The Radio Science Bulletin

ISSN 1024-4530

INTERNATIONAL
UNION OF
RADIO SCIENCE

UNION
RADIO-SCIENTIFIQUE
INTERNATIONALE

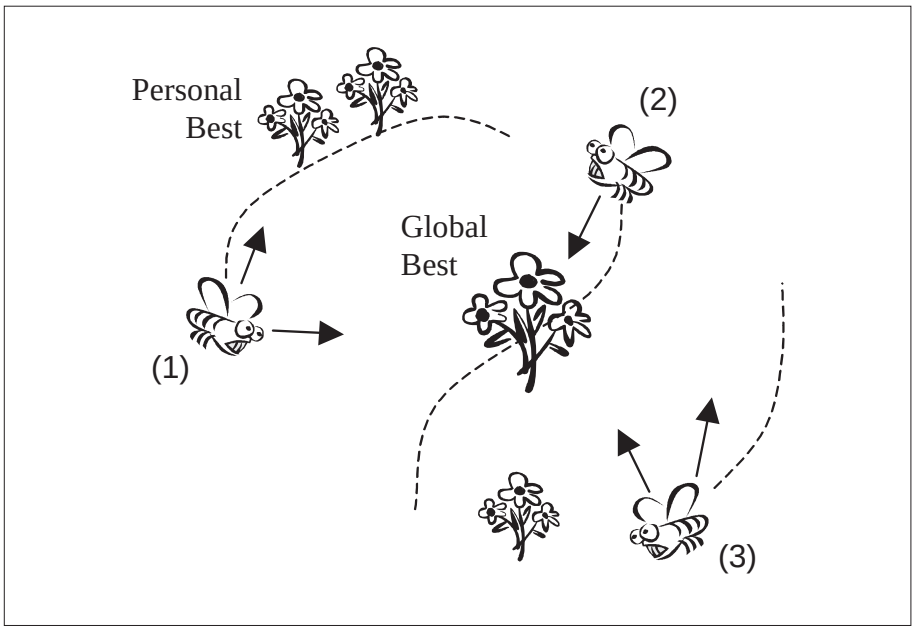

No 305
September 2003

Publié avec l'aide financière de l'ICSU
URSI, c/o Ghent University (INTEC)
St.-Pietersnieuwstraat 41, B-9000 Gent (Belgium)

Contents

Front cover: Figure 1 from "Particle Swarm Optimization (PSO): A Novel Pardigm for Antenna Designs (more on pp. 12-20)

For information, please contact :
The URSI Secretariat
c/o Ghent University (INTEC)
Sint-Pietersnieuwstraat 41, B-9000 Gent, Belgium
Tel.: (32) 9-264 33 20, Fax: (32) 9-264 42 88
E-mail: ursi@intec.rug.ac.be
http://www.ursi.org

The International Union of Radio Science (URSI) is a foundation Union (1919) of the International Council of Scientific Unions as direct and immediate successor of the Commission Internationale de Télégraphie Sans Fil which dates from 1913.

Editorial

A Second Very Special Issue

This is the second of two special issues of the *Radio Science Bulletin*. The papers in this issue and the June issue were written in honor of and are dedicated to Jean Van Bladel, on the occasion of his 80th birthday. Jean has had a tremendous positive personal impact on radio science, as teacher, mentor, and friend to many radio scientists – and in particular, to many of URSI's Young Scientists – and as Secretary General of URSI for more than 14 years. I am personally very grateful for his help, kindness, and support.

This issue and the June issue have been guest-edited by Chalmers Butler, Daniël De Zutter, Ken Mei, and Paul Lagasse. Their dedication and efforts are what have made these special issues possible, and are greatly appreciated. There is a separate introduction to these issues that concentrates on the purpose of the issues, and I will therefore again forego the usual introductions to the papers.

Also in this Issue

Jim Lin's "Radio Frequency Radiation Safety and Health" column considers an interesting outgrowth of the advance of technology. With wireless networking and cellular telephone devices taking on multiple functions, they are being used in proximity and contact with the body in ways that are dramatically different from the traditional cell phone held next to the ear. A picture phone held in front of the eye is just one example. What is the likely effect of such differences in use on the formation of cataracts in the eye? Jim's column looks at what is known in terms of answers to this interesting and important question.

The Open Radar Initiative is an effort to develop reusable, readily available technology for radio science. The proposed initial project involves developing hardware and software for ionospheric radio science, using what has been termed a Software Radar architecture. A description of this initiative appears in an open letter to the radio science community in this issue, along with a call for participation. Your input and participation are welcomed.

The December issue of the *Radio Science Bulletin* will mark a new milestone: it will contain the first of this triennium's *Reviews of Radio Science* (*RRS*), and the first of the *Reviews* to be published in the *Bulletin*. This will be just the beginning. Phil Wilkinson, our Senior Associate Editor for the *RRS*, has been working with the Commission Associate Editors to prepare an ongoing schedule of *Reviews*. Each issue starting with December should contain at least one – and more usually, several – of the *Reviews*. Of course, we will also be bringing you our usual selection of papers.

Many will be starting a new academic year about the time this issue arrives. I hope it is productive, and also fun. I also hope you will consider sharing the results of your work with your colleagues through our pages.

In Memoriam

Shortly before going to press we received the sad announcement that Mrs. Ielena (Yela) Stevanovitch, the former executive secretary of URSI, passed away at the age of 77. The next issue will contain an in memoriam.

P. Lagasse, Secretary General

Mrs. Stevanovitch and Dr. C.M. Minnis, Secretary General, at the URSI General Assembly of Helsinki (Finland) in 1978

Guest Editors' Comments

The June and September, 2003, issues of the URSI *Radio Science Bulletin* are published in honor of Professor Jean Van Bladel to celebrate his eightieth birthday. Four former students of Professor Van Bladel's chose the publication of these two special issues as a way to express their long-term affection and gratitude to their mentor and friend. As guest Editors of the two special issues, they issued invitations to participate to former students and selected professional colleagues and friends who are close to Professor Van Bladel. Although several invitees no longer work in radio science or related areas of electromagnetics and some preferred to decline our invitation due to other commitments, the response has been most gratifying. We hope you, the reader, derive as much pleasure from the papers in these two issues as we have derived in the opportunity to honor our former teacher, and, if you infer devotion to him on the parts of the Editors and authors, your senses do not deceive you.

Jean G. Van Bladel was born eighty years ago in Antwerp, Belgium, on July 24, 1922. Brussels University conferred the Electromechanical Engineer and the Radio Engineer degrees upon him in 1947 and 1948, respectively, and he received the MS and PhD degrees in electrical engineering in 1949 and 1950 from the University of Wisconsin, Madison. He was Head of the Radar Department of the Manufacture Belge de Lampes et de Matériel Electronique in Brussels during 1950 to 1954 and was an associate professor at Washington University, St. Louis, MO, from 1954 to 1956. In 1956, Professor Van Bladel became an associate professor at the University of Wisconsin, Madison, where he rose to the rank of full professor in 1960. In 1964 he returned home to Belgium to become Professor of Electrical Engineering and Director of the Laboratory for Electromagnetism and Acoustics at the University of Ghent, which he founded. In addition, during 1976 through 1978, Professor Van Bladel served as Dean of the Faculty of Applied Science of the University of Ghent and, from 1981 to his mandatory retirement in 1987, he was a member of the University Board.

In 1962-63, Professor Van Bladel was a Guggenheim fellow and a visiting professor at the Royal Institute of Technology, Stockholm, and was the Brittingham Visiting Professor at the University of Wisconsin in 1974. He was a visiting professor at the National University of Zaire in 1976 and held the Francqui Chair at the Free University of Brussels in 1978-79 and, again, in 1982.

Among numerous other international offices of importance that he has held, Professor Van Bladel was for more than ten years Secretary General of the International Union of Radio Science and now holds the title, Honorary President of URSI. He is a fellow of the IEEE and of the IEE, has served as Chairman of the European Microwave Conference, was the recipient of the Montefiore Prize in 1965, and has been a member of several editorial boards. He is a member of the Royal Academy of Sciences of Belgium (1984), a member of the Electromagnetics Academy (1990), a foreign member of the Real Academia de Ciencias, Spain (1989), and is a Corresponding Astronomer of the Royal Observatory of Belgium (1990). In 1987, the University of Liège conferred the Honorary Doctor's Degree upon Professor Van Bladel. From the IEEE, Professor Van Bladel received the 1995 Heinrich Hertz Medal and the Antennas and Propagation Society's 1997 Distinguished Achievement Award. A complete list of his noteworthy professional service and other honors and awards is simply too lengthy to delineate here.

As an author of textbooks and monographs, Professor Van Bladel has guided many of us to a better understanding of electromagnetics and has revealed to us a storehouse of techniques for solving a variety of problems. He is the author of *Les Applications du Radar à l'Astronomie et à la Météorologie* (Gauthier-Villars, Paris, 1955), *Relativity and Engineering* (Springer-Verlag, Berlin, 1984), and *Singular Electromagnetic Fields and Sources,* (Oxford University Press, Oxford, 1991; reprinted by IEEE Press, Piscataway, 1995). To those of us in the radio science community his best-known work is *Electromagnetic Fields* (McGraw-Hill, New York, 1964; reprinted by Hemisphere, New York, 1985), a tome on analytical methods for solving boundary-value problems in fields and waves. An extensive revision of the last volume is in process, so we all look forward to seeing the second edition on our bookshelves in the not-too-distant future. In addition, Professor Van Bladel has contributed chapters to several books edited by others. He also has published many papers in leading research journals.

Professor Van Bladel is a man of truly remarkable achievement in the international community of electrical scientists, radio scientists, and electrical engineers, and, by any measure, he must be listed among the handful of leading researchers of the past thirty years in electromagnetic theory and numerous of its applications. In several facets of electromagnetics – guided waves, aperture theory, dielectric resonator theory, the concept of field singularities near edges, among others – Professor Van Bladel's contributions have had significant influence on subsequent researchers and their work. In addition to fundamental contributions in the above areas, Professor Van Bladel has made relativity accessible to electrical engineers. He has shown us the utility of this arcane concept in solving everyday problems in electrical engineering, ranging from rotational and

translational media to electromagnetic scattering from moving objects. In the early 1960s, it was Professor Van Bladel who first advanced a method for solving an electrodynamic integral equation by numerical methods. At the time, electrostatic and magnetostatic integral equations had been solved by Professor Van Bladel and several others, but he was the first to lead us to the use of a digital computer to solve a time-harmonic integral equation.

Professor Van Bladel's research contributions to electromagnetic theory and applications are vast. His books and papers have been important resources to researchers and teachers alike, and they will stand the test of time with grace. Over a long and distinguished career, which continues at a frantic pace today, he has exhibited a rare depth of understanding and originality. Professor Van Bladel commands the respect of everyone in the electromagnetics community and he enjoys rapport with his colleagues around the world. He is exceptionally articulate, perceptive, personable, and reflects genuine concern for his friends and professional colleagues. He appreciates the arts and music and has a deep sense of history. These qualities are intricately woven into an exquisite and rare Belgian fabric.

Jean Van Bladel and his wife Hjördis (Pettersson) reside in Deurle, Belgium, and spend their summers in Nieuwpoort on the Belgian coast. Their three children, Vivica, Eric, and Sigrid, live in the US.

The authors, the Editors, his former students, and many colleagues dedicate the June and September, 2003, issues of the URSI *Radio Science Bulletin* to Jean Van Bladel on the occasion of his eightieth birthday. We hope this modest tribute to a distinguished scientist conveys to our gentle friend the intensity and depth of our gratitude, affection, and admiration.

Chalmers M. Butler
Daniël De Zutter
Kenneth K. Mei
Paul Lagasse

Chalmers Butler is with the Holcombe Department of ECE, Clemson University
336 Fluor Daniel EIB
Clemson, SC 29634-0915 USA
Tel: +1 (864) 656-5922; Fax: +1 (864) 656-7220;
E-mail: cbutler@ces.clemson.edu.

Daniël De Zutter is with Ghent University (INTEC)
Sint-Pietersnieuwstraat 41
B-9000 Gent, Belgium
Tel:+32 92643327;
E-mail: daniel.dezutter@intec.rug.ac.be

Kenneth Mei is with the Department of Electronic Engineering, City University of Hong Kong
83 Tat Chee Avenue
Kowloon, Hong Kong, PRC
Tel: (852) 27887769; Fax: (852) 27887189;
E-mail: eekkmei@cityu.edu.hk.

Paul Lagasse is with Ghent University (INTEC)
Sint-Pietersnieuwstraat 41
B-9000 Gent, Belgium
Tel: +32 9-264-33-20; Fax: +32 9-264-42-88
E-mail: ursi@intec.rug.ac.be.

Theory of Maxwellian Circuits

Kenneth K. Mei

Abstract

It is shown that the currents on thin wire structures including antennas and open transmission lines are solutions of ordinary differential equations as well as integral equations. The existence and uniqueness of the differential operators are proved. The differential operators naturally lead to equivalent circuits. These equivalent circuits, containing dependent sources, are not the conventional Kirchhoff type. Each solution of the equivalent circuits is the same as that of the integral equation, from which the circuit elements are obtained. Such circuits are termed "Maxwellian circuits."

1. Introduction

Currents on thin wire antennas are traditionally formulated by one-dimensional integral equations [1], and those on transmission lines by differential equations [2, 3]. It is generally accepted that the antenna problems involve radiation, which can only be accounted for in the integral equation formulation, or in a full-fledged three-dimensional set of Maxwell's equations. Recent progress in the on-surface measured equation of invariance (OSMEI) [4] suggests that the current on a dipole may also satisfy a differential equation. The sparse matrices obtained from OSMEI are indeed the discrete form of such type of differential equations. Furthermore, for thin wire structures, OSMEI is not the only method that can provide such differential equations. We can readily obtain them from solutions of the integral equations determined by the method of moments (MoM). The results presented in this paper are all obtained via MoM. This paper presents the proofs of the existence and uniqueness of the differential equations and shows how this reformulation can be done. Once the differential equations are obtained, the steps to find the circuit parameters follow naturally. However, the circuit so obtained is not the conventional Kirchhoff type. It contains voltage and current dependent sources to accommodate the solutions of Maxwell's equations. We term such circuits "Maxwellian circuits."

2. The Integral Equation and the Differential Equation of Currents

The currents on a center fed symmetrical wire antenna satisfy Hallén's integral equation,

$$\mathbf{L}I(\ell) = \mathrm{B}\cos k\ell - \frac{\boldsymbol{j}V_0}{2\mathrm{Z}_0}\sin k\ell\,, \quad \ell \geq 0 \tag{1}$$

where V_0 is the driving voltage and **L** is the integral operator,

$$\mathbf{L}I(\ell) = \int_{-L}^{L} G\left(\overline{r}/\overline{r}'\right) I\left(\ell'\right) d\ell' \cdot \tag{2}$$

$G\left(\overline{r}/\overline{r}'\right)$ is the free-space Green's function, if the structure is a straight wire antenna in open air. For wire antennas of other shapes, $G\left(\overline{r}/\overline{r}'\right)$ is an integral of the free-space Green's function [1]. For microstrip of any shape, the integral of the Hallén type can still be derived, where $G\left(\overline{r}/\overline{r}'\right)$ is replaced by a kernel of integrals of Sommerfeld type Green's dyadic. We have chosen a symmetrical wire structure to simplify the ensuing discussions. The analysis that follows should be valid for arbitrarily shaped wire structures. The constant B is a parameter adjusted to enforce the boundary condition of the vanishing current at the end of the antenna or any other impedance condition at the end of the wire.

We have also chosen a delta generator as the source model [5, 6] so that the incident field is zero everywhere on the wire except at the gap. Our objective is to find a differential operator **D**,

$$\mathbf{D}I(\ell) = \frac{d^2I}{d\ell^2} + U(\ell)\frac{dI}{d\ell} + T(\ell)I = 0 \tag{3}$$

where $U(\ell)$ and $T(\ell)$ are to be found, such that the

Kenneth K. Mei is with the Wireless Communication Research Center, City University of Hong Kong, SAR, China (CIE)

Dedicated to Professor J. Van Bladel on the occasion of his 80th birthday

solution of Equation (3) is identical to that of Equation (1). In Equation (3), the zero on the right hand side is justified because there is no incident field on the wire owing to the delta source. In fact, for every function of ℓ, there are infinite number of differential operators that can cause Equation (3) to be zero. We wish to find one which is applicable to all solutions of Equation (1) regardless of the terminating condition at $\ell = L$. And, the solution of Equation (3) should be the same as that of the integral equation (1) when the same terminating condition is applied. We prove the existence and uniqueness of such an operator and its invariance to the terminating condition in the following sections.

Operators are in general not unique, in that the product of the operator of Equation (3) with any other operator should include the same properties of the operator of Equation (3). So, our uniqueness theorem is for **D** to be the lowest-order differential operator. It is easy to eliminate a first-order operator as a possible candidate, so the second-order equation of Equation (3) is the next possible candidate.

The theorems presented rely on two assumptions:
(1) The inverse operator of the integral operator $\mathbf{L}$ exists,
(2) The current on the structure can be adequately represented by a complex Fourier series of finite terms.

3. Existence Theorem of the Differential Operator $\mathbf{D}$

Let I_i and I_j be two solutions of the integral equation (1) subject to different terminating conditions at $\ell = L$. Then, there exists a differential operator $\mathbf{D}$, defined in Equation (3), such that $\mathbf{D}I_i = 0$ and $\mathbf{D}I_j = 0$.

Proof: Substituting these two solutions into Equation (3), we get two equations from which we can solve for the coefficients U and T. The solutions for U and T should exist and be unique unless the following determinant vanishes:

$$\begin{vmatrix} \dfrac{dI_i}{d\ell} & I_i \\ \dfrac{dI_j}{d\ell} & I_j \end{vmatrix} = 0 \cdot \tag{4}$$

Vanishing of the determinant (4) means

$$\ln I_i - \ln I_j = \text{Constant} \cdot \tag{5}$$

In other words, the ratio I_i/I_j must be a constant, which is not possible if I_i and I_j have different terminating conditions. Because a current can be approximated by finite terms of a complex Fourier series, then for Equation (4) to be true within a finite nonzero interval of $\Delta\ell$, say at the neighborhood of a point $\ell = \ell_0$, should imply $I_i^{(n)}(\ell_0) = CI_j^{(n)}(\ell_0)$, for $n = 0,1,2,...,\infty$, and C is a constant. It follows that the Taylor's expansion of $I_i(\ell)$ and $CI_j(\ell)$ are identical, which leads to $I_i(\ell) = CI_j(\ell)$ over the entire length of the wire, which again contradicts the assumption of the boundary conditions. Hence, Equation (4) can be true only at discrete points where U and T may be singular but not in a finite interval $\Delta\ell$, and it follows that the existence of a differential operator valid for at least two solutions of Equation (1) is proved.

4. Uniqueness Theorem of the Differential Operator $\mathbf{D}$

The differential operator $\mathbf{D}$, defined in Equation (3), is unique for all solutions of an integral equation shown in Equation (1).

Proof: Let I_i and I_j be a pair of solutions of Equation (1) from which we obtain an operator $\mathbf{D}_{ij}$, and let $\mathbf{L}^{-1}$ be the inverse operator of the integral operator $\mathbf{L}$. Thus,

$$\mathbf{D}_{ij}I_{\binom{i}{j}} = \mathbf{D}_{ij}\mathbf{L}^{-1}\left(B_{\binom{i}{j}}\cos k\ell - \frac{jV_0}{2Z_0}\sin k|\ell|\right) = 0 \cdot \tag{6}$$

The right-hand side of Equation (6) must vanish for two different values of B, because the left-hand side must vanish for both I_i and I_j, which satisfy different terminating conditions. For Equation (6) to vanish for two different values of B, it is necessary that the two terms in the right hand side of Equation (6) vanish separately after being operated on by $\mathbf{D}_{ij}\mathbf{L}^{-1}$. It follows that

$$B_{\binom{i}{j}}\mathbf{D}_{ij}\mathbf{L}^{-1}\cos k\ell = 0 \cdot \tag{7}$$

Since the $B_{\binom{i}{j}}$ govern the terminating conditions and $B_i \neq B_j$, at least one of them does not vanish and $\mathbf{D}_{ij}\mathbf{L}^{-1}\cos k\ell = 0$ independent of the parameter B. Therefore $\mathbf{D}_{ij}I_{\binom{i}{j}} = 0$ has to be an invariance of the terminating conditions.

Since $\mathbf{D}_{ij}$ exists and is unique between I_i and I_j, the same is true for $\mathbf{D}_{ik}$ between I_i and I_k. But, $\mathbf{D}_{ij}$ is also applicable to I_i and I_k because of its invariance to the terminal condition. It follows that $\mathbf{D}_{ij} = \mathbf{D}_{ik}$. It is thus proved that the $\mathbf{D}$ is the same for all solutions I, since $\mathbf{D}_{ij}$ is unique for I_i and I_j and $\mathbf{D}_{ik}$ is unique for I_i and I_k.

5. Finding the Operator $\mathbf{D}$ from Numerical Results

The integral equation of the type in Equation (1) is most conveniently solved numerically [1]. To find the operator $\mathbf{D}$ numerically we assume the wire structure to be subdivided into equal segments and the values of the currents are found numerically at the middle of each segment.

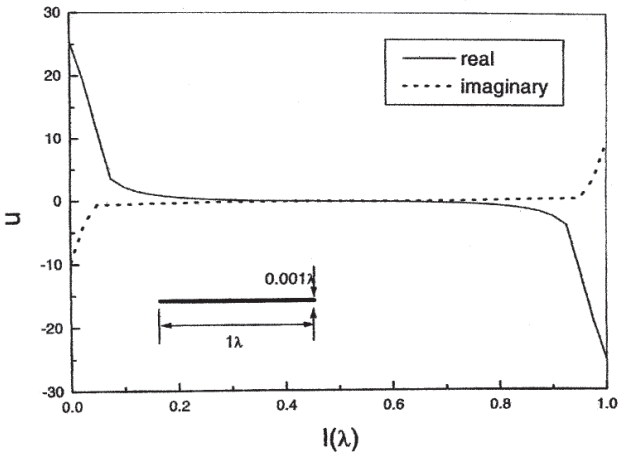

Figure 1a. The coefficient $U(z)$ of a dipole antenna ($L = 1\lambda$).

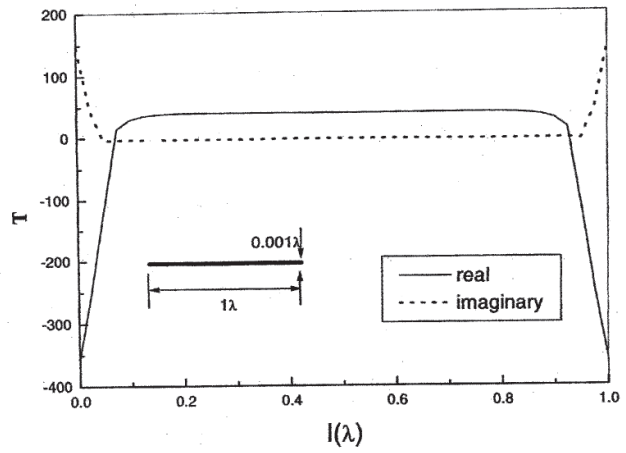

Figure 1b. The coefficient $T(z)$ of a dipole antenna ($L = 1\lambda$).

A second-order differential operator may be represented by the linear equation

$$I_{n+1} + a_n I_n + b_n I_{n-1} = 0 \tag{8}$$

at a point n, ($n = 1, 2, ..., N$). Substituting two numerical solutions for I into Equation (8), we can solve for a_n and b_n. The values of U_n and T_n can be obtained readily by comparing Equation (8) to the finite-difference form of Equation (3), which yields

$$U_n = 2\frac{(1-b_n)}{(1+b_n)\Delta\ell} \tag{9a}$$

and

$$T_n = \frac{2(1+a_n+b_n)}{\Delta\ell^2(1+b_n)}. \tag{9b}$$

6. Numerical Results

We have used MoM and the terminating conditions, $I(L) = c$ and $I'(L) = \alpha I(\ell)$ with various values of c and α to find the current along the wire. Values of coefficients U and T for a dipole and a wire antenna with two right-angle bends are given in Figures 1 and 2, respectively. It is interesting to observe that the value of U is practically zero in the mid-section of a long straight wire antenna. The value of T there is the square of the free-space wavenumber, which indicates that the current travels along a straight wire antenna with the velocity of light, almost without attenuation. Most of the radiation, therefore, takes place near the ends of the antenna where both U and T change drastically. Another interesting feature of the differential equations is that the coefficients U and T are very sensitive functions of the local geometry of the wire. From the currents it is hard to see where the bends are, but from U and T it is quite obvious where the bends are located. Conversely the currents are not very sensitive to the errors of the differential equations. Since the functions U and T near the bends are fairly easily characterized, one can make use of their approximations to form the differential equation of the current. Figure 3 shows the results of the current on a long antenna with a 90° bend, computed from the differential equation solution incorporating the U and T for a shorter wire together with the current obtained from MoM solution. One should observe very close agreement even at the driving point where the input impedance may be determined. Figure 4 shows values of the current on a rectangular helical antenna determined by the MoM and the differential equation. The parameters of the differential equations are obtained from the MoM solutions subject to the boundary conditions $I'(L) = \alpha I(L)$ with $\alpha = 0$ and 1. The currents in the figure incorporate the conditions $I(0) = I(L) = 0$.

7. Extraction of Maxwellian Circuit Parameters from Full-wave Results

One of the important applications of the differential-equation formulation is that it is amenable to the extraction of circuit components from the full-wave results that might be found, for example, by the MoM. Actually, wire antennas and microstrips belong to the same class of problems that can be solved by integral equations of the type in Equation (1). Circuit parameter extraction is important for IC interconnects, which is done traditionally from static results [7] on open transmission systems. Although several researchers have succeeded in obtaining full-wave solutions of microstrips of various shapes [8, 9, 10], none has made any attempt to extract circuit parameters from the dynamic results. Using the differential equation of the current we are able to extract circuit parameters for both transmission and radiating systems at any frequency at which we can obtain the solution.

Having shown that the solution of the differential Equation (3) truly reproduces the MoM solution, our next

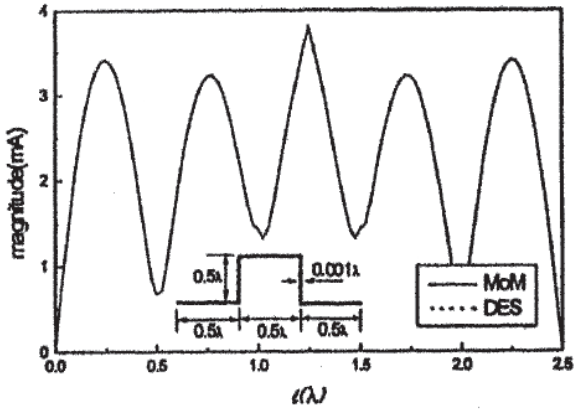

Figure 2a. The current $|I|$ on a double bend wire antenna.

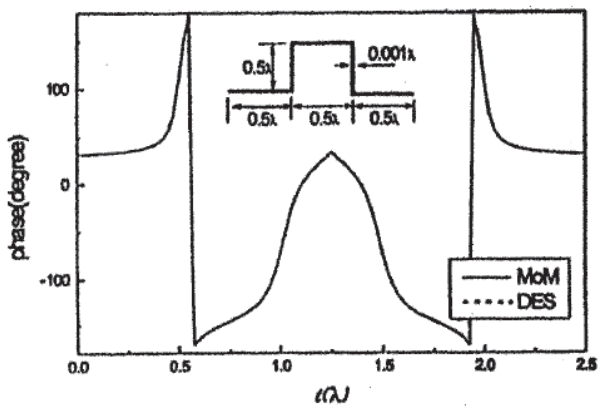

Figure 2b. The phase angle of the current of Figure 2a.

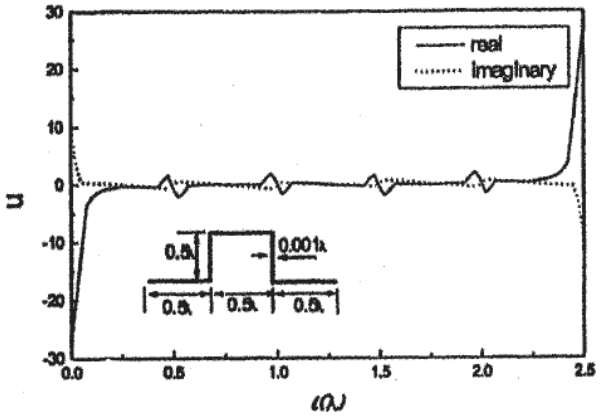

Figure 2c. The coefficient $U(\ell)$ of a double bend wire antenna.

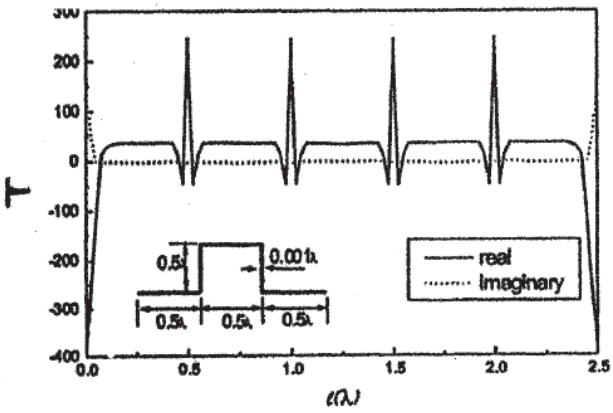

Figure 2d. The coefficient $T(\ell)$ of a double bend wire antenna.

step is to split Equation (3) into two coupled first-order equations involving current and voltage. The general homogeneous first-order linear system of differential equations [11] that can reproduce Equation (3) may be written in the form

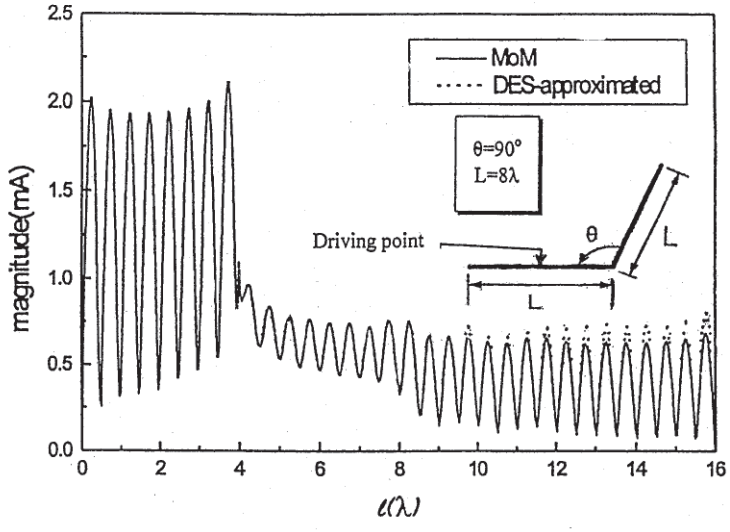

Figure 3. The calculated current $|I|$ from approximate $U(\ell)$ and $T(\ell)$ for a 90° bent wire antenna.

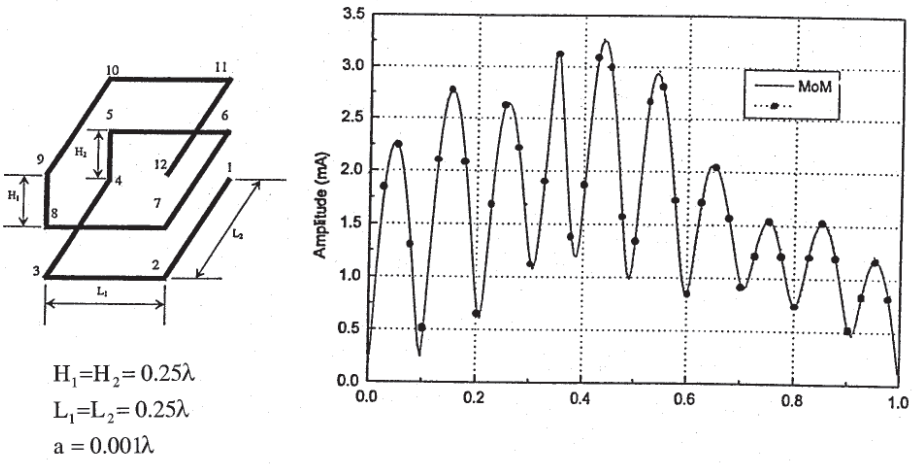

Figure 4. The currents on a rectangular helical antenna driven at node 5, computed by the MoM and from the solution of the wire differential equation

$$\frac{dV}{d\ell} = -j\omega L(\ell) I + \alpha(\ell) V\,, \tag{10}$$

$$\frac{dI}{d\ell} = -j\omega C(\ell) V + \beta(\ell) I\,, \tag{11}$$

where the factor $j\omega$ is inserted for convenience in the ensuing discussions relating L and C to circuit elements. Since $I(\ell)$ is found by the MoM and $V(\ell)$ can be found from $I(\ell)$, we need two independent solutions of $I(\ell)$ to find L and α from Equation (10), and C and β from Equation (11). These parameters in Equations (10) and (11) are found by a procedure similar to that used to determine the parameters in the differential operator **D** of Equation (3). After the parameters are found, V may be eliminated from Equations (10) and (11) to get a second-order differential equation of $I(\ell)$, which, by the uniqueness theorem, should be identical to Equation (3).

Since **D** is proven to be invariant to the terminating conditions, so should be the parameters L, C, α, and β, from which we can derive **D**. The L, C, α, and β are circuit components familiar to circuit engineers, where α and β are parameters of the voltage- and current-dependent sources, respectively. The novelty is that the exact solution of an antenna problem can now be obtained by solving a circuit problem. Since such circuits are formulated via solutions of Maxwell's equations instead of the conventional Kirchoff's laws, they are termed "Maxwellian circuits."

8. Line and Load

In the classical theory of uniform transmission lines, an infinite line is indistinguishable from a finite-length line with a matched load. In this new formulation, we should notice that a load has to be different from a line.

The parameters L, C, α, and β are invariants of the load, but they are not invariants of the length or shape of the line. A pure load is defined as a circuit parameter that does not produce external fields to influence the other parameters of the system. Since a piece of open transmission line is considered to be a radiating or receiving element, it cannot be considered a load. The combination of a load and a transmission line is not a pure load. The attached transmission line must be accounted for in the determination of the equivalent circuit parameters. For the same reason, an antenna is not a pure load unless it can be shown that its radiation has no effect on the transmission system. Because of the variation of the equivalent circuit parameters near the line termination, an exact matching load may not be easy to find. The conventional matching load, the characteristic impedance, may be a good approximation, but there is no guarantee that it is the optimum.

9. Numerical Results – Circuit Parameters

The circuit parameters are not calculated from the second-order differential equations. They are calculated

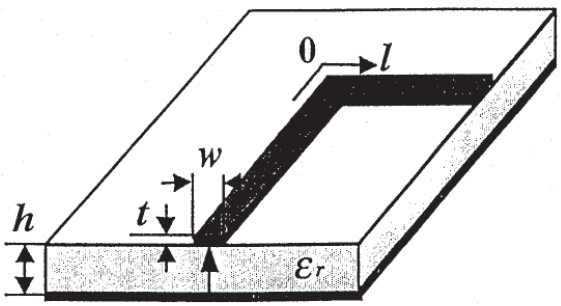

Figure 5a. The microstrip, with $\varepsilon_r = 9.8$ *for* $f = 50$ *to* 900 *MHz.*

directly from the solutions $I(\ell)$, as mentioned in the previous section. To show the versatility of the theory, we present the circuit parameters of microstrips, where they are most needed.

Figure 5 shows L, C, α, and β of a microstrip with a 90° bend. An interesting feature of these figures is that L and C are now almost independent of frequency. There are small drifting changes, which may partially be attributed to the numerical inaccuracies in the computation. An average value within an operating band may be adequate for most applications. The parameter a is essentially frequency independent. Only β is dependent on frequency, and our calculations show that its variation is proportion to ω^2. Even the ω dependence of β can be avoided if we choose to use a mitered 90° bend. β is independent of ω if the bend is 45°. A 90° bend can be achieved by two 45° bends. β becomes ω dependent when the two varying parts of β overlap, which happens when the inner mitered distance is less than the width of the strip. Using these parameters to solve for the current on the bent microstrip, one should obtain results identical to those from the MoM. It is noted that in the computation of the parameters, all are considered to be complex, but the results show that all are real. Using these real parameters, one can readily calculate the current of any load. Figure 6 shows the comparisons of the results of the equivalent circuits and those of MoM over a wide band of frequencies. The parameters are found from $Z_L = 0, \infty$. The curves are for $Z_L = 50 + j50$. The robustness of the equations is confirmed.

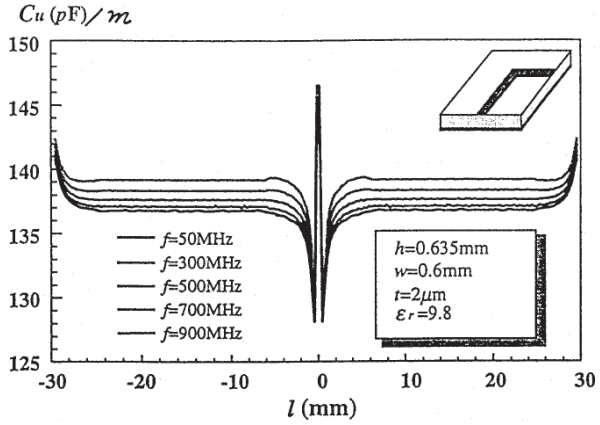

Figure 5b. $C(\ell)$ of a microstrip of $\varepsilon_r = 9.8$ for $f = 50$ to 900 MHz, applicable to all loads.

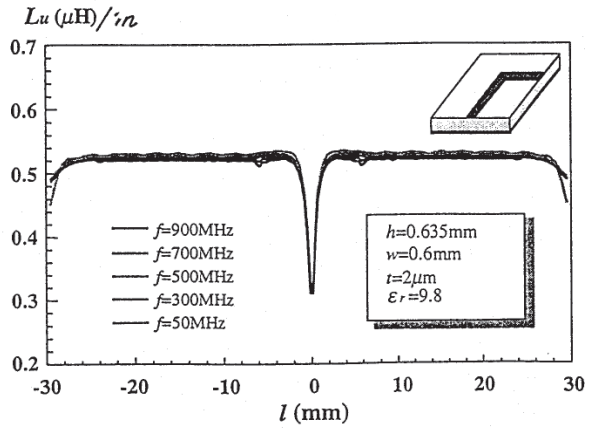

Figure 5c. $L(\ell)$ of a microstrip of $\varepsilon_r = 9.8$ for $f = 50$ to 900 MHz, applicable to all loads.

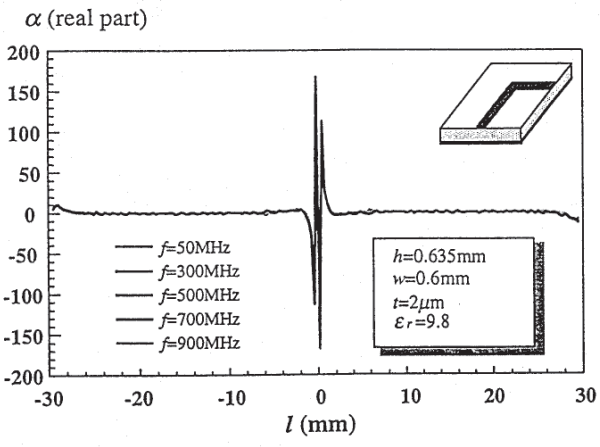

Figure 5d. $\alpha(\ell)$ of a microstrip of $\varepsilon_r = 9.8$ for $f = 50$ to 900 MHz, applicable to all loads.

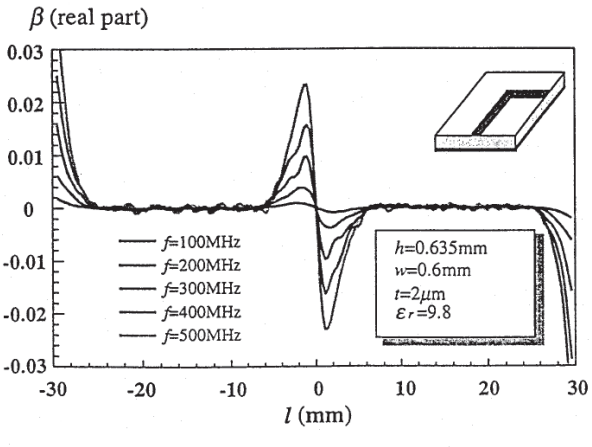

Figure 5e. $\beta(\ell)$ of a microstrip of $\varepsilon_r = 9.8$ for $f = 50$ to 900 MHz, applicable to all loads.

10. Interpretation of the Dependent Sources

Without α and β, Equations (10) and (11) are the textbook equations of nonuniform transmission lines [2, 3], which are derived from Kirchoff's laws. By including the dependent sources we have essentially modified Kirchoff's laws, but the physical conditions we have used to replace Kirchoff's laws are not explicit here. However, the dependent sources α and β are not arbitrary. They are found by fitting the equations to the solutions of Maxwell's equations. The significance lies in the fact that one pair of α and β should work for all solutions of the Maxwell's equations of the specific system, which implies that the pair (α, β) is a part of Maxwell's equations. In contrast to Kirchoff's laws of conservation of current, Maxwell's equations stipulate the conservation of charge, so α and β must support this physical condition. Another interpretation of the role of the dependent sources is that an open transmission line is not a pure passive system. When a section of line radiates, it behaves as a sink insofar as the system is concerned, because energy is removed. Conversely, when energy is received from outside, it behaves like a source. So, a section of line can be passive or active depending on the direction of current flow, a role that cannot be fulfilled by an active or passive component. But a dependent source fits naturally. There is very strong evidence to support the claim that the missing links between a theory based on Maxwell's equations and one based on the laws of circuits are the dependent sources. Without them, the model is incomplete, and discrepancies arise as erratic frequency and load dependencies of the circuit parameters. With the dependent sources, the solutions of the equivalent circuit problem become the same as those of Maxwell's equations for all loads over a wide band of frequencies.

11. Conclusion

We have shown that to every integral equation of the thin wire structure type, there exists a unique second-order differential operator, the solutions of which are identical to those of the integral equation if identical boundary conditions are applied in the solution to the integral and differential equations. Existence and uniqueness theorems were proved. When the second-order differential equations are rewritten as two first-order differential equations involving voltage and current, equivalent circuits evolve naturally. We have shown that the telegrapher's equations for nonuniform lines, given by most text books of electromagnetic field theory, are incomplete. We have appended dependent sources to the equations to make them complete and the ensuing results are most remarkable. It makes the passive components almost independent of frequency, which preserves the simple relationship between voltage and current of circuit theory. The dependent sources appear to be the missing link between circuit theory and electromagnetic theory. Only by including them can the currents in a circuit obtained from the solution of equations based on circuit laws be the same as currents obtained from the solution of Maxwell's equations. The theorems and ensuing equivalent circuits not only have improved our physical insights but also have accelerated computations because of the broadband nature of the circuit parameters.

While we have demonstrated the validity of the theory, we also wish to remind the reader that it is still an approximation. The limit of the "thin wire" condition must be adhered to when the theory is applied. Further development to cover multi-wire systems, branching, and patches are needed, before the theory can be put to widespread practical use. However, each of the above mentioned topics requires

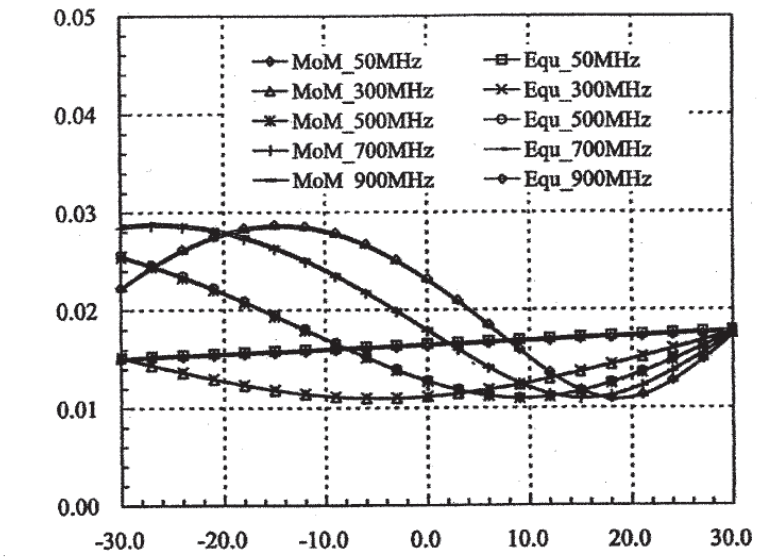

Figure 6. The currents on the structure of Figure 5, computed from its equivalent circuit and by the MoM.

extensive mathematical derivations and numerical confirmation, which are beyond the limit of a single journal paper. We shall present them in follow-up papers.

12. Dedication

This paper is dedicated to celebrate the 80th birthday of Prof. J. B. Van Bladel, my PhD thesis adviser at the University of Wisconsin, Madison. I obtained my doctorate in 1962. Every mathematical reasoning and physical concept needed in the writing of this paper can be traced back either to the classroom lectures by him or research discussions with him. It is fair to say that I have learned all my trade skill from him. It also seems that I have not learned much new, since I left the apprenticeship 41 years ago. Perhaps, there is no need to, because learning Maxwell's equations from the good professor is like learning martial art from the Shaoling temple master, in that a few secret punches and kicks can last a lifetime for one to survive in the jungle of electromagnetic theory.

13. Acknowledgement

This research is supported in part by research grant CERG no. 9040265 of the Hong Kong Research Grant Council (RGC) and by the SRG no. 7000862 and no. 7001024 of the City University of Hong Kong. The calculations of the differential equations of the dipoles were done by Dr. K. Lan (now at the University of Waterloo, Canada), and the data on microstrip transmission lines were calculated by Dr. J. H. Wang (now at the Northern Jaotung University in Beijing). Their faith in my pursuit of the differential operator is greatly appreciated. The author also appreciates the valuable discussions with Dr. Y. W. Liu.

14. References

1. K. K. Mei, "On the Integral Equations of Thin Wire Antennas," *IEEE Transactions on Antennas and Propagation*, **AP-13**, 3, May 1965, pp. 374-378.

2. S. Ramo, J. R. Whinnery and T. Van Duzer, *Fields and Waves of Communication Electronics, 3rd Edition*, New York, Wiley, 1994.

3. David Chang, *Field and Wave Electromagnetics, 2nd Edition*, Reading, Addison-Wesley, 1990.

4. Y. Liu, K. Lang and K. K. Mei, "Application of On-Surface MEI Method on Wire Antennas," *IEEE Transactions on Antennas and Propagation*, **AP-47**, 8, August 1999, pp. 1301-1304.

5. R. E. Collin, *Antennas and Radiowave Propagation*, New York, McGraw-Hill, International Edition, 1985.

6. R. W. P. King, *Theory of Linear Antennas*, Cambridge, MA, Harvard University Press, 1956.

7. P. Silvester and P. Benedek, "Equivalent Discontinuities Capacitance for Right-Angle Bends, T-Junctions, and Crossings," *IEEE Transactions on Microwave Theory and Techniques*, **MTT-21**, May 1973, pp. 341-346.

8. W. Sun, W. W. M. Dai, and W. Hong, "Fast Parameter Extraction of General Interconnects using Geometry Independent Measured Equation of Invariance," *IEEE Transactions on Microwave Theory and Techniques*, **MTT-45**, 5, May 1997, pp. 827-836.

9. X. Zhang and K. K. Mei, "Time-Domain Finite Difference Approach to the Calculation of the Frequency-Dependent Characteristics of Microstrip Discontinuities," *IEEE Transactions on Microwave Theory and Techniques*, **MTT-36**, 12, December 1988, pp. 1775-1787.

10. W. Harokopus and P. B. Katehi, "Characterization of Microstrip Discontinuities on Multilayer Dielectric Substrates including Radiation Losses," *IEEE Transactions on Microwave Theory and Techniques*, **MTT-37**, 12, December 1989, pp. 2058-2066.

11. I. G. Petrovski, "Ordinary Differential Equations," (English edition translated by Richard A. Silverman), New York, Dover Publications, 1973.

Particle Swarm Optimization (PSO): A Novel Paradigm for Antenna Designs

Y. Rahmat-Samii
Dennis Gies
Jacob Robinson

Abstract

The particle swarm optimization (PSO) algorithm represents a new approach to optimization problems in electromagnetics. Based upon a mathematical model of the social interactions of swarms, the algorithm has been shown to be effective at finding good solutions to a number of complicated EM design problems. This paper provides a conceptual overview of the algorithm, keeping at all times the focus on implementing PSO to solve practical problems. In this vein, selected recent applications of the method to real-world design examples are presented.

1. Introduction

1.1 Celebrating Prof. Jean Van Bladel's 80th Birthday

We are delighted to contribute this paper to the 80th birthday special issues of the URSI *Radio Science Bulletin* honoring Prof. Van Bladel, whose contributions to the electromagnetic and URSI communities are immeasurable. We have all benefited from his wisdom and his technical wit. His papers are original, mathematically detailed and always address some interesting conceptual phenomena. His books have inspired and provided solid foundations for the educations of other authors. One of the authors of this article, Rahmat-Samii, has also tremendously enjoyed his friendship with Prof. Van Bladel. It is so humbling to be able to honor Prof. Van Bladel with this contributed paper. Two of my students (one MS and one BS) and I have assembled this paper in order to bring to the attention of the URSI community a powerful optimization paradigm based on our recent research activities [1-3]. It is in the spirit of Prof. Van Bladel's research style to strive for new directions in research and apply it to useful engineering problems. Prof. Rahmat-Samii is also thankful to the Special Issue Editors for extending the invitation to contribute this paper. We hope that the URSI community will find it interesting and useful.

1.2 Evolutionary Optimization Techniques: GA and PSO

As access to previously unimaginable computational resources has become commonplace, many aspects of electromagnetic design have undergone titanic shifts. In particular, the ability to accurately evaluate the relative quality of a given design based on numerical methods has opened the door for stochastic global optimizers to augment design processes for everything from antenna design to RCS reduction to microwave circuit analysis. Having repeatedly proven its worth through a broad selection of difficult problems [4], the genetic algorithm (GA) is the most popular of the so-called evolutionary methods in the electromagnetics community [5],[6]. More recently, however, a new stochastic algorithm called particle swarm optimization (PSO) has surfaced, and early research indicates that this method should prove to be a valuable addition to the electromagnetic design engineer's toolbox [1].

GA consists of a population composed of numerous individuals, each of which contains a binary string that encodes a potential solution to a problem. The algorithm specifies the process through which the genetic information of the population is combined to form new generations as time progresses. In contrast, PSO models the social interaction of a group of individual agents operating together as a swarm, where the position of each particle represents potential designs. The particles update their positions according to how successful their present positions are in relation to the rest of the swarm's positions.

Both methods are inherently well-suited for electromagnetic optimization, but substantial differences between the two algorithms lead us to believe that one may be better than the other for certain applications. A critical difference between GA and PSO is the number and type of operators available for each method. GA traditionally makes use of three operators: crossover, selection, and mutation. Each of these has multiple implementations and parameters

Yahya Rahmat-Samii, Dennis Gies, and Jacob Robinson are with the Department of Electrical Engineering, University of California, Los Angeles, Los Angeles, California 90095-1594 USA; E-mail: rahmat@ee.ucla.edu

Dedicated to Professor J. Van Bladel on the occasion of his 80th birthday

that must be chosen according to the problem. The particle swarm, on the other hand, has only one operator: velocity calculation. This step of the algorithm is subject to modification by a number of algorithm parameters and also subsumes the process of calculating the distance between two particles. Distance calculation is generally trivial, but can take either the form of numerical difference or the Hamming distance between two binary strings [7]. Being subject to only one operator simplifies the PSO algorithm and can reduce the complexity of applying a global optimization routine to an arbitrary problem.

PSO also differs from GA in that the convergence behavior of the swarm can be closely controlled by algorithm parameters. Both the rate of convergence and the level of stagnation ultimately reached by the swarm can be fine tuned by the designer. In addition to avoiding the serious stagnation problems of GA [8], convergence control is useful for engineering applications because it is often more important to continuously test new solutions than it is to ensure that all the particles have converged to a single point. Like GA, certain algorithm parameters must be specified by the designer. Of particular importance, of course, is the specification of the range over which each design parameter can vary. In PSO, the parameters can take any real value between the two limits, whereas in GA one must also specify the number of discrete values that the parameter can take.

For the purpose of illustrating some of these properties of particle swarm optimization, we present in this paper three examples of electromagnetic designs accomplished by means of particle swarm optimization. First, we consider the problem of corrugated horn design. Corrugated horns have a large number of design parameters, so it is difficult to find the optimum trade-off for a given design goal. It is shown that using the particle swarm to determine the horn's parameters can result in improved radiation characteristics and smaller physical size. Second, the particle swarm is used to optimize the element excitations of an antenna array such that the array can radiate with two different power patterns depending only on the phases of the excitation. Finally, a non-uniform Luneburg lens is designed using the particle swarm to specify the layer thicknesses and dielectric constants.

2. Particle Swarm Optimization

Particle swarm optimization can be understood by imagining a swarm of bees that encounter in their travels an open field spotted with wildflowers. The natural desire of the swarm is to locate the position in the field that has the highest density of flowers. Because the swarm has no a priori knowledge of the field, the individual bees spread out and begin their search in random locations. Each bee can remember the locations that it found the most flowers, and somehow communicates this information to the rest of the swarm. As time goes on, each bee is torn between returning to the position that it was previously successful in finding flowers and heading toward the location that the rest of the swarm has reported as having the most flowers. The ambivalent bee therefore accelerates in both directions, altering its trajectory to fly somewhere between the two points depending on whether nostalgia or social influence dominates its decision. Occasionally, a bee may fly over a place with more flowers than had been encountered by any bee in the swarm. The whole swarm would then be drawn in part toward that location (see Figure 1).

In this way the bees explore the field: continuously updating their speed and direction of travel depending on how successful at finding flowers they have been in comparison to the rest of the swarm. Constantly, they're checking the territory they fly over against previously encountered locations of highest concentration hoping to find the highest concentration of flowers. Eventually, the bees will have explored the entire field, and will end up swarming around the location with the absolute highest concentration of flowers.

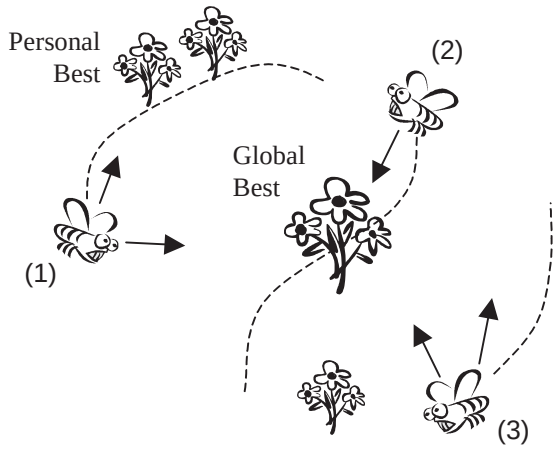

Figure 1. Particle Swarm Optimization as modeled by a swarm of bees searching for flowers. Dashed lines trace the paths of our imaginary agents, and the solid arrows show the two components of their velocity vector. The first bee here (1) has found a personal best location, and one component of his velocity vector points to that position. The other vector points to the global best position, which was found by bee (2). Finally, the third bee shows that although a particle may not have found a useful personal best, it still is drawn to the same global best position.

In 1995, Kennedy and Eberhart [7] attempted to model naturally occurring swarming behavior in a computer program. They shortly realized that in the process they had developed an optimization algorithm and called their creation particle swarm optimization (PSO), using the more general term "particle" to represent bees, fish, birds, or any other type of natural agent that exhibits swarming behavior. As shown in the block diagram of Figure 2, the first step of the algorithm is to randomly initialize the position and velocity of each particle in the swarm, dispersing them uniformly across the search space. The number of particles is a parameter of the algorithm, generally specified between 10 and 20 [9].

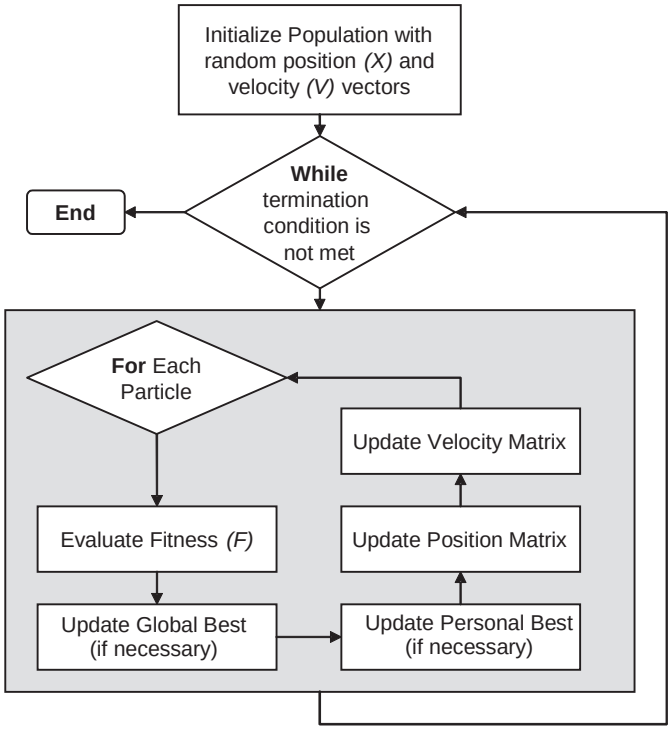

Figure 2. A flow chart describing the Particle Swarm Optimization (PSO) algorithm. The termination condition can be the number of iterations, the convergence of the swarm, or the achievement of a particular goal fitness value.

The fundamental process of particle swarm optimization is how the particles move through solution space. Like our ambivalent bee, PSO posits that particles should move toward some combination of their personal best position and the global best position. Therefore, all of the data required to update the particle positions for every time step can be stored in four $M \times N$ matrices, where M is the number of particles in the simulation and N is the number of dimensions of the problem. The positions of all of the particles in the swarm are stored in the position matrix $\mathbf{X} = \left(x_{ij}\right)$ where $1 \le i \le M$ and $1 \le j \le N$. Each row of this matrix represents a potential solution for the function to be optimized. The velocity of each particle in N-dimensional space is stored in another $M \times N$ matrix $\mathbf{V} = \left(v_{ij}\right)$.

Like the bees in our example, every particle must know the locations in solution space where they have previously been successful and the location that the rest of the swarm has found to be most successful. This information is represented by the personal best and global best position matrices, respectively. The personal best position matrix specifies the position at which any given particle achieved its best fitness value up to the current iteration. Similarly, the global best position vector specifies the location in solution space at which the best fitness value was obtained. The global best may be attained by any particle at any iteration up to the present one. Therefore, although every particle in the swarm accesses the same global best position, the personal best positions are specific to a given particle. The personal and global best positions can also be represented by the $M \times N$ matrices $\mathbf{P} = \left(p_{ij}\right)$ and $\mathbf{G} = \left(g_{ij}\right)$, respectively. Because the global best for each particle is the same, the rows of the $\mathbf{G}$ matrix must all be identical.

The position and velocity of each particle is updated at discrete intervals according to

$$\mathbf{V}_{\text{updated}} = \mathbf{V}_{\text{previous}} + c_1\eta_1(\mathbf{P} - \mathbf{X}) + c_2\eta_2(\mathbf{G} - \mathbf{X}) \quad (1)$$

where $\eta_{1,2}$ is a uniform random variable in the range $0 \le \eta_{1,2} \le 1$ and c_1 and c_2 are constants that determine the relative impact of social influence or nostalgia on a particle's trajectory. The three terms of this expression are the initial velocity of the particle at the beginning of the iteration, and the distance of the particle from the personal and global best positions. Hence, the particle velocities are likely to be large in the early stages of the optimization and will become substantially smaller as the swarm converges to the optimum. Finally, for every dimension, the particles move in the direction specified by the velocity matrix according to a simple relationship given by

$$\mathbf{X}_{\text{updated}} = \mathbf{X}_{\text{previous}} + \mathbf{V} \cdot \Delta t \quad (2)$$

where Δt is either a unit time step (as in the examples presented in this work) or specified in combination with c_1 and c_2 such that it has the same effect as the constriction factor proposed in [10].

2.1 Fitness Evaluation

Determination of the $\mathbf{P}$ and $\mathbf{G}$ vectors requires a way of specifying the relative quality of potential solutions. As in all evolutionary optimization algorithms, this is achieved by means of the concept of fitness evaluation. Returning to the example of bees in a field, good fitness values are achieved when a bee reaches an area with many flowers.

Likewise, areas without substantial flora would result in bad fitness values. The terms "good" and "bad" are used here because, although the fitness is always represented by a numeric quantity, the best fitness may be either a global maximum or a global minimum.

In engineering problems, fitness evaluation is often the most crucial part of the entire optimization process. If the fitness of potential solutions is not properly quantified, then the optimization will not be successful. The process is deceptively difficult, however, because engineering problems often require finding the best trade-off between a number of relevant design goals. Designs that achieve just one of the goals are often easy to find, but determining the design that represents the best possible tradeoff among all of the goals brings into the picture each parameter's magnitude (normalization is often impossible because the maximum achievable value is unknown) and the relative importance of each parameter to the others. For example, in antenna design one might wish to find a design that achieves high gain, low side lobes, and small physical size, but the designer may wish to emphasize high gain over the other two parameters.

The problem facing the designer becomes how to distill a multitude of disparate values into a single fitness value that accurately represents how closely an arbitrary design conforms to the desired result. A common means for doing so is called the method of weighted aggregation (MWA). The aggregate fitness is calculated by [11]

$$F = \sum_{i=1}^{N} w_i f_i \qquad (3)$$

where N is the number of fitness factors, f_i is the value of the i th fitness factor, and w_i is a weighting coefficient that must be specified by the designer. This method is simple and effective but often requires extensive tuning of the weighting coefficients, particularly for problems where each domain is unrelated to the others, as is usual in engineering.

3. Design Examples

3.1 Corrugated Horn Antenna Design

The first electromagnetic design example considered is the case of corrugated horn antenna design [3]. The physical and electromagnetic characteristics of the horn can be controlled by a combination of five parameters (see Figure 3):

1. S-parameter relating to length, $s = a^2/(2\lambda L)$
2. Number of corrugations per wavelength
3. Ratio of tooth width to total corrugation width, (t/w)
4. Profile parameter (relating to the overall shape of the horn)
5. Matching section parameter

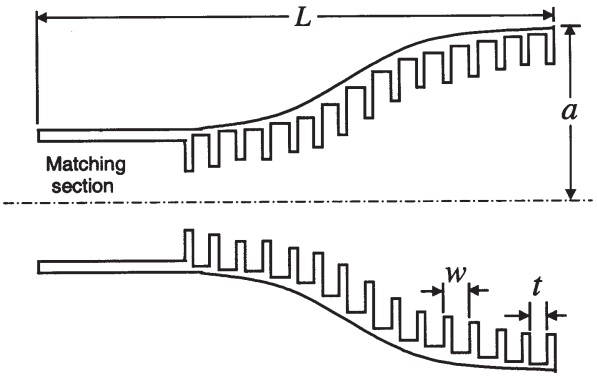

Figure 3. The cross-sectional geometry of a corrugated horn antenna.

These parameters define a five-dimensional solution space in which the PSO searches for the optimum design. Each five-coordinate position in this solution space represents a possible horn design where each coordinate corresponds to its respective parameter value. The five design parameters are specified by the particle swarm and then passed to a separate program that simulates the horn's far-field pattern and cross-sectional geometry. The horn, designed as a space-borne feed for a reflector antenna, must be light weight and must exhibit a desired beamwidth (BW_{target} *t)*. It is also desirable for the horn to have a low $Xpol$ and S_{11}. Because the horn is to be a reflector feed, it is only important that the cross polarization be low within the reflector subtended angle, which, for this design, is ±36° [12]. Thus $Xpol$ is computed only within this subtended angle. Largely through trial and error, a successful fitness function was found to be

$$F = -0.5\,\mathrm{Weight(lbs)} - 0.2Xpol(\mathrm{dB}) - (BW_{target} - BW)^2 - S_{11}(\mathrm{dB}) \qquad (4)$$

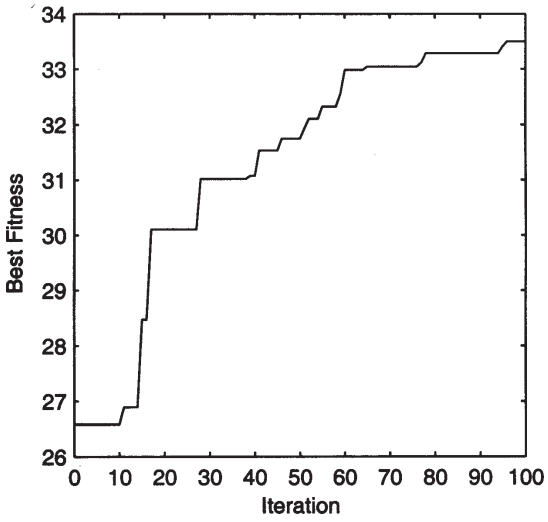

Figure 4. The convergence behavior of the particle swarm for the corrugated horn design. In this case, PSO was used to maximize the fitness function

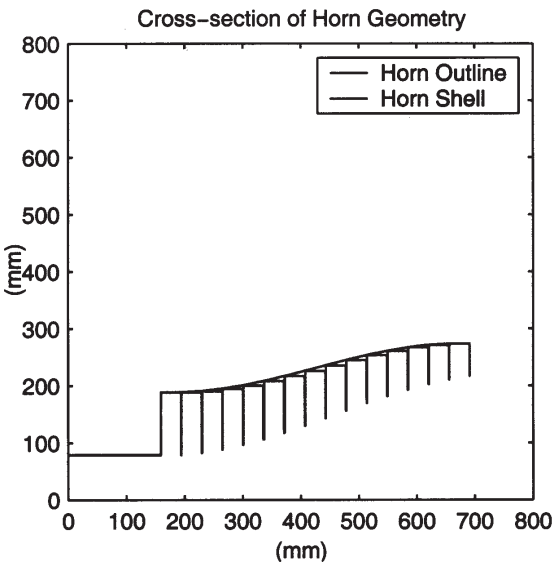

Figure 5a. A plot showing half of a cross section of the optimized profiled corrugated horn.

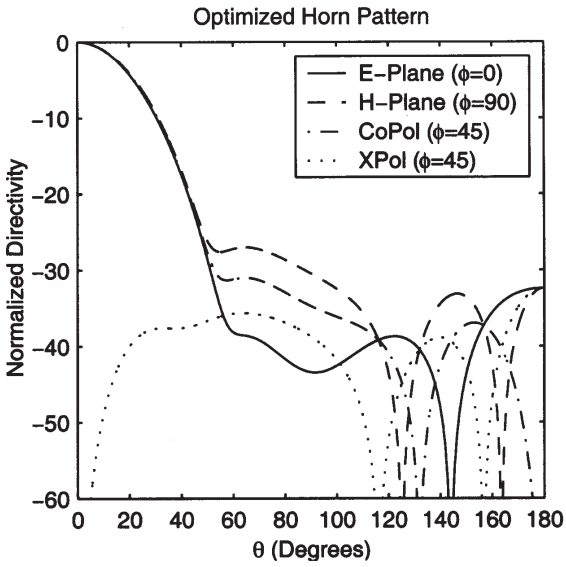

Figure 5b. The far field pattern for the optimized horn. Plus or minus 36° is the subtended angle for an offset reflector antenna illuminated by the horn.

and in this example the PSO was used to maximize the fitness value. Furthermore, a swarm size of 10 was selected, c_1 and c_2 were both set to 2.0, and the inertial weight (w) was varied linearly from 0.9 to 0.4 over 100 iterations. Figure 4 shows the convergence behavior of the swarm over the course of the optimization.

The results of the optimization are shown in Figure 5. The optimized horn showed improvement in every category over the best horn in the initial random population. It had 16 corrugations, an outer shell thickness of 1 mm, approximate weight of 8.2 lbs, and total length of 713.2 mm. Specifically the optimized horn had lowered its S_{11} by over 6 dB, it's *Xpol* by almost 1 dB, was two pounds lighter and matched the target beamwidth of 34° perfectly. This corresponded to a fitness value increase from 26.6 to 33.5. The performance of the horn resulting from this optimization is comparable to the performance achieved through other methods of optimization such as GA, and microGA (iGA) [3],[9].

3.2 Reconfigurable Array Design

A second interesting application of PSO to electromagnetics is in the design of reconfigurable antenna arrays. The next example illustrates the use of the particle swarm algorithm to find excitation coefficients of a 20 element array such that it is capable of radiating two different patterns, but can be fed by a static power division network, as shown in Figure 6. The implication of this is that the two patterns must be solely phase-differentiated [13]. We further stipulate that one of the patterns should radiate with an optimized amplitude distribution but with zero phase to all of the elements.

Two patterns are desired: a high-directivity, low-side-lobe pencil-shaped beam, and a wider sector pattern. Graphically, the pencil and sector patterns should fit within the design masks specified by dashed lines in Figures 7a and 8a, respectively. The amplitude and phase of the excitation

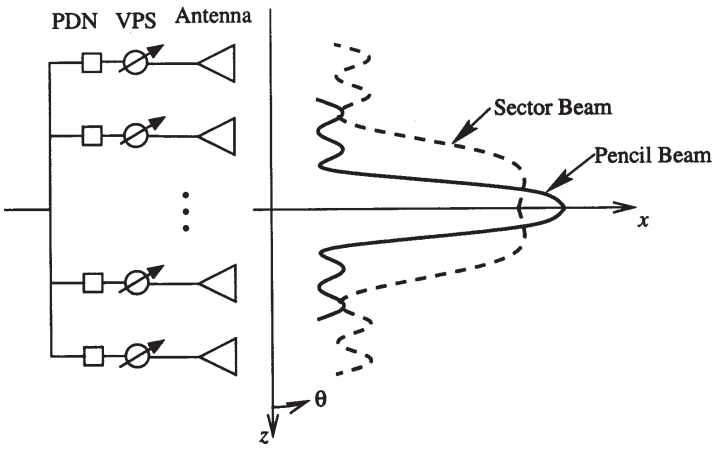

Figure 6. The geometry of the reconfigurable array problem. The goal is to design an array which can radiate two beams (as shown) using the same power dividing network (PDN). Only the variable phase shifters (VPS) need to be reconfigured in order to change the radiation pattern.

coefficients for each element were specified by the particle swarm, which consisted of 20 agents. It follows that this is a problem with the number of dimensions equal to twice the number of elements. Linear inertial weighting was applied with an upper limit of 0.9 and a lower limit of 0.4. The fitness of potential solutions was evaluated according to

$$F = \sum_{i=1}^{3}\left(P_{i,d}^{(p)} - P_i^{(p)}\right)^2 + \sum_{i=1}^{4}\left(P_{i,d}^{(s)} - P_i^{(s)}\right)^2 \qquad (5)$$

where the superscript p indicates a fitness factor for the pencil beam and the superscript s specifies a fitness factor for the sector beam. The subscript d indicates the desired value for the parameter specified by P, which may represent SLL, HPBW, HPBW at the first side-lobe level, or beam ripple. Essentially, the first summation is performed over the second column of Table I and the second summation is performed over the third column. Note that unlike the fitness value for the pencil beam pattern (which requires just three fitness factors), the sector pattern fitness must also take into account the pattern ripple.

Design Param	Pencil Pattern	Sector Pattern
SLL	-30 dB	-25 dB
HPBW	6.4°	24°
BW at SLL	20°	40°
Peak-to-Peak Ripple	N/A	0.5 dB

Table1: The design parameters for beam patterns

The optimized pencil-shaped power pattern is shown in Figure 7a. This beam fits within the required design mask and, therefore, meets the requirements for beamwidth and sidelobe level. The element excitations that generate this pattern are shown in Figure 7b. As expected for a problem with low sidelobes, the amplitude distribution shows a significant taper. Also, the phase of all element excitations is equal to zero. The optimized sector pattern is shown in Figure 8a. Again, the beam meets the design requirements for sidelobe level, beamwidth, and ripple. The width of the beam at –25 dB is slightly wider than specified, and this was reflected in the fitness value of the final design, i.e., the fitness was not equal to exactly zero. The excitation for this pattern, shown in Figure 8b, has the same amplitude distribution as for the pencil beam. This feature of the

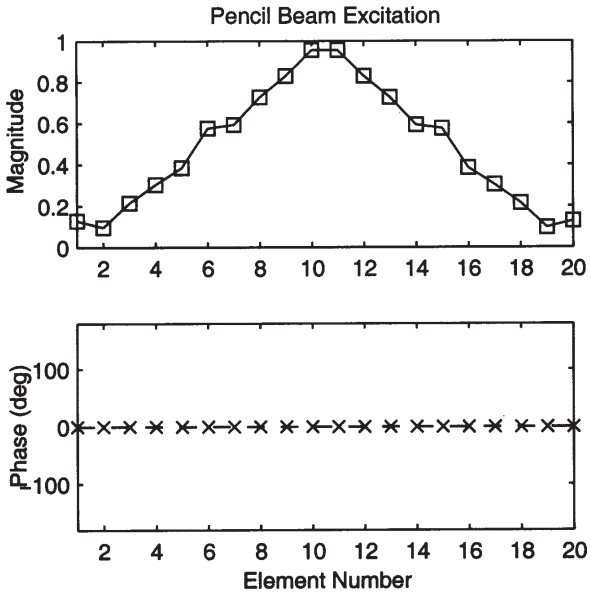

Figure 7b. Shown here are the excitation magnitude and phase required to achieve the pencil-shaped beam of Fig. 7a. Note that the phase of each element is equal to zero

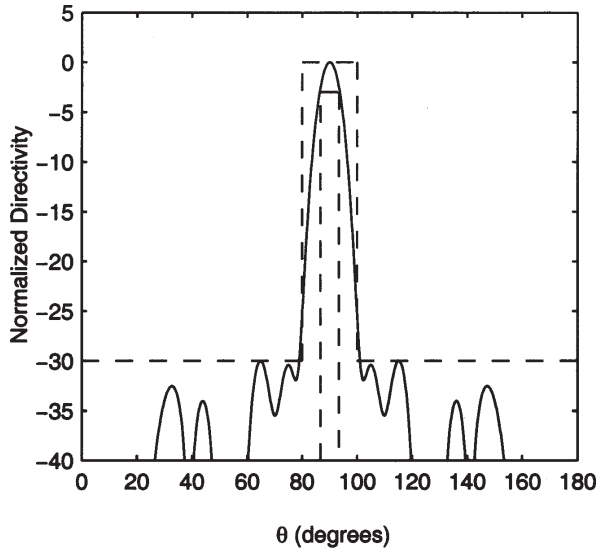

Figure 7a. The dashed lines show the desired mask for the pencil-shaped beam. The optimized radiation pattern (shown in solid line) meets all of the constraints

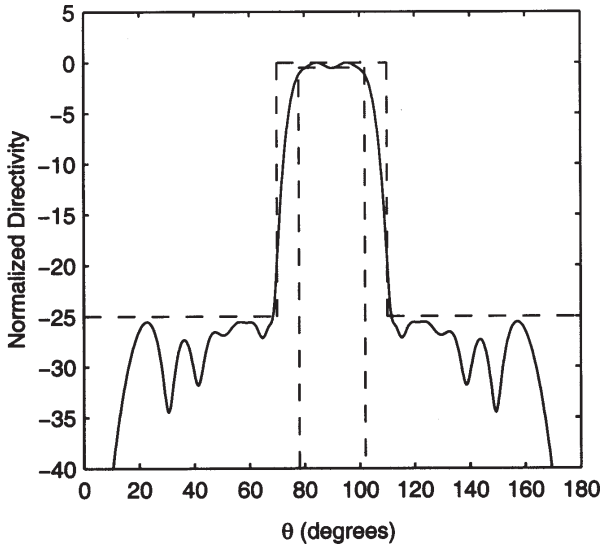

Figure 8a. The dashed lines show the desired shape of the sector beam. Again, the optimized radiation pattern is very good.

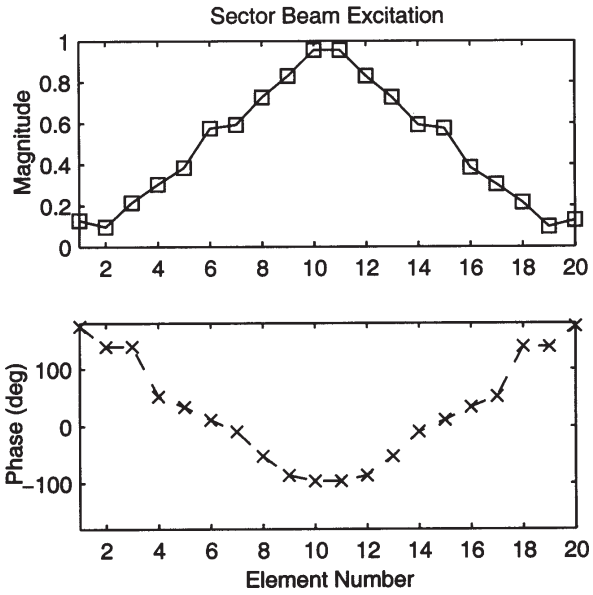

Figure 8b. The excitation required for the sector pattern can be achieved using the same power division network but with the addition of tunable phase shifters for each element

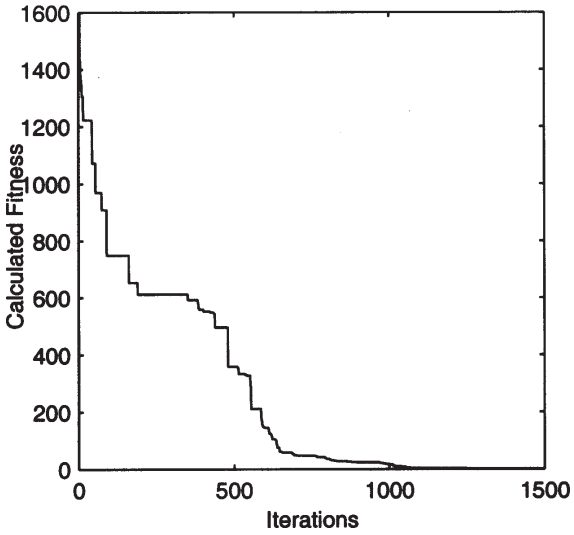

Figure 9. The convergence curve for dual beam array optimization using PSO. In this case the particle swarm was being used to minimize the fitness function.

solution would allow the array to be implemented with a single power division network, which improves the cost and efficiency of reconfigurable arrays. The phase of each element is therefore the only thing that needs to change in order to switch between the two radiation patterns, and this can be achieved by implementing phase-shifters inline with each antenna element. Finally, the convergence behavior of the optimization is shown in Figure 9. The swarm was used to minimize the fitness function in this case, in contrast to the corrugated horn example, demonstrating that PSO can easily find either global maxima or minima.

3.3 Luneburg Lens Design

A Luneburg lens is a dielectric sphere or half-sphere that is capable of focussing a plane wave incident on one side of the sphere to the point diametrically opposite to the incident field. This is accomplished because the lens's dielectric constant varies continuously according to [14]

$$\varepsilon_r(r) = 2 - \left(\frac{r}{a}\right)^2, (0 \le r \le a), \qquad (6)$$

where a is the radius of the lens and r is the distance from the center of the lens. Because it is generally very difficult to manufacture a lens with continuously varying dielectric constant, Luneburg lenses are most often approximated by a number of homogenous concentric spherical shells, each of which has a constant permittivity determined according to the Luneburg design equation. When each of the shells has equal thickness, this kind of lens approximation is said to be a uniform design. Figure 10 shows a schematic model of a uniform Luneburg lens with 5 layers. In practice, a Luneburg lens is usually fed by a horn antenna placed close to the outer surface of the lens. In our simulations, however, this feed structure was represented by a rectangular array of four infintesimal dipoles. The spacing of the array elements in the y- and z-directions was a half wavelength and a quarter wavelength, respectively. Due to the focussing effects of the lens, a radiation pattern is generated in the far-field along the z-axis. It is the properties of this pattern that we wish to optimize.

Global optimization techniques have in the past been used to optimize the design of Luneburg lenses with good results. In [15], a genetic algorithm was used to find optimized 5-shell lens designs that approached the performance of a lens with twice as many shells.

Following this work, in this example we consider the design of a 30λ diameter lens approximated by five concentric shells. The particle swarm is used to specify the thickness and dielectric constant of each layer, making this a 10-dimensional problem. As before, the fitness of a potential design is evaluated by the method of weighted aggregation, and therefore the fitness function must be carefully chosen such that it properly represents the design goals. For lenses consisting of a small number of shells, grating effects can significantly increase the side lobe levels of the lens pattern for certain angular regions. Therefore, the primary goal of the optimization is to improve the side lobe performance of the lens. Specifically, we seek a design such that the side-lobe envelope of an optimized 5-shell lens is the same as that of a uniform 10-shell lens, which is given by [15]

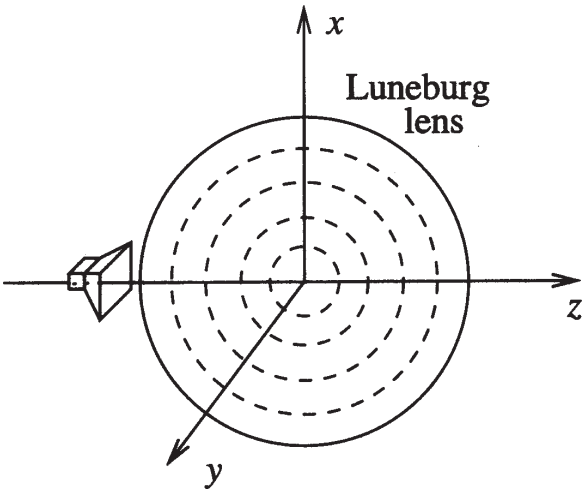

Figure 10. The geometry of the Luneburg lens. The lens itself is made up of a number of homogeneous shells, and is fed by a small horn antenna. For the purpose of simulations, the horn is modeled by an array of four infintesimal dipoles.

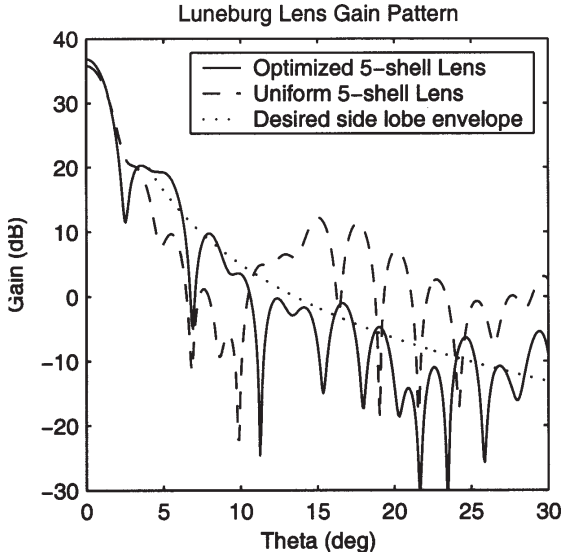

Figure 11. The optimized radiation pattern (shown in solid line) shows significant side-lobe performance improvement over the uniform 5-shell lens pattern (shown in dashed line). For reference, the desired side lobe envelope is shown in dotted line

$$f(\theta) = 12 - 38\log(\theta^\circ / 5.8^\circ) \quad (\mathrm{dB}) \cdot \tag{7}$$

At the same time, the boresight gain of the lens is maximized. A fitness function that represents a trade-off between these two objectives is

$$F = (40 - G)^2 + (E)^2 , \tag{8}$$

where G is the boresight gain of the antenna and E is a composite parameter that represents how well the side lobe envelope of the solution matches the desired envelope. Via trial and error, it was determined that good designs could be achieved if the parameter E is calculated to be the average of the difference between side-lobes that are above the desired envelope and the envelope itself:

$$E = \frac{1}{N}\sum_{i=1}^{N}\left[f(\theta_i) - G(\theta_i)\right], \tag{9}$$

Shell	ε_r	Thickness (λ)
1	1.152	2.725
2	1.609	3.003
3	1.722	1.585
4	1.826	1.438
5	1.932	6.253

Table 2: Optimized design criteria for a 5-shell Luneburg lens

where N is the number of side lobes that are above the desired envelope, θ_i represents the angular location of these side lobes, and $G(\theta)$ is the radiation pattern of the lens.

The results of the optimization are shown in Table 2, in which the PSO-specified values for the dielectric constant and thickness of each layer are given. The lens pattern that corresponds to these values is shown in Figure 11, along with the pattern of a uniform five-shell lens and the desired side lobe envelope. It can be seen that the impact of grating effects has been significantly reduced by the optimization while the peak gain magnitude is increased (in this case approximately 1 dB). The parameters of the optimized design are in line with expectations; the dielectric constant of the outer layer is very low while that of the inner-most layer is nearly equal to 2. Furthermore, the inner-most layer is very thick because focusing the energy along or near the diameter is not as difficult as it is toward the outside of the lens.

4. Conclusion

The enormous interest in evolutionary optimization techniques like genetic algorithms is evidence of the wide range of electromagnetics problems to which these algorithms can be applied. Particle swarm optimization is a new algorithm to the EM community, but it has already been applied to a number of interesting problems, three of which have been described in this paper. These three problems –design of a corrugated horn antenna, design of a reconfigurable array, and design of a Luneburg lens –have in common certain features that make them suitable for

particle swarm optimization. They are all, like most engineering problems, highly multi-objective. The goal of real-world design is rarely to maximize a single parameter. In particular, antenna designers must be concerned with gain, side-lobe level, efficiency, size, weight, and many other factors. It is shown that, in the three example design problems, all of these parameters showed improvement in designs obtained through particle swarm optimization.

The particle swarm technique is also simple and intuitive. It is therefore relatively easy to apply to a variety of problems without making significant changes to the implementation of the algorithm in a computer program. In fact, there were effectively no changes made to the core particle swarm code developed at UCLA for all three of the problems presented here. Only the implementation of the fitness evaluation routine must be modified. In light of these features of the algorithm, particle swarm optimization stands poised to make significant contributions to the field of electromagnetics.

Furthermore, like GA, the PSO algorithm can be efficiently adapted to parallel computing architectures. A preliminary parallel PSO implementation on a Beowulf Linux cluster has resulted in substantial reductions in optimization time for the dual-beam and Luneburg lens design problems. Current and future work will extend the multi-objective paradigms developed primarily for GA to PSO. These methods will allow designers to find the optimal trade-off surfaces for complex real-world design problems.

5. References

1. J. Robinson and Y. Rahmat-Samii, "Particle Swarm Optimization (PSO) in Electromagnetics," *IEEE Trans. Antennas Prop.* (in press).

2. D. Gies and Y. Rahmat-Samii, "Particle Swarm Optimization for Reconfigurable Phase-Differentiated Array Design," *Microwave and Optical Technology Letters* (in press).

3. J. Robinson, S. Sinton, and Y. Rahmat-Samii. "Particle Swarm, Genetic Algorithm, and their Hybrids: Optimization of a Profiled Corrugated Horn Antenna," *IEEE International Symposium on Antennas and Propagation*, San Antonio, Texas, June, 2002.

4. Y. Rahmat-Samii and E. Michielssen (eds.), *Electromagnetic Optimization by Genetic Algorithms.* New York, Wiley, 1999.

5. D. S. Weile and E. Michielssen, **"Genetic Algorithm Optimization Applied to Electromagnetics: A Review."** *IEEE Trans. Antennas Prop.*, **AP-45**, 3, pp. 343-353, 1997.

6. J. M. Johnson and Y. Rahmat-Samii, "**Genetic Algorithms in Engineering Electromagnetics,**" *IEEE Antennas and Propagation Magazine*, **39**, 4, pp. 7-21, 1997.

7. J. Kennedy and R. Eberhart. "Particle Swarm Optimization," *Proc. the 1995 IEEE Int. Conf. Neural Networks (Perth, Australia)*, 1995, Vol. IV, pp. 1942-1948.

8. F. Herrera and M. Lozano, "Gradual Distributed Real-Coded Genetic Algorithms," *IEEE Trans. Evolutionary Comput.*, **4**, 1, 2000, pp. 43-62.

9. Y. Shi and R. C. Eberhart. "Empirical Study of Particle Swarm Optimization," *Proc. 1999 Congress on Evolutionary Computation*, July 6-9 1999, pp. 1945-1950.

10. M. Clerc and J. Kennedy, "The Particle Swarm –Explosion, Stability, and Convergence in a Multidimensional Complex Space," *IEEE Trans. Evolutionary Comp.* , **39**, 7, 2002, pp. 58-73.

11. Y. Jin, M. Olhofer, and B. Sendhoff, "Dynamic Weighted Aggregation for Evolutionary Multi-Objective Optimization: Why Does It Work and How?," *Proceedings of the Genetic and Evolutionary Computation Conference (GECCO-2001)*, 2001, pp. 1042-1049.

12. E. Njoku, W. Wilson, S. Yueh, and Y. Rahmat-Samii, "A Large-Antenna Microwave Radiometer Concept for Ocean Salinity and Soil Moisture Sensing," *IEEE Transactions on Geoscience and Remote Sensing,* **GRS-38**, November 2000, pp. 2645-2655.

13. O. M. Bucci, G. Mazzarella, and G. Panariello, "Reconfigurable Arrays by Phase-only Control," *IEEE Trans. Antennas Propagat.*, **AP-39**, 7, 1991, pp. 919-925.

14. R. K. Luneburg, *The Mathematical Theory of Optics*, Providence, RI, Brown University Press, 1944.

15. H. Mosallaei and Y. Rahmat-Samii, "Nonuniform Luneburg and Two-shell Lens Antennas: Radiation Characteristics and Design Optimization." *IEEE Trans. Antennas Propagat.*, **AP-49**, 1, 2001, pp. 60-69.

Low-Frequency Illumination by an E Wave of Infinitely Long, Parallel, Perfect Conductors

Ronald De Smedt

Abstract

The low-frequency illumination by an E wave of one or more perfectly conducting cylinders of arbitrary shape is studied. The induced current, the radiation pattern and the scattering cross section exhibit a frequency dependent logarithmic and the complete, frequency independent part in their low frequency behavior. They can be derived from an equivalent radius, which depends on the shape of the conductor. The relative current on each conductor of a bundle is studied in detail. Asymptotic expressions are derived when the conductors of a bundle are loosely coupled. Results are presented for a single conductor with various shapes, ellipse, rectangle, diamond, rounded rectangle and regular polygon, as well as for a number of symmetrical and asymmetrical bundles of circular conductors.

1. Introduction

Forty years have passed since the first extensive investigations of the problem of low frequency scattering by cylindrical bodies [1-9], but was already addressed earlier as well [10-12]. In the low frequency case the dimensions of the cross section of the conductor are assumed to be small with respect to the wavelength. The advantage is that only a static potential problem has to be solved instead of the full frequency dependent dynamic problem. Furthermore, explicit expressions of the frequency behavior are found.

In the present paper we restrict ourselves to perfect conductors. Indeed, the thickness of the cable screen or of the wire diameter, being of the order of a 1 mm, is much larger than the skin depth of copper, being about 70 μm at a low EMC frequency, such as 1 MHz. A detailed study of the penetration into and the scattering by a conducting cylinder, when the diameter is of the same order as the skin depth, can be found in [13-16].

A particular low frequency case is the illumination by an E wave of a cylinder, in which the electric field is polarized parallel to the cylinder [3,4,17] or the equivalent problem of a TE wave, which penetrates through a slot [7,8,11]. A typical example is the normal incidence illumination of a bundle of (unshielded) wires [18]. Instead of solving the complete three-dimensional problem [2,5,9], the problem can be reduced and simplified to two dimensions, when we assume that the cables are infinitely long. This is acceptable, as in practice the cables are close together over a long distance, e.g., a few 100 m, while the diameters of the cables are only a few centimeters and the spacings are typically 0.01 m to 1 m. By this approximation the solution no longer exhibits resonances in the longitudinal direction, but the behavior in the transverse direction remains essentially unaltered [3,4]. In this low frequency case it is found that the dominant term exhibits a logarithmic frequency dependence.

In the present paper the low frequency approximation is refined. Besides the frequency dependent, logarithmic term the complete frequency independent part is included, which allows the low frequency expansion to be valid in a larger frequency range. In this frequency independent term appears the equivalent radius. It is defined in such a way that the total current, the radiation pattern and the radar cross section of the original conductor (or bundle) are identical to that of a circular cylinder with such a radius [8]. The equivalent radius depends on the dimensions and shape of the conductor (and the relative position of the wires in a bundle). It is deduced from the solution of an appropriate static potential problem. The relative current on each conductor of a bundle is studied in detail. Asymptotic expressions are derived when the conductors of a bundle are loosely coupled. Results are presented for a single conductor with various shapes, ellipse, rectangle, diamond, rounded rectangle and regular polygon, as well as for a number of symmetrical and asymmetrical bundles of circular conductors.

Ronald De Smedt is with Alcatel Bell, Francis Wellesplein 1, B-2018 Antwerpen (Belgium);
Tel: +32 3 240 4650; Fax: +32 3 240 9845
E-mail: ronald.de_smedt@alcatel.be

Dedicated to Professor J. Van Bladel on the occasion of his 80th birthday

2. Illumination of a Single Conductor

2.1 Theoretical Background

An infinitely long, perfect conductor is illuminated by an E wave ($\mathbf{E}^i$ parallel to the conductor, taken in the $\mathbf{u}_z$ direction). Figure 1a shows the cross section. C is the contour of the cross section of the conductor. The incident field induces on the conductor a longitudinal current $\mathbf{J}_s = J_{sz}\mathbf{u}_z$, which creates a scattered field [17]

$$E_r^{sc}(\rho) = \frac{j\omega\mu_0}{2\pi}\int_C J_{sz}(\rho')\, j\frac{\pi}{2} H_0^{(2)}\left(k|\rho-\rho'|\right) dc', \quad (1)$$

where $H_0^{(2)}(k|\rho-\rho'|)$ is the Hankel function. An $e^{+j\omega t}$ time dependence is assumed. Throughout the present document ρ is used instead of $\mathbf{r}$ to stress that the coordinates are located in a 2D plane (x,y) and that no variation in the third dimension (z) exists.

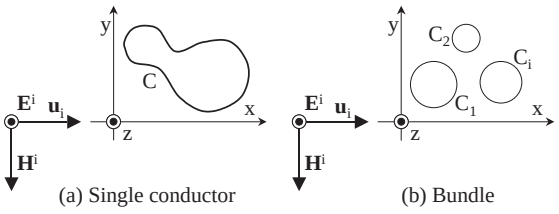

Figure 1. Cross section of a conductor or bundle illuminated by an E-wave.

From the requirement that the total tangential electric field vanish on the surface of the conductor it follows that J_{sz} satisfies the integral equation [17]

$$\frac{1}{2\pi}\int_C J_{sz}(\rho')\, j\frac{\pi}{2} H_0^{(2)}\left(k|\rho-\rho'|\right) dc' = \frac{-E_z^i(\rho)}{j\omega\mu_o}\ ,$$

$$\rho \text{ on C.} \quad (2)$$

When the dimensions of the cross section are small with respect to the wavelength we can replace the kernel of Equation (2) by its low frequency approximation [3,4,7,811,12,17], which yields

$$\frac{1}{2\pi}\int_C J_{sz}(\rho')\left(\ln\frac{\gamma' k|\rho-\rho'|}{2} + j\frac{\pi}{2}\right) dc' = \frac{-E_z^i}{j\omega\mu_0},$$

$$\rho \text{ on C,} \quad (3)$$

where $\gamma' = e^{\gamma} = 1.78107241...$, and $\gamma = 0.57721566...$ (γ is Euler's constant). At low frequencies the incident field is assumed to be constant in the neighborhood of the conductor.

Instead of solving (3) directly, we first look for the solution of the following normalized static potential equation:

$$\frac{1}{2\pi}\int_C \rho_0(\rho')\ln\frac{L}{|\rho-\rho'|}\frac{dc'}{L} = \phi_0\,,\ \rho \text{ on C,} \quad (4)$$

with the additional condition

$$\int_C \rho_0(\rho)\frac{dc}{L} = 1\cdot \quad (5)$$

Whereas in [2-4,17] L is defined as the length of the contour, here, we take L to be an arbitrary reference length, to which all dimensions are normalized. ϕ_0 is an unknown constant potential, to which the conductor is raised. We can always put it in the following form,

$$\phi_0 = \frac{1}{2\pi}\ln\frac{L}{R}\,, \quad (6)$$

where R is the radius of an equivalent circular conductor with unit total charge raised at a potential ϕ_0. Together with the charge density $\rho_0(\rho)$, ϕ_0 and R R are found from the solution of (4) and (5).

Once the charge density $\rho_0(\rho)$ is known, the current density $J_{sz}(\rho)$ can be expressed as a multiple of $\rho_0(\rho)$. From (3), the low frequency behavior is seen to be [8]

$$J_{sz}(\rho) = \frac{-E_z^i}{j\omega\mu_0 L}\frac{2\pi}{\ln\dfrac{\gamma' kR}{2} + j\dfrac{\pi}{2}}\rho_0(\rho)\cdot \quad (7)$$

From (7) we easily derive an expression of the total current on the conductor [8]

$$I = \int_C J_{sz}(\rho)\,dc = \frac{-E_z^i}{j\omega\mu_0}\frac{2\pi}{\ln\dfrac{\gamma' kR}{2} + j\dfrac{\pi}{2}}\cdot \quad (8)$$

Apart from the general capacitive behavior $1/j\omega$ a logarithmic dependence of the frequency is found. In contrast to [3,4,17] all the frequency independent terms are included in the denominator as well. Not the length of the contour, but the equivalent radius R, as defined in (6), appears in the logarithm.

The scattered field in the far field zone can generally be expressed as [2,5,17]

$$E_z^{sc,far} = \frac{e^{-jk\rho}}{\sqrt{\rho}}F(\varphi)\,, \quad (9)$$

where the radiation pattern $F(\varphi)$ is

$$F(\varphi) = j^{3/2}\sqrt{\frac{\pi}{2k}}\frac{j\omega\mu_0}{2\pi}\int_C J_{sz}(\rho')\,e^{+jk\mathbf{u}\cdot\rho'}dc' \cdot \quad (10)$$

Substituting the current density (7) and using the low frequency assumption, one finds the radiation pattern

$$F(\varphi) = -\,j^{3/2}\sqrt{\frac{\pi}{2k}}\frac{E_z^i}{\ln\dfrac{\gamma' kR}{2} + j\dfrac{\pi}{2}} \cdot \quad (11)$$

At low frequencies the radiation pattern is omni-directional and proportional to the inverse of the square root of the frequency. The denominator contains a frequency dependent, logarithmic term $\ln(k)$ and a frequency independent part $\ln(\gamma' R/2) + j\pi/2$. Higher order terms in frequency are neglected in this low frequency approximation. At very low frequencies the logarithmic frequency dependence is dominant. Although the radiation pattern is omni-directional the magnitude depends on the shape of the conductor through the presence of the equivalent radius in the frequency independent part of the denominator.

The radar cross section σ_{sc} is the ratio of the scattered power to the incident power density. It is given by [2-5,8,17,19]

$$\sigma_{sc} = \frac{1}{\left|E_z^i\right|^2}\int_0^{2\pi}\left|F(\varphi)\right|^2 d\varphi \cdot \quad (12)$$

Using (11) allows one to find the low frequency expression for σ_{sc},

$$\sigma_{sc} = \frac{\pi^2}{k}\frac{1}{\left(\ln\dfrac{\gamma' kR}{2}\right)^2 + \dfrac{\pi^2}{4}} \cdot \quad (13)$$

The scattering cross section contains a factor inversely proportional to the wavenumber k and, thus, to frequency. There is, in addition, a logarithmic dependence on the frequency in the denominator. This logarithmic term is dominant at very low frequencies. All frequency independent terms are included as well. The dependence on the shape of the conductor is embedded in the equivalent radius.

2.2 Check: Single, Circular Conductor

We apply the above theory to the particular case of a circular conductor with radius a. Due to the rotational symmetry and the condition (5) it follows that the charge density $\rho_0(\rho)$ is constant:

$$\rho_0(\rho) = \frac{L}{2\pi a} \cdot \quad (14)$$

Substitution of (14) into the integral (4) yields the potential ϕ_0

$$\phi_0 = \frac{1}{2\pi}\ln\frac{L}{a} \cdot \quad (15)$$

Comparison of this with (6) immediately shows that the equivalent radius "R", as defined by (6), is equal to the radius "a" of the circular conductor.

The low frequency behavior of the current density, the total current and the scattering cross section are found by replacing "R" by "a" in the respective equations (7), (8) and (13). These results are confirmed if we first solve the full frequency dependent problem and then introduce the low frequency expansion [4,17,19].

2.3 Other Examples of a Single Conductor

In the previous paragraphs it is shown that the key parameter in the low frequency illumination problem is the equivalent radius R, by which the total current, the radiation pattern and the scattering cross section can be constructed. In the present paragraph we compute the equivalent radius for a number of different shapes, shown in Figure 2.

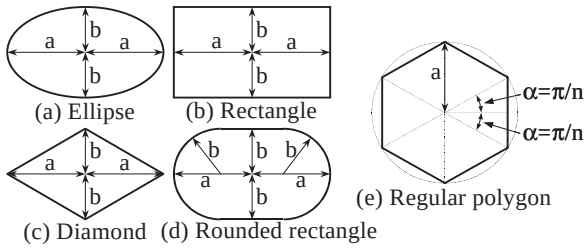

Figure 2: Cross-sections of a single conductor

The first shape is the *ellipse* with half principal axes a and b (Figure 2a). In this case the potential problem (4,5) can be solved analytically. From (6) we find the equivalent radius R

$$R = \frac{a+b}{2}, \quad (16)$$

which is simply equal to half of the sum of the half principal axes. The values of R, normalized to half the largest principal axis "a" as a function of the width to length ratio, are shown in Figure 3. Due to the simple relationship (16) this is a linear function. Two particular cases are the circle ($a = b$), for which the equivalent radius is the radius of the conductor itself (c.f. paragraph 2.2), and the strip ($b = 0$), for which the equivalent radius is one quarter of its total length [4,8,19].

A second shape, which has received great attention in [2,3], is the *rectangle* with length $2a$ and width $2b$ (Figure 2b).

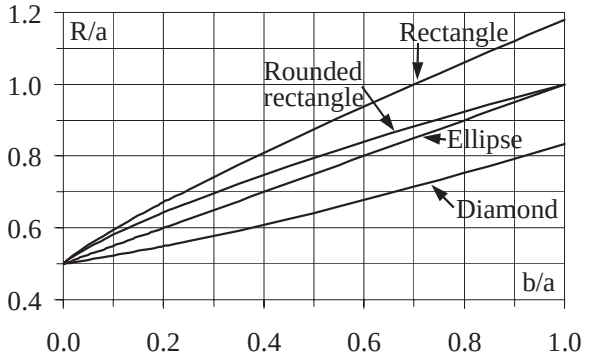

Figure 3. The equivalent radius R/a, normalized to the half-length, as a function of the aspect ratio b/a.

In this case the potential problem (4,5) must be solved numerically, e.g., by the Method of Moments (which has been used here to obtain all results). The numerical values of R, normalized to half of the total length "$2a$," are shown in Figure 3. The numerical results for the rectangle are well represented by the approximation,

$$R = \frac{a+b}{2}\,\frac{a^2 + 6.111ab + b^2}{a^2 + 4.881ab + b^2}, \qquad (17)$$

which is constructed by fitting numerical values. The relative deviation of these values is less than 0.5% for all values of a and b. Note the symmetry in a and b, which allows both $a > b$ and $a < b$.

A third shape, which is handled in a very similar way, is the *diamond* with total length $2a$ and total width $2b$ (Figure 2c). The numerical results of the equivalent radius R, normalized to half of the total length "$2a$," are shown in Figure 3. Again, we can cast the numerical results into an approximate expression,

$$R = \frac{a+b}{2}\,\frac{a^2 + 0.7893ab + b^2}{a^2 + 1.341ab + b^2}, \qquad (18)$$

which deviates less than 0.03% from the numerical values. Also in (18) a and b a and b can be freely interchanged. The *square* is the limiting case of both a rectangle and a diamond ($a = b$). From (17,18) we respectively find $R = 1.18a$ and $R = .0835a$. The ratio between these values is $\sqrt{2}$, which originates from the different definitions of the length "a" (see Figure 2b and c).

A fourth shape is the *rounded rectangle*, where the long sides (half-lengths "a") are terminated with semi-circles with radius b (equal to the half-length of the short sides). The numerical results for the equivalent radius R, normalized to half of the total length "$2a$", are shown in Figure 3. To approximate the numerical values, a slightly more complicated expression than (17,18) is needed,

$$R = \frac{a+b}{2}$$

$$\times\frac{a^4 + 14.399ab(a^2+b^2) - 28.23a^2b^2 + b^4}{a^4 + 12.952ab(a^2+b^2) - 25.34a^2b^2 + b^4}. \qquad (19)$$

The relative deviation of R is less than 0.75% from the numerical values. It is evident in (19) that the long and short sides, a and b, can be switched arbitrarily.

A fifth interesting shape is the *regular polygon* with n sides, enclosed in a circle with radius "a." A half-opening angle α is defined as (Figure 2e)

$$\alpha = \frac{\pi}{n}. \qquad (20)$$

Here, again, numerical methods are needed. Results are displayed in Figure 4 as a function of the number of sides. They are normalized to the radius of the enclosing circle. Some interesting values are: $n = 2$ corresponds to a strip ($R = 0.5a$); $n = 4$ corresponds to a square ($R = 0.835a$); $n = \infty$ corresponds to a circle ($R = a$).

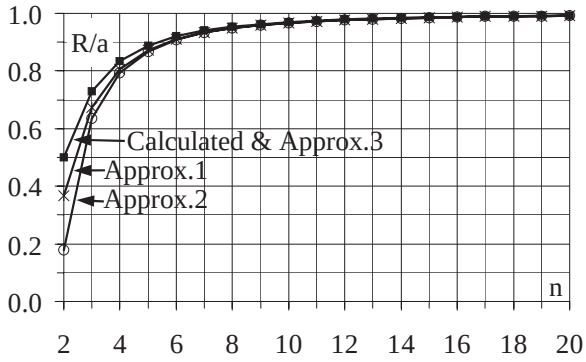

Figure 4. The equivalent radius R/a, normalized to the radius of the enclosing circle of the regular polygon, as a function of the number of sides, n.

Assuming a constant charge density $\rho_0(\mathbf{r})$ one finds the following approximations of the equivalent radius:

$$R \approx a\exp\left[-1 + \frac{\alpha}{\tan\alpha}\right] \text{ (Approx. 1)},$$

$$\approx a\left(1 - \frac{1}{3}\alpha^2\right) \text{ (Approx. 2)}. \qquad (21)$$

Results from these approximations are shown in Figure 4 as well. They exhibit an excellent match with the numerically obtained values for $n > 6$ (with relative deviations of 1%

and 1.3% respectively). An even better correspondence is found by adding more terms to (21):

$$R \approx a\frac{1+6.7188\alpha^2-0.7722\alpha^4}{1+7.0521\alpha^2+1.2103\alpha^4} \text{ (Approx. 3)}, \quad (22)$$

which deviates less than 0.05 % from the numerical values for all values of n. Instead of using the radius of the circumscribed circle as reference, we can correlate R with the radius of the circle with the same area as the polygon. One finds that R deviates less than 1% from this reference for $n > 6$. However, for smaller values of n the correlation is worse. For $n = 2$ (strip) it even completely fails as the area is zero in this particular case.

3. Current Distribution in a Bundle of Conductors

3.1 Theoretical Background

Consider the situation of a number of parallel conductors illuminated by an electromagnetic field, with the electric field $\mathbf{E}^i$ parallel to the conductors (Figure 1b) taken to be the $\mathbf{u}_z$ direction. When the cross section of the whole bundle of conductors is small with respect to wavelength, we can repeat the theory of the previous Section 2. We only need to replace the contour C by the ensemble of contours

$$C = \bigcup_i C_i \cdot \quad (23)$$

As a result we obtain the charge density $\rho_0(\rho)$ on all the contours C_i, the common constant potential ϕ_0 to which every contour is raised, and the equivalent radius R of the whole bundle. From these results the total relative current on a single conductor (with contour C_i) is determined to be

$$F_i = \int_{C_i} \rho_0(\rho)\frac{dc}{L} \cdot \quad (24)$$

From (5) it immediately follows that

$$\sum_i F_i = 1, \quad (25)$$

proving that indeed the sum of all relative currents is unity.

3.2 Simplified Solution

In general the normalized static potential problem must be solved numerically, e.g., by the Method of Moments. When the conductors have circular cross sections, which are small relative to the distances between the conductors, we can solve the integral equation (4), subject to (5), in an approximate, simplified way (the theory remains valid for non-circular conductors if they are replaced by the corresponding circular conductors, as defined in Section 2). The potential, created by a charge density on a circular conductor, can be expanded into a series of harmonic functions. As a simplification we only retain the first term, which is a logarithmic function. The total potential $\phi(\rho)$ at any point ρ then becomes

$$\phi(\rho) = \frac{L}{2\pi}\sum_i F_i \ln\frac{L}{\rho_i}, \quad (26)$$

where ρ_i is the distance between the point ρ and the center of the i th conductor. From (26) the charge distribution $\rho_0(\rho)$ can be derived. In line with the above simplification we only take the constant term into account. For each conductor,

$$\rho_0\left(\text{on } C_i\right) = \frac{L}{2\pi}\frac{F_i}{a_i}, \quad (27)$$

where a_i is the radius of the i th conductor. From (27) it follows that the constants F_i are the relative current densities, as defined in (24). The integral equation (4) with the additional condition (5) is now turned into a matrix equation by forcing (26) to be equal to ϕ_0 on each conductor:

$$\sum_{\substack{j \\ j\neq i}} F_j \frac{1}{2\pi}\ln\frac{L}{\rho_{ij}} + F_i\frac{1}{2\pi}\ln\frac{L}{a_i} - \phi_0 = 0, \quad \forall i \quad (28)$$

$$\sum_i F_i = 1$$

where ρ_{ij} is the distance between the respective centers of the i th and the j th conductors. The solution of (28) yields the relative current distributions F_i and the potential ϕ_0, from which the equivalent radius R is derived through (6).

When the distance between the conductors is very large compared to the radii, the solution can be further simplified. In this case the coupling between the conductors becomes negligible and the currents on the conductors are the same. With n conductors present, the relative current F_i simply becomes

$$F_{i\infty} = \frac{1}{n} \cdot \quad (29)$$

Introducing this asymptotic behavior of F_i into (28) and adding all equations together allow one to find an asymptotic expression for ϕ_0, from which the asymptotic behavior of the equivalent radius is derived:

$$R_\infty = \left[\prod_i a_i \left(\prod_{\substack{j \\ j\neq i}} r_{ij}\right)\right]^{1/n^2} \cdot \quad (30)$$

We use this simplified procedure to find approximate solutions for a number of practical cases, which are discussed in the next paragraphs with examples of symmetrical and asymmetrical configurations.

3.3 Examples: Symmetrical Configurations

We consider a number of symmetrical configurations with two to five conductors, as shown in Figure 5 (cases a to i). The conductors are arranged along one line, as a star or positioned on a regular polygon. We take the radii of all conductors equal to a common value a. We introduce a distance D between the centers of the conductors in such a way that $D = 2a$ represents the most dense spacing. We look for the behavior of the relative currents F_i and the equivalent radius R, when this distance D varies between $2a$ and ¥.

When the conductors are arranged on a regular polygon, they are all geometrically equivalent and the relative currents F_i are exactly

$$F_i = \frac{1}{n}, \quad i = 1...n, \tag{31}$$

regardless of the distance D. This is true for cases a, c, e, h of Figure 5. In all other cases the relative currents F_i vary as a function of D, as shown in Figure 6a-e. For large D, they tend to the asymptotic value (29). From Figure 6 it follows that the center conductors are somewhat shielded by the conductors on the outside. This shielding is more pronounced when the center conductor(s) are densely surrounded by others, e.g., compare the case of aligned conductors with the star shaped configurations.

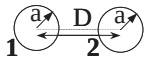

Case a: 2 wires - parallel

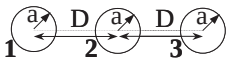

Case b: 3 wires - parallel

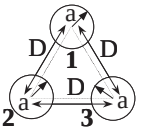

Case c: 3 wires - triangle

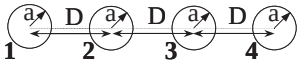

Case d: 4 wires - parallel

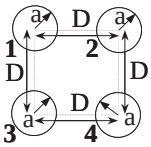

Case e: 4 wires - square

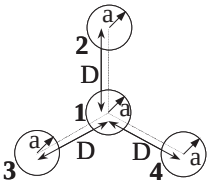

Case f: 4 wires - star

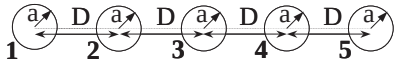

Case g: 5 wires - parallel

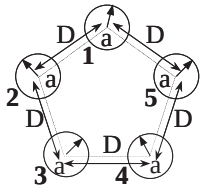

Case h: 5 wires - quintic

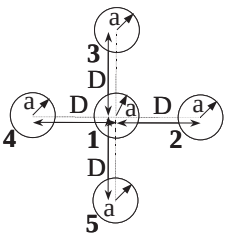

Case i: 5 wires - star

Figure 5: Symmetrical configurations

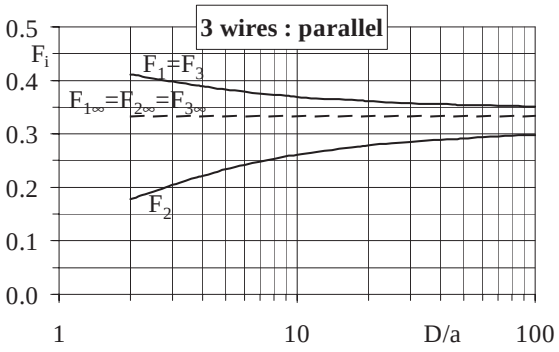

1. Case b: 3 wires - parallel

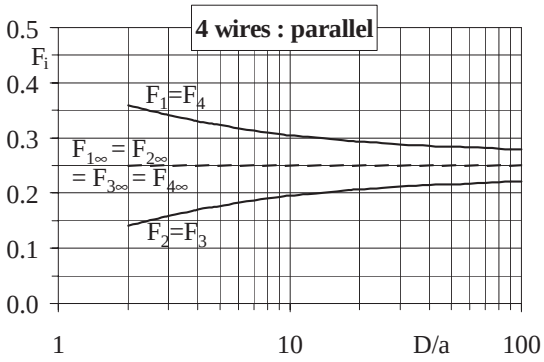

2. Case d: 4 wires - parallel

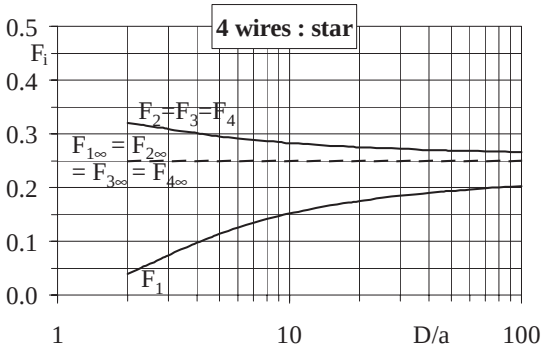

3. Case f: 4 wires - star

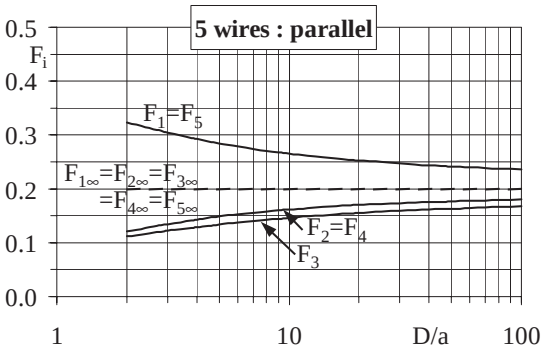

4. Case g: 5 wires - parallel

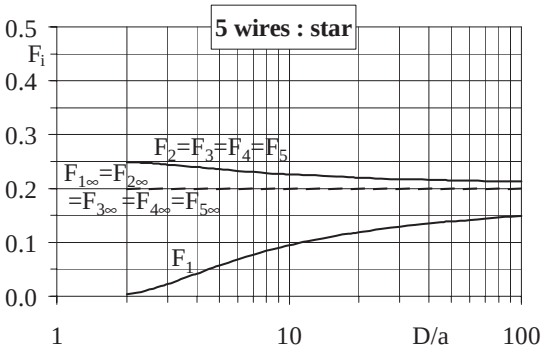

5. Case i: 5 wires - star

Figure 6. The relative current F_i on each conductor as a function of D/a, the ratio of the spacing to conductor radius, for the cases b, d, f, g, i of Figure 5.

Applying the simplified approach of (30), one finds it possible to derive asymptotic expressions for the equivalent radius R_∞ for each of the cases of Figure 5:

(a): $R_\infty = (aD)^{1/2}$

(b): $R_\infty = 2^{2/9}(aD^2)^{1/3} = 1.17(aD^2)^{1/3}$

(c): $R_\infty = (aD^2)^{1/3}$

(d): $R_\infty = 2^{1/4}3^{1/8}(aD^3)^{1/4} = 1.36(aD^3)^{1/4}$

(e): $R_\infty = 2^{1/8}(aD^3)^{1/4} = 1.09(aD^3)^{1/4}$ (32)

(f): $R_\infty = 3^{3/16}(aD^3)^{1/4} = 1.23(aD^3)^{1/4}$

(g): $R_\infty = 2^{2/5}3^{4/25}(aD^4)^{1/5} = 1.57(aD^4)^{1/5}$

(h): $R_\infty = 1.21(aD^4)^{1/5}$

(i): $R_\infty = 2^{8/25}(aD^4)^{1/5} = 1.25(aD^4)^{1/5}$

As a general rule it follows that the equivalent radius, for large values of the distance D, is proportional to $(\text{conductor radius } a)^{1/n}$ and $(\text{distance } D)^{(n-1)/n}$, with n conductors present. In Figure 7 we present the variation of the equivalent radius normalized to the respective asymptotic value (32) as a function of the distance. The numerically obtained values confirm that the asymptotic behavior (32) is a good approximation when the conductors are not too close with respect to the conductor radius.

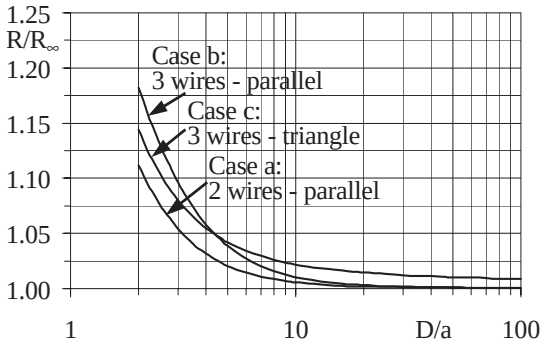

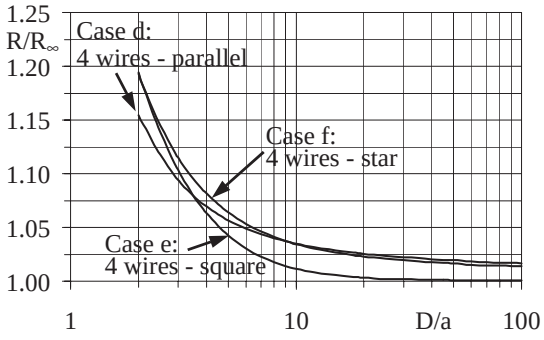

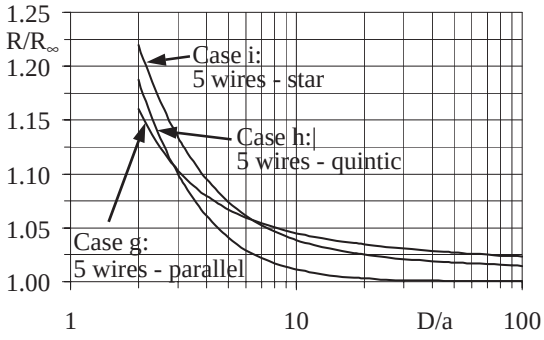

Figure 7. R/R_∞, the ratio of the equivalent radius to its asymptotic value as a function of D/a, the ratio of the spacing to conductor radius, for the cases a-i of Figure 5

3.4 Examples: Asymmetrical Configurations

As an example of an asymmetrical configuration we take n conductors in one line. The first conductor is at a distance D from the other $n-1$ conductors, which remain at their closest distance. Figure 8 shows three examples with $n = 3, 4,$ and 5 conductors.

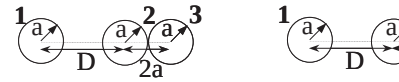

Case j: 3 wires (2 + 1)

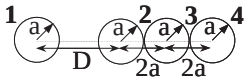

Case k: 4 wires (3 + 1)

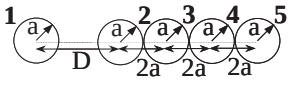

Case ℓ: 5 wires (4 + 1)

Figure 8: Asymmetrical configurations

Figure 9a-9c shows the behavior of the relative currents F_i as a function of the distance D. The current on the first separated conductor tends to an asymptotic value of 1/2. That is, when the conductors become uncoupled this single conductor takes half of the total induced current. The other conductors, bundled together, take the other half. The conductors along a line spaced close together, as presented in the previous paragraph on symmetrical configurations. The convergence towards these limiting values can however be very slow, due to the $1/\ln(D/a)$ dependence of the correction term (this $\ln(D)$ behavior originates from the 2D logarithmic behavior of the potential). This is confirmed by detailed computations with separations as large as $D/a = 10^6$, which still fail to exhibit a very close match between the actual and limiting values.

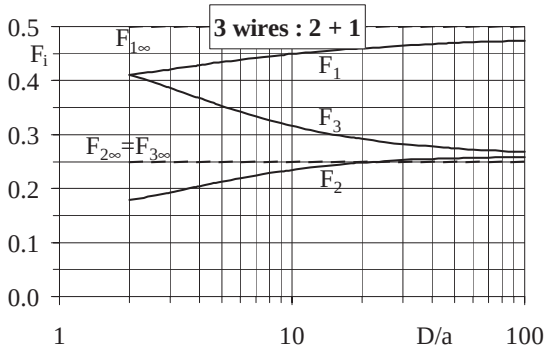

(a) Case j: 3 wires (2 + 1)

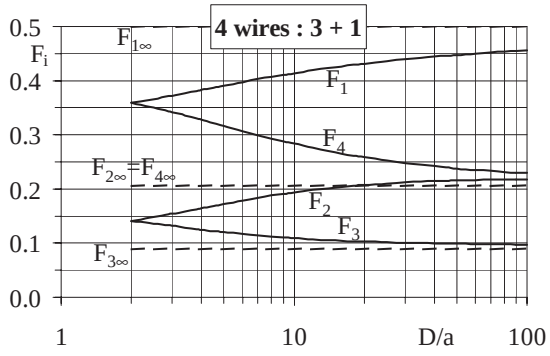

(b) Case k: 4 wires (3 + 1)

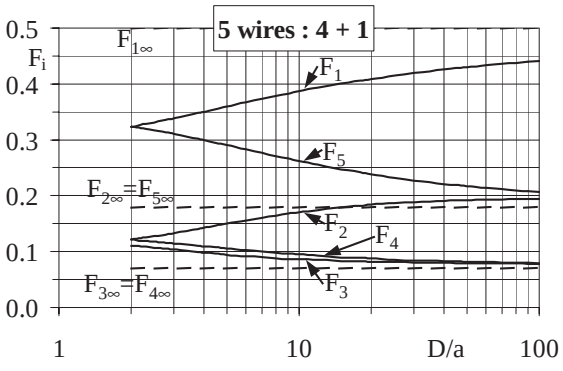

(c) Case l: 5 wires (4 + 1)

Figure 9. The relative current F_i on each conductor as a function of D/a, the ratio of the spacing to conductor radius, for the cases j-l of Figure 8.

To find the asymptotic behavior of the equivalent radius of the cases of Figure 8 we represent them by two conductors: first, conductor #1, with radius a; second, the other conductors, represented by an equivalent radius as found in the previous paragraph, i.e., $1.57a$, $2.12a$, $2.65a$ for cases j, k, l of Figure 8, respectively. This allows one to find the following asymptotic expressions of the equivalent radii of the complete configurations:

$$\begin{aligned} &\text{(j):}\ R_\infty = 1.12[a(D+a)]^{1/2}, \\ &\text{(k):}\ R_\infty = 1.21[a(D+2a)]^{1/2}, \\ &\text{(l):}\ R_\infty = 1.28[a(D+3a)]^{1/2}. \end{aligned} \qquad (33)$$

In Figure 10 we show the equivalent radii normalized to the respective expressions of (33) as a function of the distance. It is seen that for large values of D/a (33) are good approximations.

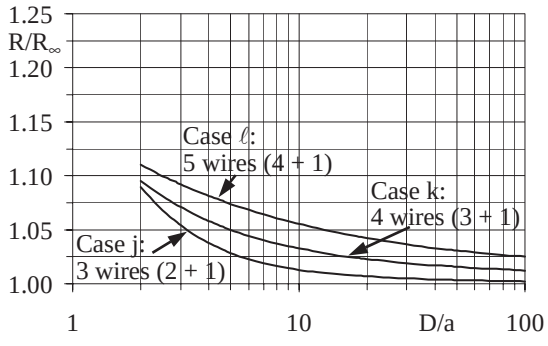

Figure 10. R/R_∞, the ratio of the equivalent radius to its asymptotic value as a function of D/a, the ratio of the spacing to conductor radius, for the cases j-l of Figure 8.

4. Conclusions

The Figure 10. R/R_∞ , the ratio of the equivalent radius to its asymptotic value as a function of D/a , the ratio of the spacing to conductor radius, for the cases j-l of Figure 8.low frequency illumination of a cylindrical conductor or bundle of conductors by an E wave is revisited. Apart from the dominant logarithmic frequency dependent term, the complete, frequency independent part is included in the low frequency behavior. An equivalent radius is defined as the radius of a circular cylinder on which the same total current is induced as would exist on the original conductor.

The low frequency behavior of the total current, the radiation pattern and the scattering cross section are determined. The denominator contains a frequency dependent logarithmic term (which is dominant at very low frequencies) and a frequency independent part. The shape-dependence shows up through the appearance of the equivalent radius. The radiation pattern is omni-directional. In the case of a bundle of wires the relative current on each wire is studied in detail. Asymptotic expressions are derived when the conductors of a bundle are loosely coupled.

A first series of configurations to which the theory is applied, concerns a single conductor with various shapes: ellipse, rectangle, diamond, rounded rectangle and regular polygon. The strip with zero thickness is a special, limiting case of these examples. Explicit expressions for the equivalent radius are derived either analytically (ellipse) or from numerical results (all other shapes). In the latter case, we use the boundary element method to solve the potential problem. The approximate expressions deviate less than 1% from the numerical values, from which they are derived. A second series of configurations deals with a number of symmetrical and asymmetrical bundles of circular conductors. In this case our main attention is focused on the relative current on the various conductors and the equivalent radius of the whole bundle. It has been found that the inner conductors in a bundle are somewhat shielded by the outer conductors. This effect is more pronounced when several conductors are present. When one or all conductors are separated by large distances the behavior agrees well with the results of the simplified analysis. In this case each conductor (or group of close or touching conductors) tends to carry equal amounts of the total current.

5. References

1. J. Van Bladel, "Good Conductors in Low-Frequency Fields," *IRE Trans. Antennas Propagat.*, **AP-10**, 1962, pp. 625-633.

2. K. Mei and J. Van Bladel, "Low-Frequency Scattering by Rectangular Cylinders," *IEEE Trans. Antennas Propagat.*, **AP-11**, 1963, pp. 52-56.

3. K. Mei and J. Van Bladel, "Scattering by Perfectly Conducting Rectangular Cylinders," *IEEE Trans. Antennas Propagat.*, **AP-11**, 1963, pp. 185-192.

4. J. Van Bladel, "Low-Frequency Scattering by Cylindrical Bodies," *Appl. Sci. Res.*, **10B**, 1963, pp. 195-202.
5. M. G. Andreasen, "Scattering from Parallel Metallic Cylinders With Arbitrary Cross-sections," *IEEE Trans. Antennas Propagat.*, **AP-12**, 1964, pp. 746-754.

6. J. Van Bladel, "Circuit Parameters from Maxwell's Equations," *Appl. Sci. Res.*, **28**, 1973, pp. 381-397.

7. C. M. Butler, and D. R. Wilton, "General Analysis of Narrow Strips and Slots," *IEEE Trans. Antennas Propagat.*, **AP-28**, 1980, pp. 42-48.

8. C. M. Butler, "The Equivalent Radius of a Narrow Conducting Strip," *IEEE Trans. Antennas Propagat.*, **AP-30**, 1982, pp. 755-758.

9. D. Felbacq, G. Tayeb, and D. Maystre, "Scattering by a Random Set of Parallel Cylinders," *J. Opt. Soc. Am. A*, **11**, 1994, pp. 2526-2538.

10. Lord Rayleigh, "On the Passage of Waves Through Apertures in Plane Screens and Allied Problems," *Phil. Mag.*, **43 - series 5**, 1897, pp. 259-272.

11. P. M. Morse and P. J. Rubenstein, "The Diffraction of Waves by Ribbons and by Slits," *Phys. Rev.*, **54**, 1938, pp. 895-898.

12. C. J. Bouwkamp, "Diffraction Theory," *Rep. Progr. Phys.*, **17**, 1954, pp. 35-100.

13. J. Van Bladel, "Penetration of a Low-Frequency E-Wave into a Conducting Circular Cylinder," *IEEE Trans. Electromagn. Compat.*, **EMC-37**, 1995, pp. 536-542.

14. J. Van Bladel, "Penetration of a Low-Frequency H-Wave into a Conducting Circular Cylinder," *IEEE Trans. Electromagn. Compat.*, **EMC-38**, 1996, pp. 441-449.

15. J. Van Bladel, "Deep Field Penetration into a Conducting Cylinder," *IEEE Trans. Electromagn. Compat.*, **EMC-38**, 1996, pp. 549-556.

16. P.-R. Renaud and J.-J. Laurin, "Shielding and Scattering Analysis of Lossy Cylindrical Shells Using an Extended Multifilament Current Approach," *IEEE Trans. Electromagn. Compat.*, **EMC-41**, 1999, pp. 320-334.

17. J. Van Bladel, *Electromagnetic Fields*, New York, Hemisphere Publishing Corp., pp. 376-381, 1985, 393-394.

18. C. W. Harrison Jr., "Generalized Theory of Impedance Loaded Multiconductor Transmission Lines in an Incident Field," *IEEE Trans. Electromagn. Compat.*, **EMC-14**, 1972, pp. 56-63.

19. R. W. P. King and T. T. Wu, *The Scattering and Diffraction of Waves*, Cambridge, MA, Harvard University Press, 1959, pp. 44, 115-116.

Spectral Domain Calculation of the Excess Capacitance Matrix for a Stripline Crossing

Daniël De Zutter
Jegannathan Srinivasan

Abstract

In this paper, we present a method for calculating the excess capacitance matrix of a stripline crossing. We use a spectral domain formulation of the method of moments. By making use of the circular symmetry of the kernels and by introducing a sinc function expansion basis, it is shown that the calculation of the moment method matrix is considerably simplified. Numerical simulations demonstrate the accuracy of the proposed method.

1. Introduction

In high speed digital interconnects, packages and VLSI circuits, parasitic couplings such as that exist between neighbouring lines, via-holes, via-holes and lines etc. can have a significant impact on signal integrity [1]. A lot of effort has been spent in order to model these effects in an efficient way, as for example in [2] and [3]. Recently 3-D capacitance extraction techniques based on a multiresolution method of moments approach [4] and on a novel dimension-reduction technique to subdivide some typical 3-D structures into a set of 2-D problems [5] have been put forward. Their common aim is to reduce the computation time. In this paper we investigate one important structure namely the line crossing. It is our purpose to show that a suitably formulated method of moments in the spectral domain yields accurate and fast results. Our approach is inspired by similar approaches for the analysis of microstrip-like transmission lines published many years ago [6,7]. It will be shown that by taking advantage of the circular symmetry of the integral equation kernels and by introducing a sinc function expansion basis, the calculation of the moment method matrix can be considerably simplified and hence speeded up. Results are presented in terms of an excess capacitance matrix and can easily be included in a circuit simulator as the excess capacitance matrix can be cast into the form of a π-network consisting of one coupling capacitor between the crossing lines (themselves represented by their transmission line equivalent) and two capacitors, one for each line, in parallel over the line. Special attention is devoted to assessing the accuracy of the obtained results by comparison with reliable results for parallel lines. This is certainly necessary as the excess quantities are very small (typically of the order of femtofarad!). In this paper we have restricted ourselves to the stripline crossing, albeit embedded in a multilayered but planar stratified medium and infinitely thin perfect conductors to show the potential benefits of the proposed method.

2. Mathematical analysis

The strip to strip crossing is depicted in Fig. 1.

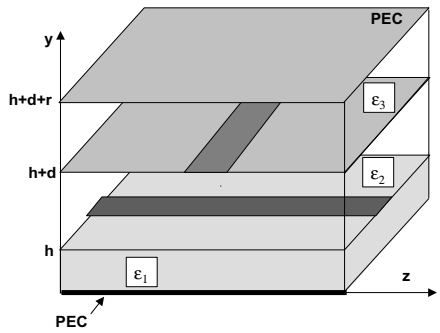

Figure 1: Crossing strips in a stripline configuration.

The static potential distribution $\phi(x, y, z)$ and the charge density distribution $\rho(x, y, z)$ in the structure

The first author is the head of the Electromagnetics Group of the Department of Information Technology (INTEC) of Ghent University;
the second author was a post-doc researcher at INTEC
Sint-Pietersnieuwstraat 41
9000 Ghent, Belgium
T: 32-9-2643327
F: 32-9-2643593
E: daniel.dezutter@ugent.be

Dedicated to Professor J. Van Bladel on the occasion of his 80th. birthday.

must obey the Poisson's equation:

$$\nabla^2\phi\left(x,y,z\right)=\frac{-\rho\left(x,y,z\right)}{\epsilon} \tag{1}$$

where ϵ is the permittivity. In the following analysis, we consider infinitely thin perfectly conducting (PEC) strips. We can express the charge density distribution as:

$$\rho=\delta\left(y-h\right)f_b\left(x,z\right)+\delta\left(y-h-d\right)f_t\left(x,z\right) \tag{2}$$

where δ is the Dirac delta function.

With the Fourier transform defined as:

$$\mathbf{\Phi}\left(y\right)=\int_{-\infty}^{\infty}\phi e^{-jk_xx}e^{-jk_zz}dxdz \tag{3}$$

(where, to simplify the notation, the single integral sign stands for both the integration over x and over z) the Poisson equation becomes:

$$\left(\frac{\partial^2}{\partial y^2}-k_x^2-k_z^2\right)\mathbf{\Phi}\left(y\right)=0 \tag{4}$$

$(y\neq h, y\neq h+d)$, which has the solution:

$$\mathbf{\Phi}\left(y\right)=C_1e^{\sqrt{k_x^2+k_z^2}y}+C_2e^{-\sqrt{k_x^2+k_z^2}y} \tag{5}$$

in the bounded region; the arbitrary constants C_1 and C_2 are decided by the appropriate boundary conditions.

The boundary conditions and the continuity conditions in the Fourier transform domain read

$$\mathbf{\Phi}\left(0\right)=0 \tag{6a}$$
$$\mathbf{\Phi}\left(h+0\right)=\mathbf{\Phi}\left(h-0\right) \tag{6b}$$
$$\epsilon_2\frac{\partial}{\partial y}\mathbf{\Phi}\left(h+0\right)=\epsilon_1\frac{\partial}{\partial y}\mathbf{\Phi}\left(h-0\right)-\mathbf{F_b} \tag{6c}$$
$$\mathbf{\Phi}\left(h+d+0\right)=\mathbf{\Phi}\left(h+d-0\right) \tag{6d}$$
$$\epsilon_3\frac{\partial}{\partial y}\mathbf{\Phi}\left(h+d+0\right)=\epsilon_2\frac{\partial}{\partial y}\mathbf{\Phi}\left(h+d-0\right)-\mathbf{F_t} \tag{6e}$$
$$\mathbf{\Phi}\left(h+d+r\right)=0 \tag{6f}$$

where the argument of $\mathbf{\Phi}$ is the value of the height y, where ϵ_1,ϵ_2,ϵ_3 are the dielectric constants shown in Fig. 1; $\mathbf{F_t}$ and $\mathbf{F_b}$ are the Fourier transforms of the charge density functions $f_t\left(x,z\right)$ and $f_b\left(x,z\right)$, respectively. Imposing these conditions on the solution of Eqn. (4) and eliminating the arbitrary constants, we find that:

$$\mathbf{\Phi_b}=\mathbf{A}\left(k_x,k_z\right)\sinh\left(k_rh\right) \tag{7}$$

$$\mathbf{\Phi_t}=\mathbf{A}\left(k_x,k_z\right)\left[\sinh\left(k_rh\right)\cosh\left(k_rd\right)+\frac{\epsilon_1}{\epsilon_2}\cosh\left(k_rh\right)\sinh\left(k_rd\right)\right]-\frac{\mathbf{F_b}}{\epsilon_2k_r}\sinh\left(k_rd\right) \tag{8}$$

where $\mathbf{\Phi_b}=\mathbf{\Phi}\left(h\right)$, $\mathbf{\Phi_t}=\mathbf{\Phi}\left(h+d\right)$, and $k_r=\sqrt{k_x^2+k_z^2}$. In the above equations $\mathbf{A}\left(k_x,k_z\right)$ is given by:

$$\mathbf{A}\left(k_x,k_z\right)=\mathbf{P_1F_b}+\mathbf{P_2F_t} \tag{9}$$

where

$$\mathbf{P_1}=\frac{\epsilon_3}{\epsilon_2}[\coth\left(k_rr\right)\sinh\left(k_rd\right)+\frac{\epsilon_2}{\epsilon_3}\cosh\left(k_rd\right)]\mathbf{P_2} \tag{10}$$

and

$$\mathbf{P_2}=\{k_r\epsilon_3[\sinh\left(k_rh\right)(\coth\left(k_rr\right)\cosh\left(k_rd\right)+\tfrac{\epsilon_2}{\epsilon_3}\sinh\left(k_rd\right))+\cosh\left(k_rh\right)(\tfrac{\epsilon_1}{\epsilon_2}\coth\left(k_rr\right)\sinh\left(k_rd\right)+\tfrac{\epsilon_1}{\epsilon_3}\cosh\left(k_rd\right))]\}^{-1} \tag{11}$$

Rearranging the above equations, we obtain:

$$\begin{pmatrix}\mathbf{R_{11}} & \mathbf{R_{12}}\\ \mathbf{R_{21}} & \mathbf{R_{22}}\end{pmatrix}\begin{pmatrix}\mathbf{F_t}\\ \mathbf{F_b}\end{pmatrix}=\begin{pmatrix}\mathbf{\Phi_t}\\ \mathbf{\Phi_b}\end{pmatrix} \tag{12}$$

where

$$\mathbf{R_{11}}=\mathbf{P_2}(\sinh\left(k_rh\right)\cosh\left(k_rd\right)+\frac{\epsilon_1}{\epsilon_2}\cosh\left(k_rh\right)\sinh\left(k_rd\right)) \tag{13}$$

$$\mathbf{R_{12}}=\mathbf{P_2}\sinh\left(k_rh\right) \tag{14}$$

$$\mathbf{R_{21}}=\mathbf{P_2}\sinh\left(k_rh\right) \tag{15}$$

$$\mathbf{R_{22}}=\mathbf{P_1}\sinh\left(k_rh\right) \tag{16}$$

We note that

$$\phi_t=\frac{1}{\left(2\pi\right)^2}\int_{-\infty}^{\infty}\mathbf{\Phi_t}e^{jk_xx}e^{jk_zz}dk_xdk_z \tag{17a}$$
$$\phi_b=\frac{1}{\left(2\pi\right)^2}\int_{-\infty}^{\infty}\mathbf{\Phi_b}e^{jk_xx}e^{jk_zz}dk_xdk_z \tag{17b}$$

The potential functions must satify:

$$\lim_{x,z\rightarrow topstrip}\phi_t\left(x,z\right)=c_t \tag{18a}$$
$$\lim_{x,z\rightarrow bottomstrip}\phi_b\left(x,z\right)=c_b \tag{18b}$$

In the above equations, c_t and c_b are the constant potentials at which the top and bottom strips are held. The task is to solve (12) subject to the conditions expressed by (18). A moment method formulation is employed towards this purpose. Let us first focus our attention on the top strip. Let it be divided into M equal square cells. Upon implementing (18a) on the i^{th} cell in an integral sense, we get:

$$\frac{1}{A_{cell}}\int_i\phi_t\left(x,z\right)dxdz=c_t \tag{19}$$

where A_{cell} is the area of a cell. From (17a) and (19) we have

$$\frac{1}{A_{cell}} \int_i [\frac{1}{(2\pi)^2} \int_{-\infty}^{\infty} \mathbf{\Phi_t} e^{jk_x x} e^{jk_z z} dk_x dk_z] dx dz = c_t \quad (20)$$

Interchanging the order of the integrations, we get

$$\frac{1}{A_{cell}} \int_{-\infty}^{\infty} \mathbf{\Phi_t} [\frac{1}{(2\pi^2} \int_i e^{jk_x x} e^{jk_z z} dx dz] dk_x dk_z = c_t \quad (21)$$

After some calculations, the final result obtained for c_t is:

$$\frac{1}{(2\pi)^2} \int_{-\infty}^{\infty} \mathbf{\Phi_t} e^{jk_x x_{ci}} e^{jk_z z_{ci}} \operatorname{sinc}\left(\frac{k_x \Delta x}{2}\right) \operatorname{sinc}\left(\frac{k_z \Delta z}{2}\right) dk_x dk_z = c_t \quad (22)$$

where x_{ci} and z_{ci} are the (x, z) coordinates of the centre of the i^{th} cell on the top strip and Δx and Δz are the sampling intervals in the x and z directions respectively. We expand the charge density function using a sinc function basis:

$$f_t(x, z) = \sum_{i=1}^{M} f_{ti} \operatorname{sinc}[\frac{\pi}{\Delta x}(x - x_{ci})] \times \operatorname{sinc}[\frac{\pi}{\Delta z}(z - z_{ci})] \quad (23)$$

Taking the Fourier transform on both sides:

$$\mathbf{F_t} = A_{cell} \sum_{i=1}^{M} f_{ti} e^{-jk_x x_{ci}} e^{-jk_z z_{ci}} \quad (24)$$

for $\frac{-\pi}{\Delta x} < k_x < \frac{\pi}{\Delta x}$ and $\frac{-\pi}{\Delta z} < k_z < \frac{\pi}{\Delta z}$ and zero otherwise. From (12) and (22) we have:

$$\int_{-\infty}^{\infty} \mathbf{R_{11}} \mathbf{F_t} \mathbf{T}(k_x, k_z) e^{jk_x x_{ci}} e^{jk_z z_{ci}} dk_x dk_z + \int_{-\infty}^{\infty} \mathbf{R_{12}} \mathbf{F_b} \mathbf{T}(k_x, k_z) e^{jk_x x_{ci}} e^{jk_z z_{ci}} dk_x dk_z = \frac{1}{(2\pi)^2} c_t \quad (25)$$

where

$$\mathbf{T}(k_x, k_z) = \operatorname{sinc}\left(\frac{k_x \Delta x}{2}\right) \operatorname{sinc}\left(\frac{k_z \Delta z}{2}\right) \quad (26)$$

Substituting in (25) for $\mathbf{F_t}$ from (24), and for $\mathbf{F_b}$ a similar expression, we get:

$$\sum_{j=1}^{M} f_{tj} \int_{-\infty}^{\infty} \mathbf{R_{11}} \mathbf{W}(k_x, k_z) \mathbf{T}(k_x, k_z) f dk_x dk_z + \sum_{l=1}^{N} f_{bl} \int_{-\infty}^{\infty} \mathbf{R_{12}} \mathbf{W}(k_x, k_z) \mathbf{T}(k_x, k_z) f dk_x dk_z = c_1 \quad (27)$$

with

$$f(k_x, k_z) = e^{jk_x(x_{ci} - x_{cj})} e^{jk_z(z_{ci} - z_{cj})} \quad (28)$$

and where $c_1 = \frac{(2\pi)^2 c_t}{A_{cell}}$. The window function $\mathbf{W}(k_x, k_z)$ is equal to one for: $\frac{-\pi}{\Delta x} < k_x < \frac{\pi}{\Delta x}$ and $\frac{-\pi}{\Delta z} < k_z < \frac{\pi}{\Delta z}$ and zero otherwise. In (27), the number of cells in the bottom strip is taken to be N and for simplicity, their area is taken to be the same as the area of the cells in the top strip. The coordinates of the centres of the cells where the potential is imposed are (x_{ci}, z_{ci}) while (x_{cj}, z_{cj}) and (x_{cl}, z_{cl}) are the centres of the cells on the top and bottom cells respectively over which the summation is carried out. We also choose $\Delta x = \Delta z = \Delta$ for convenience. The above equation can be written as:

$$\sum_{j=1}^{M} \alpha_{ij} f_{tj} + \sum_{l=1}^{N} \beta_{il} f_{bl} = c_t \quad (29)$$

where

$$\alpha_{ij} = A_{cell}(FT^{-1}[\mathbf{R_{11}} \mathbf{W}(k_x, k_z) \mathbf{T}(k_x, k_z)]) \quad (30)$$

$$\beta_{il} = A_{cell}(FT^{-1}[\mathbf{R_{12}} \mathbf{W}(k_x, k_z) \mathbf{T}(k_x, k_z)]) \quad (31)$$

and with the above expressions evaluated at $x = x_{ci} - x_{cj}$ and $z = z_{ci} - z_{cj}$. Similarly, by imposing the constant potential at the bottom strip, we arrive at another system of equations:

$$\sum_{j=1}^{M} \gamma_{ij} f_{tj} + \sum_{l=1}^{N} \delta_{il} f_{bl} = c_b \quad (32)$$

where

$$\gamma_{ij} = A_{cell}(FT^{-1}[\mathbf{R_{21}} \mathbf{W}(k_x, k_z) \mathbf{T}(k_x, k_z)]) \quad (33)$$

$$\delta_{il} = A_{cell}(FT^{-1}[\mathbf{R_{22}} \mathbf{W}(k_x, k_z) \mathbf{T}(k_x, k_z)]) \quad (34)$$

From (29) and (32), we have:

$$\begin{pmatrix} [\tilde{\alpha}] & \left[\tilde{\beta}\right] \\ [\tilde{\gamma}] & \left[\tilde{\delta}\right] \end{pmatrix} \begin{pmatrix} \left[\tilde{f}_t\right] \\ \left[\tilde{f}_b\right] \end{pmatrix} = \begin{pmatrix} \left[\tilde{\phi}_t\right] \\ \left[\tilde{\phi}_b\right] \end{pmatrix} \quad (35)$$

where the elements of the matrices $[\tilde{\alpha}]$, $\left[\tilde{\beta}\right]$, $[\tilde{\gamma}]$, $\left[\tilde{\delta}\right]$ are given by (30), (31),(33), (34) respectively; the elements of the column vectors $\left[\tilde{f}_t\right]$ and $\left[\tilde{f}_b\right]$ are the unknown f_{ti}, $i = 1, 2, \cdots, M$ and f_{bi}, $i = 1, 2, \cdots, N$ respectively; the column vectors $\left[\tilde{\phi}_t\right]$, $\left[\tilde{\phi}_b\right]$ are constant column vectors having c_t and c_b as the elements, respectively. The above equation can be solved for the unknown charge densities first with the top strip at a potential of unity and the bottom strip at a potential of zero, and subsequently with the potentials reversed. The total charge on the top and bottom can be easily evaluated in both the cases giving the entries of the capacitance matrix.

3. Determination of the matrix coefficients

Equations (30)-(31) and (33)-(34) may be directly evaluated to determine the coefficient matrix in (35). We can, however make use of the circular symmetry to simplify the calculations. We will not go into detail here. It turns out and is proven by the numerical results that a sufficiently accurate approximation for α_{ij} (30) is

$$\alpha_{ij} = A_{cell}\left[r_{11}(x_{ci} - x_{cj}, z_{ci} - z_{cj})\right] \qquad (36)$$

with r_{11} given by

$$r_{11} = FT^{-1}\left\{\mathbf{R_{11}}(k_r)\mathbf{W}\left(k_x, k_z\right)\right\} \qquad (37)$$

Noting from (13) that $\mathbf{R_{11}}$ is circularly symmetric, we may represent (37) using the Fourier-Bessel transform to get:

$$\alpha_{ij} = \frac{A_{cell}}{2\pi}\int_0^\infty \mathbf{R_{11}}\left(k_r\right)\mathbf{W}\left(k_r\right)J_0\left(k_r\rho_{ij}\right)k_r dk_r \qquad (38)$$

where

$$\rho_{ij} = \sqrt{\left(x_{ci} - x_{cj}\right)^2 + \left(z_{ci} - z_{cj}\right)^2} \qquad (39)$$

In (38) we have approximated $\mathbf{W}\left(k_x, k_z\right)$ by the circularly symmetric window $\mathbf{W}\left(k_r\right)$ which has the value one in the interval $0 \le k_r \le \frac{\pi}{\Delta}$; outside this interval, it is zero. We can also make use of other circular windows to approximate $\mathbf{W}\left(k_x, k_z\right)$; circles with radius greater than the inner circle but less than or equal to the ex-circle of the square can also be used to describe the equivalent circular window. However, simulations have shown that while the choice of this radius has only a small influence on the final results, the best answers are obtained by choosing the inner circle as we have done here.

4. Numerical results

The above method was implemented in MATLAB on a PC with a 200 MHz processor. It will be instructive to consider specific numerical examples. Let $h = 200\mu m$, $d = 90\mu m$, $r = 300\mu m$. Let the dielectric constants be $\epsilon_1 = 2.0\epsilon_0$, $\epsilon_2 = 9.0\epsilon_0$, and $\epsilon_3 = 4.0\epsilon_0$. Let the width of the strips be $210\mu m$ and their length be $1050\mu m$. The sampling interval Δ was chosen as $30\mu m$, and the strips were taken to be parallel to each other ($\theta = 0$).

To verify the correctness of the results, the following approach was used: Let $\mathcal{C}$ be the capacitance matrix of the structure with strips of length l_1. Let $\mathcal{C} + \delta\mathcal{C}$ be the capacitance matrix of the same structure but with striplength $l_1 + \delta l$. The capacitance matrix per unit length of the infinite structure will then be given by $\delta\mathcal{C}$ / δl with the strips parallel. The obtained results can be compared with the accurate results based on a surface integral equation approach [8]. This is done in Tables 1-3 below.
Table 1 illustrates the effect of Δ on the accuracy of the results. The first row is the result for $\Delta = 30\mu m$, the second row is the result for $\Delta = 70\mu m$. The other parameters are: $h = 200\mu m$, $d = 90\mu m$, $r = 300\mu m$, $\epsilon_1 = 2.0\epsilon_0$, $\epsilon_2 = 9.0\epsilon_0$, $\epsilon_3 = 4.0\epsilon_0$, length=$1050\mu m$ and width=$210\mu m$.

$\mathcal{C}$ fF	$\delta\mathcal{C}$ / δl pF/m	Method of [8] pF/m
$\begin{pmatrix} 313 & -217 \\ -217 & 290 \end{pmatrix}$	$\begin{pmatrix} 281 & -206 \\ -206 & 263 \end{pmatrix}$	$\begin{pmatrix} 291 & -216 \\ -216 & 273 \end{pmatrix}$
$\begin{pmatrix} 300 & -207 \\ -207 & 278 \end{pmatrix}$	$\begin{pmatrix} 271 & -198 \\ -198 & 253 \end{pmatrix}$	$\begin{pmatrix} 291 & -216 \\ -216 & 273 \end{pmatrix}$

Table 1: effect of Δ on the accuracy.

Table 2 presents a similar result as in Table 1 but for different dielectric constants, i.e. $\epsilon_1 = 4.0\epsilon_0$, $\epsilon_2 = 2.0\epsilon_0$, $\epsilon_3 = 6.0\epsilon_0$ and only for $\Delta = 30\mu m$.

$\mathcal{C}$ fF	$\delta\mathcal{C}$ / δl pF/m	Method of [8] pF/m
$\begin{pmatrix} 159 & -51 \\ -51 & 137 \end{pmatrix}$	$\begin{pmatrix} 137 & -48 \\ -48 & 121 \end{pmatrix}$	$\begin{pmatrix} 141 & -50 \\ -50 & 125 \end{pmatrix}$

Table 2 : The same structure as in Table 1, but for different dielectric constants.

Finally, Table 3 shows results for the same layered structure as in Table 1 but for a much larger width and length ($h = 200\mu m$, $d = 90\mu m$, $r = 300\mu m$, $\epsilon_1 = 2.0\epsilon_0$, $\epsilon_2 = 9.0\epsilon_0$, $\epsilon_3 = 4.0\epsilon_0$, $\Delta = 70\mu m$, length=$3430\mu m$ and width=$910\mu m$).

$\mathcal{C}$ pF	$\delta\mathcal{C}$ / δl pF/m	Method of [8] pF/m
$\begin{pmatrix} 3.40 & -2.81 \\ -2.81 & 3.25 \end{pmatrix}$	$\begin{pmatrix} 973 & -818 \\ -818 & 934 \end{pmatrix}$	$\begin{pmatrix} 994 & -836 \\ -836 & 954 \end{pmatrix}$

Table 3 : A large structure is considered here.

As seen from these tables, the results of the surface integral equation method and the present method show good agreement. Although we have presented here only a few examples, simulations were carried out for a large number of examples. In all the cases, similar agreement was observed. This verifies the validity of the method proposed and in particular of the approximations to obtain (37) and (38).

We next consider the perpendicular case ($\theta = \frac{\pi}{2}$rad). Let us consider the capacitance matrix of the structure:

$$Q_t = C_{tt}V_t + C_{tb}V_b \quad (40)$$
$$Q_b = C_{tb}V_t + C_{bb}V_b \quad (41)$$

Let $\hat{Q}_t$ be the total charge on the top strip in the absence of the bottom strip; likewise, let $\hat{Q}_b$ be the total charge on the bottom strip in the absence of the top strip. Let

$$\hat{Q}_t = \hat{C}_{tt}V_t \quad (42)$$
$$\hat{Q}_b = \hat{C}_{bb}V_b \quad (43)$$

The excess charges $\Delta Q_t = Q_t - \hat{Q}_t$ and $\Delta Q_b = Q_b - \hat{Q}_b$ are given by:

$$\Delta Q_t = \left(C_{tt} - \hat{C}_{tt}\right) V_t + C_{tb}V_b \quad (44)$$
$$\Delta Q_b = C_{tb}V_t + \left(C_{bb} - \hat{C}_{bb}\right) V_b \quad (45)$$

Noting that $C_{tb} < 0$, we can write the above equations as:

$$\Delta Q_t = \left(C_{tt} - \hat{C}_{tt} - |C_{tb}|\right) V_t + |C_{tb}|\,(V_t - V_b) \quad (46)$$
$$\Delta Q_b = |C_{tb}|\,(V_b - V_t) + \left(C_{bb} - \hat{C}_{bb} - |C_{tb}|\right) V_b \quad (47)$$

If the structure is symmetric, we have the equivalent circuit for the excess capacitance as shown in Fig. 2(a) (inset) where $C_A = C_{tt} - \hat{C}_{tt} - |C_{tb}|$ and $C_B = |C_{tb}|$. With $h = r$ chosen so that we have 50Ω lines, and $\epsilon_1 = \epsilon_2 = \epsilon_3 = 4.0\epsilon_0$, the excess capacitance matrix was determined for various values of the strip-width and the parameter d. These results are shown in Fig. 2(a) and Fig. 2(b). Results are presented for 75Ω strips in Fig. 3(a) and Fig. 3(b). Note that the C_A values are negative. This is easily understood: charge repulsion between the individual lines reduces the originally present charge density per unit length.

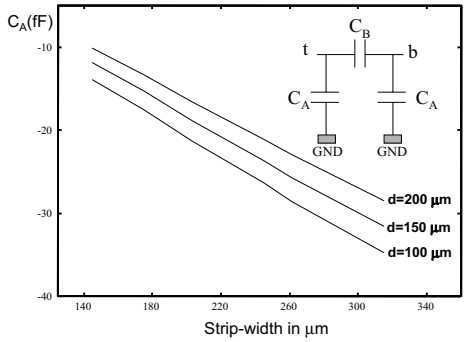

Figure 2a: C_A versus strip width for 50Ω lines crossing orthogonally.

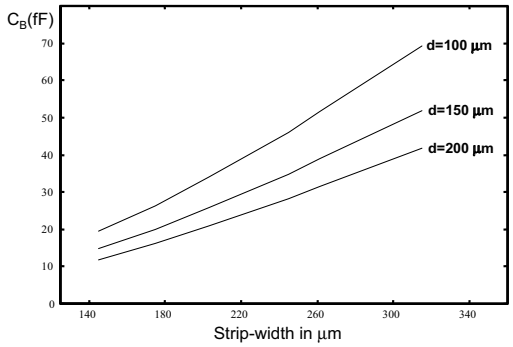

Figure 2b: C_B versus strip width for 50Ω lines crossing orthogonally.

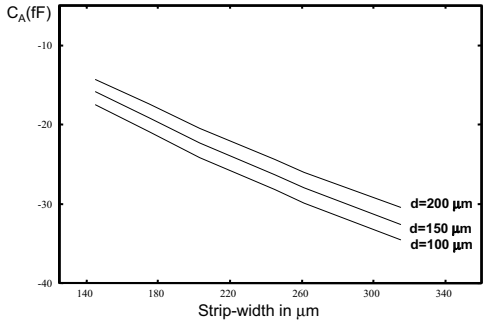

Figure 3a: C_A versus strip width for 75Ω lines crossing orthogonally.

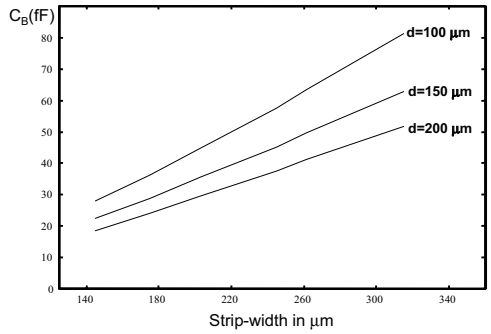

Figure 3b: C_B versus strip width for 75Ω lines crossing orthogonally.

5. Conclusion

In this manuscript, we have presented a fast method for calculating the capacitance matrix of the stripline crossing. The theory presented is quite general, in as much as the strips can be of any shape, although in our numerical examples we have dealt only with the simplest strips. Further work is needed to study the applicability of the method to multiple strip crossings, rectangular bends crossings etc.; the method should also be examined in the context of thick strips.

8. References

1. H. B. Bakoglu, *Circuits, Interconnects and Packages for VLSI*, London, Academic Press, 1995.
2. N. D. Arora, K. V. Raol, R. Schumann and L. M. Richardson, *Modeling and extraction of interconnect capacitances for multilayer VLSI circuits*, IEEE Trans. Computer-Aided Design, vol. 15, pp. 58-67, Jan. 1996.
3. K. Nabors and J. White, *Multipole-accelerated capacitance extraction algorithms for 3-D structures with multiple dielectrics*, IEEE Trans. Circuit Syst., vol. 39, pp. 936-954, Nov. 1992.
4. Ji Zheng, Zheng-Fan Li and Xia0-Ning Qian, *An efficient solver for three-dimensional capacitance of the interconnects in high speed digital circuit by the multiresolution method of moments*, IEEE Trans. Advanced Packaging, vol. 22, no. 1, pp. 9-15, Feb. 1999.
5. Wei Hong, Wei-Kai Sun, Zhen-Hai Zhu, Hao Ji, Ben Song and W. Wei-Ming Dai, *A novel dimension-reduction technique for the capacitance extraction of 3-D VLSI interconnects*, IEEE Trans. Microwave Theory and Techniques, vol. 46, no. 8, pp. 1037-1044, August 1998.
6. E. Yamashita, *Variational method for the analysis of microstrip-like transmission lines*, IEEE Trans. on Microwave Theory and Techniques, vol. MTT-16, no. 8, pp.529-535, August 1968.
7. E.Yamashita and R.Mittra, *Variational method for the analysis of microstrip lines*, IEEE Trans. on Microwave Theory and Techniques, vol. MTT-16, no. 4, pp.251-256, April 1968.
8. F. Olyslager, N. Faché and D. De Zutter, *New fast and accurate line parameter calculation of general multiconductor transmission lines in multilayered media*, IEEE Trans. on Microwave Theory and Techniques, vol. MTT-39, no. 6, pp. 901-909, June 1991.

Foundations for the Computation of the Inductance of Thin-Wire Loops in the Presence of Cylindrical Cores and Shells

Chalmers Butler

Abstract

In this paper one finds an analysis which can serve as the basis for computing inductance of thin-wire loops and helices in the presence of cylindrical shells and cores. Computation of inductance involves time-invariant magnetic fields that, in principle, are not influenced by nearby ideal conductors, yet inductance itself plays a role in circuits only in the case of time varying voltages and currents. To obtain a boundary condition needed to solve for the static magnetic field near a perfect conductor due to a time-invariant current, one appeals to a Rayleigh series analysis. With this needed condition in hand, one fashions a Fourier integral representation of the magnetic field due to stationary sources near cylinders and thereby determines inductance of loops near conducting shells and cores. Inductance is measured in the laboratory and the results are compared with those found theoretically.

Dedication

Dedicated with fondness, admiration, and gratitude to Professor Jean Van Bladel on the occasion of his 80^{th} birthday.

1. Introduction

The analysis of this paper is motivated by the need to determine the self inductance of a thin-wire, circular loop inside a conducting cylindrical shell as a first step in the computation of the self inductance of a practical helical coil. A coil must be physically supported and often is shielded. In most practical cases, the presence of a structure which serves these purposes affects the properties of the coil. Inductance is a stationary current notion whose valuation depends upon the computation of time-invariant magnetic field or flux in the loop caused by the loop current I. Even though determined from time-independent current and the flux created thereby, inductance finds its utility in circuit analyses involving time-varying quantities. Moreover, the time-independent magnetic field due to the stationary current employed in the definition of the self inductance L of the loop does not interact with the perfectly conducting wall of the surrounding shield, yet the presence of the shield does influence the current in the loop in any application of L in a circuit. Clearly, this is true because, in any circuit in which L plays a role, the current in the loop depends upon time. Thus, one faces the dilemma that the time-invariant magnetic field created by the stationary current is not influenced, theoretically, by the presence of the conducting shield, provided, of course, the circuit itself is stationary in space. Yet the presence of the nearby conductor must be accounted for in determining the value of the flux linkage employed in evaluating self inductance L. To endow the inductance of the shielded loop with the presence of the conducting shield, one defines L in terms of time-harmonic flux linkage in the limit as frequency approaches zero. This leads naturally to a *Rayleigh series* [1] analysis of the field by means of which one can deduce a needed boundary condition on the magnetic field that accounts for the presence of the conducting shield. To lay the foundation for finding the inductance of a loop near a cylindrical conductor, we present a method in this paper for computing the magnetic field due to a filamentary, time-invariant current in the presence of cylindrical structures, either conducting or of permeable material. To illustrate the use of the results obtained, we evaluate the self inductance of a thin-wire loop inside a conducting cylindrical shell and corroborate the computed values by comparison with data measured on a laboratory model.

Chalmers Butler is with the Holcombe Department of ECE, Clemson University
336 Fluor Daniel EIB
Clemson, SC 29634-0915 USA
Tel: +1 (864) 656-5922; Fax: +1 (864) 656-7220;
E-mail: cbutler@ces.clemson.edu.

Dedicated to Professor J. Van Bladel on the occasion of his 80th birthday

The inductance of wire loops and coils has drawn the attention of researchers for many years. Maxwell [2] computed the external inductance of a thin-wire loop from a model in which the current was assumed to be concentrated on the loop axis. Dwight [3] and Grover [4] each provide extensive collections of formulas and data on the inductance of coils of various configurations. Smyth [5] describes a number of methods for computing the magnetostatic field due to stationary electric currents. Young and Butler [6] examine models and present methods for computing the inductance of helical coils inside cylindrical shells at low frequencies. And they [7] investigate the effects of slots in shields as a means to mitigate the reduction in effective inductance of a coil in close proximity to a conducting shield. Extensive collections of references on the use of the so-called Rayleigh series method for solving problems of importance at low frequencies can be found in [1] by Kleinman and in [8] by Van Bladel.

Data are presented for the inductance of a circular wire loop inside a conducting cylindrical tube. The presence of the shield is fully accounted for in the data and it is observed that the inductance of the shielded loop is smaller than that of the unshielded loop. In fact, as the loop diameter approaches that of the shield, L becomes a small fraction of the inductance of the unshielded loop. Also inductance values are computed and measured for a thin-wire loop about a central conducting core and within a coaxial conducting shell.

2. Rayleigh Series and Magnetic Scalar Potential

The analysis presented in this paper is founded upon Maxwell's equations

$$\nabla \times \mathbf{H} = j\omega\varepsilon\mathbf{E} + \mathbf{J} \qquad \nabla \times \mathbf{E} = -j\omega\mu\mathbf{H} \quad (1)$$

and the derived conservation of electric and magnetic charge statements,

$$\nabla \bullet \mathbf{E} = \frac{1}{\varepsilon} q \qquad \nabla \bullet \mathbf{H} = 0\,, \quad (2)$$

for time-harmonic electric and magnetic fields $\mathbf{E}$ and $\mathbf{H}$ in regions characterized by (μ, ε). $\mathbf{J}$ is the volume electric current density and q is the volume electric charge density. Use is made also of the boundary condition exhibited by the electric field

$$\mathbf{E} \times \hat{\mathbf{n}} = \mathbf{0} \quad (3)$$

at the surface of a perfect electric conductor, the continuity of the electric field tangential to a surface devoid of surface magnetic current

$$\left(\mathbf{E}^{+} - \mathbf{E}^{-}\right) \times \hat{\mathbf{n}} = \mathbf{0}\,, \quad (4)$$

and the discontinuity condition on the magnetic field

$$\hat{\mathbf{n}} \times \left(\mathbf{H}^{+} - \mathbf{H}^{-}\right) = \mathbf{J}_s \quad (5)$$

at a surface bearing a surface electric current of density $\mathbf{J}_s$.

Because inductance, the principal application of the analysis in this paper, stems from the notion of magnetostatics, we seek relationships among quantities of interest in the limit as angular frequency ω approaches zero. To bring the frequency dependence of quantities to the fore, we expand them in power series in $j\omega$. Such a power series, the so-called Rayleigh series [1], is given by

$$\mathbf{F}(\mathbf{r}, \omega) = \sum_{p=0}^{\infty} \mathbf{F}^{(p)}(\mathbf{r})(j\omega)^p \quad (6)$$

in which $\mathbf{F}^{(p)}(\mathbf{r})$ is the frequency independent series coefficient that carries the spatial dependence of the function $\mathbf{F}(\mathbf{r}, \omega)$. If the functions in (1) through (5) are expanded in Rayleigh series and if one appeals to the uniqueness of a convergent power series and equates the coefficients of like powers of $j\omega$, equations governing the behavior of the series coefficients are found:

$$\begin{aligned} &\nabla \times \mathbf{H}^{(0)} = \mathbf{J}^{(0)} \\ &\nabla \times \mathbf{H}^{(p)} = \varepsilon\mathbf{E}^{(p-1)} + \mathbf{J}^{(p)}, \qquad p = 1,2,\ldots \end{aligned} \quad (7)$$

$$\begin{aligned} &\nabla \times \mathbf{E}^{(0)} = \mathbf{0} \\ &\nabla \times \mathbf{E}^{(p)} = -\mu\mathbf{H}^{(p-1)}, \qquad p = 1,2,\ldots \end{aligned} \quad (8)$$

$$\begin{aligned} &\nabla \bullet \mathbf{E}^{(p)} = \frac{1}{\varepsilon} q^{(p)} \\ &\nabla \bullet \mathbf{H}^{(p)} = 0, \;\; p = 0,1,2,\ldots \end{aligned} \quad (9)$$

$$\mathbf{E}^{(p)} \times \hat{\mathbf{n}} = \mathbf{0}, \quad p = 0,1,2,\ldots, \quad (10)$$

$$\left(\mathbf{E}^{+(p)} - \mathbf{E}^{-(p)}\right) \times \hat{\mathbf{n}} = \mathbf{0}, \quad p = 0,1,2,\ldots \quad (11)$$

and

$$\hat{\mathbf{n}} \times \left(\mathbf{H}^{+(p)} - \mathbf{H}^{-(p)}\right) = \mathbf{J}_s^{(p)}, \; p = 0,1,2,\ldots \quad (12)$$

Our principal interest is in the limit of the magnetic field due to a loop of filamentary current as $j\omega$ approaches zero. This limit is the zero-order magnetic field coefficient which is seen from (7)and (9) to satisfy

$$\nabla \times \mathbf{H}^{(0)} = \mathbf{0} \qquad \nabla \bullet \mathbf{H}^{(0)} = 0 \qquad (13)$$

in a source free region. If there is no static electric charge in the region of interest, which is true in the analysis of this paper, the zero-order electric field coefficient is zero, so, in the limit of zero frequency, the electric field itself is zero. However $\mathbf{H}^{(0)}$, which does survive in the limit, is related to $\mathbf{E}^{(1)}$ through (8) for $p = 1$. And it is this first-order coefficient of the electric field expansion $\mathbf{E}^{(1)}$ that provides needed boundary conditions through (10) and (11) which enables one to determine $\mathbf{H}^{(0)}$ in the limit as ω approaches zero.

Even though the magnetic field due to a filamentary loop of stationary current (Fig. 1) is not conservative in general in any region containing the current, this field can be conservative in some regions not containing the current. In particular, because of the first of (13) , $\mathbf{H}^{(0)}$ can be expressed as the gradient of a scalar

$$\mathbf{H}^{(0)} = -\nabla \Psi \qquad (14)$$

inside a cylindrical surface of radius ρ' through the loop as well as outside this surface. Application of the second of (13) to (14) reveals that the so-called magnetic scalar potential $\Psi(\rho, z)$ satisfies Laplace's equation in these two source-free regions:

$$\nabla^2 \Psi = 0 \qquad (15)$$

In the structures illustrated in Fig. 2 the source is the loop of filamentary current of Fig. 1. Field components caused by this source in open space or in the presence of one of the structures of Fig. 2 are φ independent so the magnetic scalar potential equation (15) for the source and structures of Fig. 2 reduces to

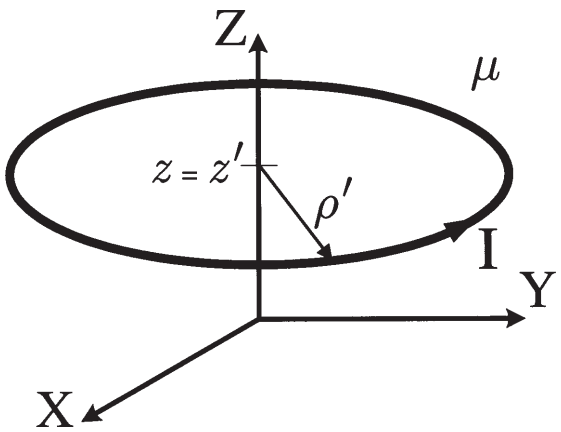

Figure 1: Circular loop of filamentary current I in free space

$$\frac{1}{\rho}\frac{\partial}{\partial \rho}\left(\rho \frac{\partial}{\partial \rho}\Psi\right) + \frac{\partial^2}{\partial z^2}\Psi = 0, \quad \rho \neq \rho' \qquad (16)$$

in circular cylindrical coordinates, where ρ' is the radius of the current loop as illustrated. A constant current in the loop creates radial and axial components of magnetic field but no component in the φ direction. This observation is consistent with the statement above about the components of the zero-order magnetic field coefficient, $\mathbf{H}^{(0)} = H_\rho^{(0)}(\rho, z)\hat{\boldsymbol{\rho}} + H_z^{(0)}(\rho, z)\hat{\mathbf{z}}$, computed from (14) :

$$H_\rho^{(0)}(\rho, z) = -\frac{\partial}{\partial \rho}\Psi(\rho, z) \quad . \qquad (17)$$

$$H_z^{(0)}(\rho, z) = -\frac{\partial}{\partial z}\Psi(\rho, z)$$

The connection between the components of the zero-order magnetic field coefficient and those of the first-order electric field coefficient comes from the second of (8) for $p = 1$:

$$H_\rho^{(0)} = \frac{1}{\mu}\frac{\partial}{\partial z}E_\phi^{(1)} \qquad H_z^{(0)} = -\frac{1}{\mu\rho}\frac{\partial}{\partial \rho}\left(\rho E_\phi^{(1)}\right) \qquad (18)$$

And from (17) and (18) one obtains

$$\frac{\partial}{\partial \rho}\Psi(\rho, z) = -\frac{1}{\mu}\frac{\partial}{\partial z}E_\phi^{(1)}(\rho, z) \qquad (19)$$

$$\frac{\partial}{\partial z}\Psi(\rho, z) = \frac{1}{\mu\rho}\frac{\partial}{\partial \rho}\left(\rho E_\phi^{(1)}(\rho, z)\right)$$

which relate the scalar potential and the components of the first-order electric field coefficient.

3. Ψ Due to Loop of Filamentary Current in Open Space

In this section one addresses the problem of finding the magnetic scalar potential due to the circular loop of filamentary current of I Amperes in infinite homogeneous space characterized by permeability μ. The current is stationary or time-invariant so the magnetostatic field is the same as the zero-order expansion coefficient $\mathbf{H}^{(0)}$. The loop center is at $z = z'$ on the z coordinate axis, its radius is ρ', and its plane is transverse to the axis as suggested in Fig. 1. The scalar potential due to the filamentary loop in open space is determined and it is used in constructing the scalar potential from which $\mathbf{H}^{(0)}$ due to the current loop in the presence of the cylinders can be found.

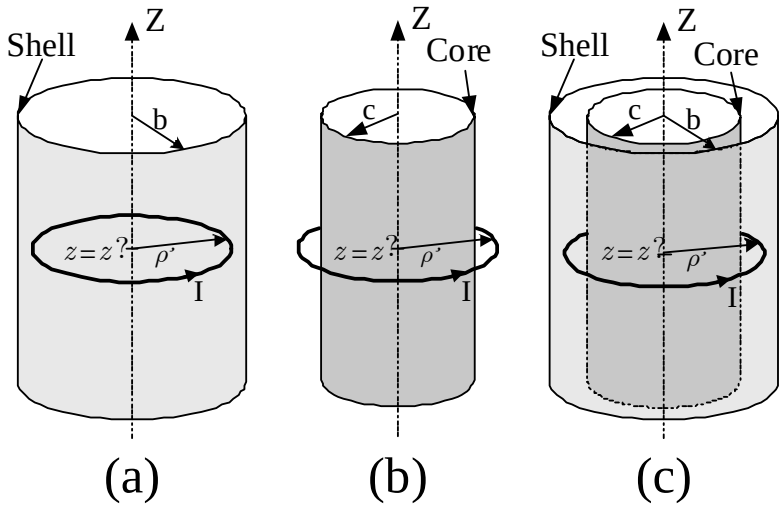

Figure 2: Loops of filamentary electric current I in presence of cylindrical shells and cores

The magnetic scalar potential due to the filamentary current loop of Fig. 1 satisfies (16) and conditions imposed through properties that must be exhibited by $H_z^{(0)}$ and $E_\varphi^{(1)}$ at the current loop. In order to obtain a solution for magnetic scalar potential for the isolated filamentary loop of current in a form amenable to extension to the case that the loop resides in the presence of the cylinders of Fig. 2, we seek a solution in separable form. To obtain such a solution, we appeal to the Fourier transform pair,

$$\tilde{f}(k_z) = \int_{-\infty}^{\infty} f(z)\, e^{jk_z z} dz \quad , \qquad (20)$$

$$f(z) = \frac{1}{2\pi} \int_{-\infty}^{\infty} \tilde{f}(k_z) e^{-jk_z z} dk_z$$

and employ it as an aid in solving the differential equation subject to conditions specified below. The transform of (16) is

$$\frac{1}{\rho}\frac{d}{d\rho}\left(\rho \frac{d}{d\rho}\tilde{\Psi}\right) - k_z^2 \tilde{\Psi} = 0, \quad \rho \neq \rho' \qquad (21)$$

where $\tilde{\Psi}$ stands for the transform of the scalar potential. Because the electric field must be continuous through a surface bearing an electric surface current, it is necessary that $E_\varphi^{(1)}$ be continuous through the cylindrical surface of radius ρ' in which the filamentary loop of current resides. From inspection of (19) one observes that this condition manifests itself as the following constraint on the scalar potential

$$\left.\frac{d}{d\rho}\tilde{\Psi}(\rho, k_z)\right|_{\rho=\rho'^{+}} = \left.\frac{d}{d\rho}\tilde{\Psi}(\rho, k_z)\right|_{\rho=\rho'^{-}} \qquad (22)$$

in the transform domain. And the presence of the current loop imposes the jump condition,

$$-\left[H_z(\rho'^{+}, z) - H_z(\rho'^{-}, z)\right] = I\delta(z - z'), \quad (23)$$

on the magnetic field. Because I is stationary, it is frequency independent and appears only in the zero-order series expansion of (23) — or of particularized to the present case – so the jump condition to be obeyed by $H_z^{(0)}(\rho, z)$ simplifies to

$$-\left[H_z^{(0)}(\rho'^{+}, z) - H_z^{(0)}(\rho'^{-}, z)\right] = I\delta(z - z'). \quad (24)$$

If $H_z^{(0)}(\rho, z)$ is represented as a function of the scalar potential as in (17) , the jump condition (24) can be expressed in the transform domain simply as

$$-jk_z\left[\tilde{\Psi}(\rho'^{+}, z) - \tilde{\Psi}(\rho'^{-}, z)\right] = Ie^{jk_z z'} \ . \quad (25)$$

The condition (22) results from the continuity of tangential electric field at a surface bearing an electric current and (25) comes from the discontinuity of magnetic field due to the presence of a surface electric current. Thus, the transform of the magnetic scalar potential $\tilde{\Psi}$ satisfies the differential equation (21) plus the two conditions (22) and (25) at $\rho = \rho'$. In addition it must be bounded at $\rho = 0$ and must decay properly as ρ becomes unbounded.

The solution of the differential equation (21) is the zero-order modified Bessel function of the first kind $I_0\left(\sqrt{k_z^2}\rho\right)$ for $\rho < \rho'$ and the zero-order modified Bessel function of the second kind, or the MacDonald function, for $\rho > \rho'$. From (22) one notes that the derivative of the

solution $\tilde{\Psi}(\rho, k_z)$ of (21) must be continuous at $\rho = \rho'$, which property is incorporated in the solution to (21) by expressing it as

$$\tilde{\Psi}(\rho, k_z) = \begin{cases} C \dfrac{I_0\left(\sqrt{k_z^2}\rho\right)}{I_0'\left(\sqrt{k_z^2}\rho'\right)}, & \rho < \rho' \\ C \dfrac{K_0\left(\sqrt{k_z^2}\rho\right)}{K_0'\left(\sqrt{k_z^2}\rho'\right)}, & \rho > \rho' \end{cases}, \quad (26)$$

where C is an arbitrary constant. Application of the transformed jump condition (25) allows one to compute the constant,

$$C = -j\rho' I \frac{\sqrt{k_z^2}}{k_z} I_1\left(\sqrt{k_z^2}\rho'\right) K_1\left(\sqrt{k_z^2}\rho'\right) e^{jk_z z'}, \quad (27)$$

and subsequently to determine the transform of the magnetic scalar potential:

$$\tilde{\Psi}(\rho, k_z) = \quad (28)$$

$$\begin{cases} -j\rho' I \frac{\sqrt{k_z^2}}{k_z} K_1\left(\sqrt{k_z^2}\rho'\right) I_0\left(\sqrt{k_z^2}\rho\right) e^{jk_z z'}, & \rho < \rho' \\ j\rho' I \frac{\sqrt{k_z^2}}{k_z} I_1\left(\sqrt{k_z^2}\rho'\right) K_0\left(\sqrt{k_z^2}\rho\right) e^{jk_z z'}, & \rho > \rho' \end{cases}$$

The somewhat cumbersome form $\sqrt{k_z^2}/k_z$ above is retained and the temptation to replace it by 1 is assiduously withstood. Taking the inverse transform of (28), one arrives at (equation 29) (see below)

which is the magnetic scalar potential from which the field of the current loop in Fig. 1 can be determined. The even- and odd-function properties of the terms in the integrands of (29) enable one to convert the expressions for the scalar potential to integrals over $(0, \infty)$: (equation 30) (see below)

$\mathbf{H}^{(0)}$ due to the current loop of Fig. 1 can be computed directly from the potential of (30).

4. Ψ Due to Loop of Current in Presence of Cylinders

In this section we determine the magnetic scalar potential due to the loop of current in the presence of the coaxial cylinders illustrated in Fig. 2. The scalar potential due to the loop in open space is used in constructing the scalar potential due to the current loop in the presence of the cylinders. The circular cylinders, either hollow tubes or solid, are of infinite extent and their axes coincide with the z coordinate axis. The structures of interest are (*i*) a loop in a hollow conducting cylinder, (*ii*) a loop about a circular conducting core, (*iii*) a loop about a conducting core in a conducting tube, (*iv*) a loop about a magnetic core of permeability μ_c, and (*v*) a loop about a magnetic core of permeability μ_c in a conducting tube. Except for the magnetic cores of (*iv*) and (*v*), all space is filled with material characterized by μ. Structure (*i*) is illustrated in Fig. 2(a), structures (*ii*) and (*iii*) are illustrated in Figs. 2(b) and 2(c) with the core a conductor, and structures (*iv*) and (*v*) are illustrated in Figs. 2(b) and 2(c), also, but with the core magnetic.

In the cylindrical regions of the structures of Fig. 2, one can express the magnetic scalar potential as

$$\Psi = \Psi_\ell + \Psi_s \quad (31)$$

in which Ψ_ℓ is the scalar potential due to the loop in open space as in (30) and Ψ_s is the secondary potential due to the presence of the cylindrical boundary or boundaries. On the surface of a perfectly conducting cylinder of radius r, the tangential electric field must be zero in the limit as ω approaches zero which through (10) with $p = 1$ implies that

$$\Psi(\rho, z) = \begin{cases} -j\rho' I \dfrac{1}{2\pi} \displaystyle\int_{-\infty}^{\infty} \frac{\sqrt{k_z^2}}{k_z} K_1\left(\sqrt{k_z^2}\rho'\right) I_0\left(\sqrt{k_z^2}\rho\right) e^{-jk_z(z-z')} dk_z, & \rho < \rho' \\ j\rho' I \dfrac{1}{2\pi} \displaystyle\int_{-\infty}^{\infty} \frac{\sqrt{k_z^2}}{k_z} I_1\left(\sqrt{k_z^2}\rho'\right) K_0\left(\sqrt{k_z^2}\rho\right) e^{-jk_z(z-z')} dk_z, & \rho > \rho' \end{cases} \quad (29)$$

$$\Psi(\rho, z) = \begin{cases} -\rho' I \dfrac{1}{\pi} \displaystyle\int_0^{\infty} K_1\left(k_z\rho'\right) I_0\left(k_z\rho\right) \sin k_z\left(z - z'\right) dk_z, & \rho < \rho' \\ \rho' I \dfrac{1}{\pi} \displaystyle\int_0^{\infty} I_1\left(k_z\rho'\right) K_0\left(k_z\rho\right) \sin k_z\left(z - z'\right) dk_z, & \rho > \rho' \end{cases} \quad (30)$$

$$E_{\varphi}^{(1)}(r,z)=0 \tag{32}$$

for all z. In turn, because the right side of the first of (19) must be zero *for all* z, one observes that

$$\frac{\partial}{\partial\rho}\Psi\bigg|_{\rho=r}=0\cdot \tag{33}$$

The boundary condition (33), inferred in the limit as ω approaches zero, is precisely the additional information needed to enable one to solve for the scalar potential in regions bound by conducting cylinders. At a cylindrical interface of radius r between two regions characterized by μ_- and μ_+, tangential components of electric and magnetic fields must be continuous. At such an interface, the scalar potential must satisfy

$$\frac{\partial}{\partial z}\Psi\left(r^-,z\right)=\frac{\partial}{\partial z}\Psi\left(r^+,z\right) \tag{34}$$

and

$$\mu_-\frac{\partial}{\partial\rho}\Psi\left(\rho,z\right)\bigg|_{\rho=r^-}=\mu_+\frac{\partial}{\partial\rho}\Psi\left(\rho,z\right)\bigg|_{\rho=r^+}. \tag{35}$$

Conditions (34) and (35) enforce continuity of $H_z^{(0)}$ and $E_{\varphi}^{(1)}$, respectively, at $\rho=r$, the interface between the magnetic core and the surrounding medium.

4.1 Ψ Due to Loop of Current inside PEC Cylindrical Shell

The magnetic scalar potential for the loop current placed inside a perfectly conducting cylindrical tube filled with material characterized by μ (Fig. 2(a)) can be expressed as in (31) where the secondary potential due to the presence of the conducting tube is

$$\Psi_s\left(\rho,z\right)= \tag{36}$$

$$\rho' I\frac{1}{\pi}\int_0^{\infty}C_s\left(k_z\right)I_0\left(k_z\rho\right)\sin k_z\left(z-z'\right)dk_z,\ \ \rho<b$$

which clearly satisfies the differential equation (16) and is bounded at $\rho=0$ as must be true. To this is added the potential due to the current, allowing one to write the total potential as

$$\Psi\left(\rho,z\right)=\rho' I\frac{1}{\pi}\int_0^{\infty}\left[C_s\left(k_z\right)I_0\left(k_z\rho\right)\right. \tag{37}$$

$$\left.+I_1\left(k_z\rho'\right)K_0\left(k_z\rho\right)\right]\sin k_z\left(z-z'\right)dk_z,\ \ \rho'<\rho<b$$

in the region between the loop and the conducting cylinder. Application of the boundary condition (33) for $r=b$ enables one to evaluate the constant $C_s\left(k_z\right)$:

$$C_s\left(k_z\right)=-\frac{I_1\left(k_z\rho'\right)K_0'\left(k_z b\right)}{I_0'\left(k_z b\right)}=\frac{I_1\left(k_z\rho'\right)K_1\left(k_z b\right)}{I_1\left(k_z b\right)} \tag{38}$$

.

Thus the total potential is the sum of the potential (30) for the isolated loop current and (36) with the constant replaced by its value from (38).

4.2 Ψ Due to Loop of Current about PEC Cylindrical Core

The procedure applied above to determine the potential for the loop in the circular conducting tube can be employed with minor modification to solve for the potential due to the loop about a perfectly conducting cylindrical core (Fig. 2(b) with the core taken to be a conductor). The secondary potential is

$$\Psi_s\left(\rho,z\right)= \tag{39}$$

$$-\rho' I\frac{1}{\pi}\int_0^{\infty}C_c\left(k_z\right)K_0\left(k_z\rho\right)\sin k_z\left(z-z'\right)dk_z,\ \rho>c$$

which satisfies (16) and decays properly for large ρ. Thus the total potential is

$$\Psi\left(\rho,z\right)=-\rho' I\frac{1}{\pi}\int_0^{\infty}\left[C_c\left(k_z\right)K_0\left(k_z\rho\right)\right. \tag{40}$$

$$\left.+K_1\left(k_z\rho'\right)I_0\left(k_z\rho\right)\right]\sin k_z\left(z-z'\right)dk_z,\ c<\rho<\rho'$$

in the region $c<\rho<\rho'$ and the constant $C_c\left(k_z\right)$ is determined by requiring (40) to satisfy the boundary condition (33) for $r=c$:

$$C_c=\frac{K_1\left(k_z\rho'\right)I_1\left(k_z c\right)}{K_1\left(k_z c\right)}. \tag{41}$$

The total potential in this case of the loop about the conducting core of Fig. 2(b) is the sum of the potential (30) for the isolated loop current and the secondary potential of (39) with the constant in (41).

4.3 Ψ Due to Loop of Current about Core inside Shell

Without elaborating upon the details, one records the secondary potential for the loop current between the conducting cylindrical core and the exterior cylindrical

conduction tube of Fig. 2(c) with conducting core,

$$\Psi_s(\rho,z)=\rho' I\frac{1}{\pi}\int_0^\infty \left[A_{cs}(k_z)K_0(k_z\rho)\right. \quad (42)$$
$$\left.+B_{cs}(k_z)I_0(k_z\rho)\right]\sin k_z(z-z')dk_z,\ c<\rho<b,$$

where the constants are

$$A_{cs}=I_1(k_zc)\frac{I_1(k_zb)K_1(k_z\rho')-I_1(k_z\rho')K_1(k_zb)}{I_1(k_zc)K_1(k_zb)-I_1(k_zb)K_1(k_zc)}$$
$$B_{cs}=K_1(k_zb)\frac{I_1(k_zc)K_1(k_z\rho')-I_1(k_z\rho')K_1(k_zc)}{I_1(k_zc)K_1(k_zb)-I_1(k_zb)K_1(k_zc)}$$
. (43)

The constants follow from enforcing the boundary condition (33) for $r=c$ and $r=b$.

4.4 Ψ Due to Loop of Current about Magnetic Core

The potential in the magnetic core of the structure illustrated in Fig. 2(b) (with the core of material exhibiting permeability μ_c) is of the form

$$\Psi(\rho,z)= \quad (44)$$
$$-\rho' I\frac{1}{\pi}\int_0^\infty C_{mc}(k_z)I_0(k_z\rho)\sin k_z(z-z')dk_z,\ \rho<c$$

which satisfies (16) and is bounded at $\rho=0$ as is necessary. Outside the core, the potential is the sum of the potential due to the loop in open space characterized by μ and a secondary potential which decays properly for large ρ:

$$\Psi(\rho,z)=\cdot \quad (45)$$
$$\cdot\ \Psi_\ell(\rho,z)-\rho' I\frac{1}{\pi}\int_0^\infty B_{mc}(k_z)K_0(k_z\rho)\sin k_z(z-z')dk_z,$$
$$\rho>c$$

The potential must satisfy the conditions (34) and (35) at $r=c$. These conditions imposed on the potential allow one to obtain equations governing the constants, which can be solved to arrive at

$$B_{mc}=\left(1-\frac{\mu_c}{\mu}\right)\frac{I_0(k_zc)I_1(k_zc)K_1(k_z\rho')}{I_0(k_zc)K_1(k_zc)+\frac{\mu_c}{\mu}I_1(k_zc)K_0(k_zc)}$$
$$C_{mc}=\frac{1}{k_zc}\frac{K_1(k_z\rho')}{I_0(k_zc)K_1(k_zc)+\frac{\mu_c}{\mu}I_1(k_zc)K_0(k_zc)}$$
(46)

4.5 Ψ Due to Loop of Current about Magnetic Core inside Shell

The potential from which the magnetic field can be computed in the structure of Fig. 2(b), with core characterized by μ_c, is (equation47) (see below) whose coefficients are computed from the solutions of the equations resulting from requiring (47) to satisfy (34) and (35) at $r=c$ and (33) at $r=b$. If these conditions are enforced, one finds that the constants A_{ms}, B_{ms}, and C_m are governed by the matrix equation, (equation 48)(see below)

With the constants available from (48) substituted into (47), one has an expression for the magnetic scalar potential in the core as well as in the region between the core and the outer conducting cylinder.

$$\Psi(\rho,z)=\begin{cases}-\rho' I\frac{1}{\pi}\int_0^\infty C_m(k_z)I_0(k_z\rho)\sin k_z(z-z')dk_z & ,\quad \rho<c \\ \Psi_\ell(\rho,z)-\rho' I\frac{1}{\pi}\int_0^\infty \left[A_{ms}(k_z)K_0(k_z\rho)\right. & \\ \left.B_{ms}(k_z)I_0(k_z\rho)\right]\sin k_z(z-z')dk_z & ,\quad c<\rho<b\end{cases} \quad (47)$$

$$\begin{bmatrix}0 & K_1(k_zb) & -I_1(k_zb)\\ I_0(k_zc) & -K_0(k_zc) & -I_0(k_zc)\\ \frac{\mu_c}{\mu}I_1(k_zc) & K_1(k_zc) & -I_1(k_zc)\end{bmatrix}\begin{bmatrix}C_m\\ A_{ms}\\ B_{ms}\end{bmatrix}=\begin{bmatrix}I_1(k_z\rho')K_1(k_zb)\\ K_1(k_z\rho')I_0(k_zc)\\ K_1(k_z\rho')I_1(k_zc)\end{bmatrix} \quad (48)$$

5. Inductance of Thin-Wire Loop in Presence of Cylinders

The self inductance L of the thin-wire loop of Fig. 3 is $L = \psi/I$ where I is the current in the loop and ψ is the magnetic flux which links the loop. For a sufficiently thin wire of radius a, the current can be approximated by a filamentary current on the axis of the wire loop as suggested in Fig. 3 and the flux through a disk of radius R whose center is at z on the coordinate axis is

$$\psi_R(z) = \tag{49}$$

$$\int_0^R \int_{-\pi}^{\pi} \mu H_z^{(0)}(\rho, z)\rho d\varphi d\rho = -2\pi R E_\varphi^{(1)}(R, z)$$

in which $H_z^{(0)}$ is the zero-order coefficient of the z component of the magnetic field due to the filament of current on the axis of the loop in Fig. 3. From the first of (19),

$$E_\varphi^{(1)}(\rho, z) = -\mu \int \frac{\partial}{\partial \rho} \Psi(\rho, z)\, dz, \tag{50}$$

in which the constant of integration is zero for, otherwise, $E_\varphi^{(1)}(\rho, z)$ would not decay as a function of z as is required. In view of (30), (50), and (49) , one can express the flux through the disk of radius R as

$$\psi_R(z) = \cdot \tag{51}$$

$$2\mu R\rho' I \int_0^\infty K_1(k_z\rho') I_1(k_z R) \cos k_z(z - z') dk_z,$$

$$R < \rho'$$

If the radius of the disk of Fig. 3 is set equal to $\rho' - a$ and the planes of the loop and disk are made the same $(z = z')$, then $\psi_{\rho'-a}(z')$ of (51) becomes the flux through the loop due to the current I. Hence a good approximation of the self inductance of the thin-wire loop is given by

$$L = \frac{\psi_{\rho'-a}(z')}{I} = \cdot \tag{52}$$

$$2\mu[\rho' - a]\rho' \int_0^\infty K_1(k_z\rho') I_1(k_z[\rho' - a])\, dk_z$$

L of (52) is a good approximation if the loop radius ρ' is very large compared to its wire radius a so that the field due to the current on the wire is well approximated by the field due to the current concentrated on the loop axis. There are other expressions [6] equivalent to (52) for the inductance of a thin-wire loop.

5.1 Inductance of Thin-Wire Loop in a Cylindrical Shell

The procedure for computing the inductance of a thin-wire loop inside a conducting cylindrical shell of radius b follows that above for computing L for the isolated loop. The difference is that one must account for the flux through the loop due to the presence of the conducting shell. It is convenient to define the inductance of the loop in the shell as

$$L_s = L^{pri} + L^{\text{sec}} \tag{53}$$

where L^{pri} is the inductance (52) of the isolated loop and L^{sec} is the contribution to the inductance due to the presence of the shell. L^{sec} is due to the contribution to the flux in the loop computed from ψ^s of (36). It is determined from the sequence of steps leading from (49) to (52) with the sole exception that the secondary potential of (36) replaces the primary potential of (30). The steps lead to

$$L^{\text{sec}} = \frac{\psi_{\rho'-a}^{\text{sec}}(z')}{I} = \cdot \tag{54}$$

$$-2\mu[\rho' - a]\rho' \int_0^\infty C_s(k_z) I_1(k_z[\rho' - a])\, dk_z$$

where the constant C_s is given in .

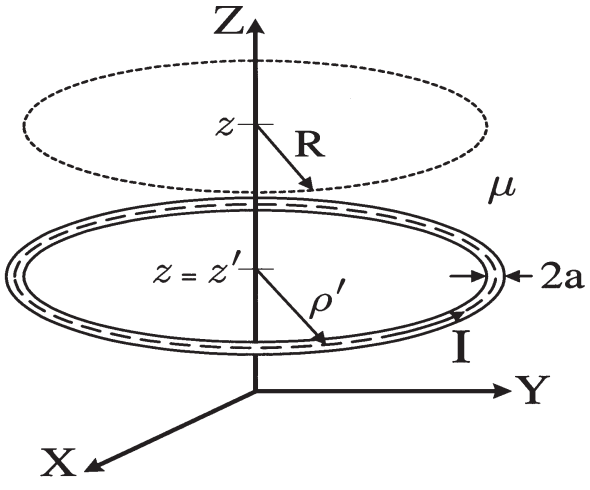

Figure 3. Current I on axis of thin-wire loop of radius ρ' and parallel disk of radius R.

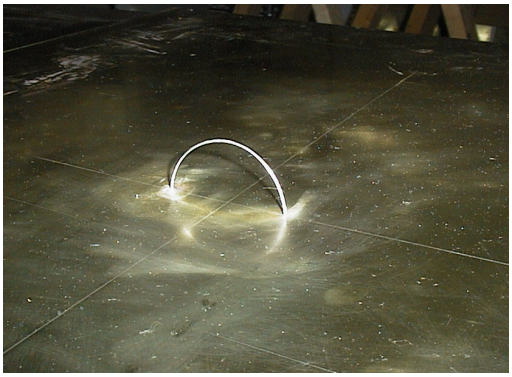

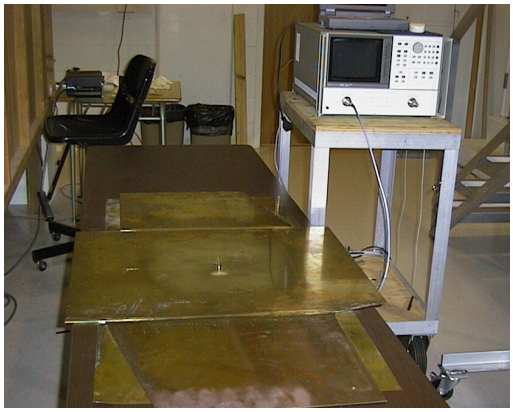

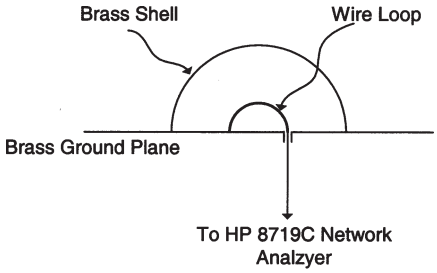

Figure 4: Apparatus for measuring inductance of thin-wire circular loop in the presence of cylindrical cores and shells

5.2 Inductance of Thin-Wire Loop about Conducting Core in Cylindrical Shell

To evaluate the inductance of a thin-wire loop in the structure of Fig. 2(c), with the core a conductor, one must know the magnetic flux in the annulus in the plane of the loop with outer radius $\rho' - a$ and inner radius c. This flux is

$$\psi^{cs}(z') = \int_{-\pi}^{\pi}\int_{c}^{\rho'-a} \mu H_z^{(0)}(\rho, z')\rho d\varphi d\rho = \quad (55)$$

$$2\pi\left[cE_{\varphi}^{(1)}(c, z') - [\rho' - a]E_{\varphi}^{(1)}([\rho' - a], z')\right]$$

where the first-order Rayleigh series coefficient $E_{\varphi}^{(1)}$ can be computed from the magnetic scalar potential $\Psi^{cs} = \Psi_{\ell} + \Psi_{s}$ whose terms are the potentials given in (30)and (42). Using the magnetic scalar potentials (30) and (42) to evaluate the right side of (55), one finds the self inductance of the thin-wire loop in the coaxial cylinder structure of Fig. 2(c) to be

$$\begin{aligned} L_{cs} = {} & 2\mu[\rho' - a]\rho'\int_0^{\infty} K_1(k_z\rho')I_1(k_z[\rho' - a])\,dk_z \\ & - 2\mu c\rho'\int_0^{\infty} K_1(k_z\rho')I_1(k_z c)\,dk_z \\ & + 2\mu[\rho' - a]\rho'\int_0^{\infty}\left[A_{cs}K_1(k_z[\rho' - a]) - B_{cs}I_1(k_z[\rho' - a])\right]dk_z \\ & - 2\mu c\rho'\int_0^{\infty}\left[A_{cs}I_1(k_z c) - B_{cs}K_1(k_z c) - \right]dk_z \ . \end{aligned} \quad (56)$$

It is of interest to note that the first term above is the same as the self inductance of the loop in open space (52) and the second term is the negative of the mutual inductance between the loop and a loop of radius c. Alternatively, one can interpret the second term as a reduction in the inductance (reduction in flux) of the loop as if it were in open space to account for the fact that flux does not penetrate the conducting core.

6. Results, Measurements, and Observations

An apparatus was designed and measurements were conducted to obtain data against which to compare the computed values of inductance. A half-loop above a ground plane was formed by means of the extension of the center conductor of a semi-rigid coax whose outer conductor was soldered to the conducting plane, as was the end of the wire loop remote from the coax feed point. As can be seen from the photograph in Fig. 4, the plane of the loop is perpendicular to the ground plane so the semicircular loop and its image form a full loop. The input impedance at the

Core Radius c (cm)	Shell Radius b (cm)	Computed L (μH)	Measured L (μH)
0	∞	0.0701	0.0704
0.970	∞	0.0648	0.0641
1.315	∞	0.0645	0.0533
0	1.830	0.0463	0.0456
0	2.150	0.0575	0.0577
0	3.800	0.0674	0.0683
0.970	2.150	0.0536	0.0552
0.970	3.820	0.0600	0.0639
1.315	2.150	0.0430	0.0476
1.315	3.820	0.0453	0.0534

Table 1: Self Inductance of Wire Loop in Various Environments

$a = 0.0475\,cm$ $\rho' = 1.585\,cm$

Core Radius c (cm)	Shell Radius b (cm)	Computed L (μH)	Measured L (μH)
0	∞	0.1423	0.1430
0.970	∞	0.1378	0.1420
1.315	∞	0.1334	0.1390
1.908	∞	0.1192	0.1270
0	0.038	0.1216	0.1235
0.970	3.820	0.1198	0.1210
1.315	3.820	0.1178	0.1240
1.908	3.820	0.1097	0.1200

Table 2: Self Inductance of Wire Loop in Various Environments

$a = 0.0475\,cm$ $\rho' = 2.763\,cm$

base of the loop was measured by means of a network analyzer at a wavelength (50 MHz to 100 MHz) much greater than the dimensions of the loop. Inductance was inferred from the impedance data. The size of the loop relative to wavelength assured a radiation resistance of essentially zero, and the dimensions of the loop were selected so that the impedance measured was near 50 Ohms. Impedance data measured via a 50 Ohm system is inaccurate if the impedance differs significantly from 50 Ohms. Semi-circular brass tubes of two different radii were placed over the half-loop to simulate a loop in a conducting shell, and a half cylinder was inserted through the loop to simulate the loop about a conducting core. A photograph of the hemi-cylindrical tube clamped to the ground plane can be seen in Fig. 4. The field in any of these configuration decays very, very rapidly with displacement from the loop, allowing one to view the shell and core as being of infinite extent. There is a small amount of capacitance between the wire and the plane at the feed, but that between the loop and the shell is negligible. Measurements were performed on two loops: wire radius 0.5 mm, loop radius 1.575 cm; wire radius 0.475 mm, loop radius of 2.75 cm.

Values of inductance determined from computations and from measurements are presented in Tables 1 and 2. In most cases the measured and computed values are in good agreement and it is observed that L is reduced by the presence of the conducting shell or core. When the wire loop is very close to a conducting wall, the proximity effect causes the current to vary noticeably as a function of circumferential displacement and computations based on the model in which the current is concentrated on the wire axis suffer accuracy. This can be seen in the data of Tables 1 and 2. Young and Butler [6] discuss models which lead to more accurate results. And they demonstrate how the basic analysis for computing self inductance of the single loop can be extended immediately to compute mutual inductance among loops as well as to compute the inductance of multi-turn coils.

7. References

1. R. E. Kleinman, "The Rayleigh region," *Proc. IEEE,* vol. 53, pp. 848-856, 1965.
2. J. C. Maxwell, *A Treatise on Electricity and Magnetism*, Third Ed., Dover, New York, 1954.
3. H. B. Dwight, *Electrical Coils and Conductors*, McGraw-Hill, New York, 1945.
4. F. W. Grover, *Inductance Calculations: Working Formulas and Tables,* D. Van Nostrand, New York, 1946.
5. W. R. Smythe, *Static and Dynamic Electricity,* Third Ed., McGraw-Hill, New York, 1968.
6. J. C. Young and C. M. Butler, "Inductance of a shielded coil," *IEEE Trans. Antennas Propagat.,* vol. 49, no. 6, pp. 944-953, June, 2001.
7. J. C. Young and C. M. Butler, "Inductance of a coil in a slotted shield," *IEEE Trans. Antennas Propagat.,* vol. 50, no. 4, pp. 475-484, April, 2002.
8. J. Van Bladel, "Low-frequency asymptotic techniques," in *Modern Topics in Electromagnetics and Antennas,* Peter Peregrinus, Ltd., Stevenage, Herts, 1977.

An open letter and call for participation

The Open Radar Initiative

Reliable Technology for Radio Science

F.D. Lind
T. Grydeland
P.J. Erickson
J.M. Holt

Abstract

The Open Radar Initiative is a project to develop reliable and reusable technology for radio science applications. The initiative will provide a resource for the development of radio science systems, reduce the duplication of effort in the community, provide a means for distributing innovative techniques, and lower the expense and difficulty of developing new experimental systems. The initial focus of the initiative is to develop reusable hardware and software components for implementing ionospheric radio science instruments based on a Software Radar architecture. The Software Radar architecture unifies monostatic and multi-static radar system designs, and enables a new generation of distributed radio science systems. Many of the hardware and software elements are also useful for implementing instruments such as riometers, sounders, beacon tomography systems, and radio telescopes. An "open source" development model is being used to distribute the resulting technology and to encourage community participation. This project is being coordinated through http://www.openradar.org.

1. Introduction

Radio science technology is the basis of experimental investigations into a variety of scientific phenomena. The Open Radar Initiative is an effort to enhance the development of this technology by encouraging the collaboration of individuals and groups involved in the development of experimental instrumentation. Although the early focus of the initiative is on the development of ionospheric radar technology, most radio science systems have many similarities to these systems, and the technologies developed for one type of instrument will often be useful in whole or part for another. By using an open source development model for hardware, software, and system architectures, we will help reduce duplication of effort in the community, aid innovation, and provide an additional means of communication among radio scientists and engineers.

This initiative is an outgrowth of recent projects to upgrade the Millstone Hill Incoherent Scatter Data Acquisition System (MIDAS) [1], and efforts to develop technology for multi-static passive radar networks [2] (e.g., the Manastash Ridge Radar). During these development efforts, it rapidly became apparent that recent technological advances in computing, networking, and software systems were converging on a comprehensive set of technologies suitable for implementing most ionospheric radar systems under a unified set of architectural patterns. The most important of these technologies include digital receivers, high-performance computer networks, software-defined radio, global positioning systems, eXtensible Markup Language, version control, advanced databases, and distributed computing.

By combining these technologies into a Software Radar framework (e.g., http://www.haystack.mit.edu/midas_w), it is possible to produce radio science systems where the vast majority of control and signal-processing functions are implemented in software running on general purpose computers and networks. This approach has a number of explicit advantages, which derive primarily from the early transformation of instrument information and data into the digital domain, the communication of this information using standard computer networks, and the rapidly increasing power of computational platforms. The foremost results of these advantages are in the control, flexibility, precision, and transparency of the experimental process.

Frank Lind, Philip Erickson, and John Holt are with the MIT Haystack Observatory, Route 40, Westford, MA 01886, USA; Tel: +1 (781) 981-5570; Fax: +1 (781) 981-5766; E-mail: flind@haystack.mit.edu.

Tom Grydeland is with the Department of Physics, University of Tromsø,Nordlysobservatoriet, Prestvannveien 38, N-9037 Tromsø, Norway.

There are other significant benefits gained through the use of software as the basis for radio science instruments, in general, and for ionospheric radars, in particular. Fully digital operation allows the state of an experimental system to be completely recorded for later analysis. Software components do not degrade or suffer calibration problems due to aging, changing environmental conditions, or component obsolescence. Another benefit is that new components and architectures can be tested and implemented in parallel with an existing operational system. This is especially important for encouraging the development of innovative new techniques in a manner that allows robust comparisons to proven existing methods.

A system composed primarily of software is also inherently ready for automated remote operations, networked global data distribution, and the provision of input in real time to diagnostic and forecasting models. The strong coupling to computer networks also allows the production of instruments that share resources, data, and operational schedules. This is particularly important for distributed instrument arrays, but can also be useful in more specialized applications (e.g., sharing a high-speed correlator between multiple radar systems).

A Software Radar approach is not without its difficulties. Software is precise, but it is not inherently flexible without specific attention, at an early stage, to adaptability and ease of use. These qualities must be explicitly designed into a software system. How to best accomplish this is not always easy to determine, and is always a function of the available development tools. Properly writing, debugging, and documenting a software system is almost always a complicated and time-consuming task. Often, the complex interdependencies associated with software components makes them as difficult to change as the physical hardware in a system. This is particularly true in systems with stringent operational requirements for fault-tolerant or failure-free operation. The key to producing a precise and flexible software system is to gradually evolve a robust architecture in response to real-world requirements and usage. This architecture must have at its core a strictly enforced modularity, to ensure that system elements are small enough in scale to be properly designed and debugged.

An evolutionary approach to software development also encourages the identification of recurrent software patterns [3]. By identifying the underlying architectural patterns inherent in experimental radio science system implementations, it is possible to develop a radio science software pattern language. In the context of software engineering, a pattern is a general solution to a recurring problem that has well-understood consequences and implications for the software system in which it is used. A pattern language is a collection of such patterns that are relevant to a particular problem domain. This language forms the basis for describing the software system design and organization at a very high level, which is independent of any particular implementation.

One of the major efforts of the Open Radar initiative is to identify and document the important patterns for radio science applications, and to create interfaces, protocols, and reference implementations that allow new radio science systems to be constructed in terms of these patterns. By modularizing the functionality of our instruments in terms of well-defined software patterns, we can provide building blocks that ease the construction of instruments tailored to particular purposes. Once these components are developed, the implementation of a given Software Radar architecture becomes less expensive as time goes on, due to the availability of the fundamental building blocks combined with the continued improvement of computing and networking hardware. The common patterns, interfaces, and protocols will also allow the signal-processing, visualization, and data-management capabilities developed for one system to be shared by another, in many cases.

The effort required to develop a robust production-quality Software Radar architecture, and to incorporate emerging technologies into ionospheric radar systems, is not insignificant. While larger research groups may be able to support the cost of developing custom solutions using the latest technologies, it will be difficult for smaller programs and projects to take full advantage of these developments. A portion of this development burden can be offset by the reuse of radar hardware and software designs and ideas through online, open-source repositories. The Open Radar Initiative will encourage this reuse by maintaining an online resource for radio-science-related reference designs, software patterns, hardware components, documentation, advice, and data protocols.

The availability of well-defined and documented building blocks will also have the added benefit of allowing new investigators to construct radio science systems to address particular scientific issues in a manner that takes advantage of design experience gained from other systems. This may be most attractive to individuals or organizations that would prefer to focus their effort on solving scientific problems, and not on mastering the full complexity of modern technology.

Beyond the context of ionospheric radar, these technologies have fundamental importance to the entire radio science community. The hardware and software components required to construct and operate a radar system are functionally similar to those needed in riometers, beacon tomography and scintillation systems, ionospheric sounders, and radio-astronomy telescopes. While the Open Radar Initiative will not always be able to directly address the needs of these diverse communities, it will form both an example and a resource for those interested in applying similar techniques to other problem domains.

2. Community Participation

The Open Radar Initiative functions as an online community through the Web site http://www.openradar.org, and this is where the designs, software components, and mailing lists are available. Individuals or groups interested in participating in the initiative can easily start by joining the mailing lists and contributing to the discussions. We also encourage the community to let others know about the initiative, especially graduate students whose formative research might benefit significantly from collaborative efforts. Those with a strong interest in a particular topic may wish to consider organizing a special-interest group. We are also interested in hosting brief contributed tutorials that address particular aspects of experimental radio science at a level appropriate for beginning graduate students.

We encourage those with radio science related hardware or software architectures, whether conceptual or concrete, to contribute their ideas to the Open Radar Initiative. In particular, if you have radio science related instrument designs, hardware, or software you would like to contribute, please contact us regarding the possibility. Contributions to discussions of interfaces and protocols are especially welcome, and we urge the community to consider these topics when constructing new instrumentation in order to facilitate systems that are compliant with open protocols. Finally, feedback is especially needed for designs from the Open Radar Initiative, whether in the form of suggestions, improvements, or problems encountered.

3. Conclusion

Ultimately, the reason we develop radio science instrumentation is to produce tools that can address fundamental scientific problems in space physics, radio science, plasma physics, aeronomy, and astronomy. Ionospheric radars encompass many important radio science related technologies, and are prime contributors to real-time space-weather diagnostic and forecasting efforts. The growing importance of these activities requires significant refinement of experimental systems to take advantage of the great leaps made possible by modern technologies. In particular, the full exploitation of information technology is a great and growing challenge to the community. The goal of the Open Radar Initiative is to meet this challenge and enable these scientific and operational endeavors.

By coordinating community development efforts, the Open Radar Initiative will help to reduce duplication of effort. As part of this process, the Initiative will develop reference designs for Software Radar systems, establish a unified Radio Science Software Architecture, encourage the free distribution of innovative techniques, and create a forum for the discussion of radio science design and development. These efforts will also enable new participants to begin experimental investigations without the burden of starting major engineering efforts from scratch. In the longer term, the Open Radar Initiative will provide a foundation for the development of a Global Radio Science Network (www.openradar.net) by enabling new classes of distributed radio science instruments. Such a network will soon be possible, and will be a key element for monitoring our geospace environment, and for conducting coordinated global investigations of scientifically interesting phenomenon.

4. Acknowledgment

The authors would like to thank John D. Sahr for useful discussions on these topics.

5. References

1. J. M. Holt, P. J. Erickson, A. M. Gorczyca, and T. Grydeland, "MIDAS-W: A Workstation Based Incoherent Scatter Radar Data Acquisition System," *Annales Geophys.*, **18**, 9, 2000, p. 1234.

2. J. D. Sahr and F. D. Lind, "The Manastash Ridge Radar: A Passive Bistatic Radar for Upper Atmospheric Radio Science," *Radio Science*, **32**, 1997, p. 2345.

3. E. Gamma, R. Helm, R. Johnson, and J. Vlissides, *Design Patterns: Elements of Reusable Object-Oriented Software*, Reading, PA, Addison-Wesley, 1994.

Radio-Frequency Radiation Safety and Health

James C. Lin

Lens Opacification and Radio-Frequency Electromagnetic Radiation

The induction of lens opacity, or cataracts, in the human eye has often been implicated as a potential adverse effect of human exposure to personal-communication radiation, and radio-frequency radiation in general. In the case of mobile phones, some concerns have been expressed when the user holds the mobile-phone handset, or the microwave radiating device, directly in front of the face, exposing the eye to a straight-on incidence of the mobile-phone radiation. Thus, the eyes could potentially be subjected to a higher level of microwave radiation relative to exposures from the side of the head, where the handset is in contact with or next to an ear, and the amount of microwaves reaching the eyes would be substantially lower.

As more high-speed, WiFi (wireless fidelity), and third-generation (3G) personal-communication services are launched worldwide, advanced mobile telecommunication services such as smart phones will enable advanced video and multimedia capabilities. Photo phones or camera phones that allow users to take pictures and send them as e-mail attachments will become more ubiquitous worldwide. The manner in which a handset is held in common usage is about to be radically altered along with the technology of wireless telecommunication. The handset will no longer need to be placed next to the ear. The common usage position of the handset would migrate from the side of the head to anywhere from the side to in front of the face.

A recent paper, which reported numerical computations of the specific absorption rates (SARs) and temperature increases in the human eye for exposure to obliquely incident plane waves, predicted that SAR averaged over the eyeball depends on the angle of incidence and on the frequency of operation [1]. At 900 MHz, the maximum SAR occurs when the wave is incident straight on, while at 1.9 GHz, the SAR is maximum at an incidence angle of 40° relative to normal incidence. This result is not a surprise, but it does provide substantive data, putting any concerns – or lack thereof – and any arguments on the angular dependence of the SAR and its distribution inside the head of a mobile-phone user on more quantitative grounds.

In fact, it is fundamental knowledge that the reflection, scattering, and transmission of microwave energy into material media are functions of the frequency, angle of incidence, curvature, and dielectric permittivity of the material body [2]. They are also a function of the direction of the wave's polarization. For example, at the Brewster angle (45° to 90°, for air-tissue interfaces at 2.5 GHz), a plane wave of microwave radiation, polarized in the plane of incidence (parallel polarization), is almost completely transmitted into a tissue medium [3]. (Most of the energy carried by the incident plane wave in air would be deposited inside the tissue medium.) The magnitude of the reflected microwave is reduced to a minimum at the Brewster angle. Similarly, computed results of the scattering of 915 MHz and 2450 MHz microwaves from prolate spheroidal tissue models showed that the scattered energy varies widely with the angle of observation [4]. It reaches a minimum between the angles of 60° to 90° for a model of the adult head size.

There have been medical case reports of cataract formation in humans following accidental exposure to microwave radiation [5]. Some clinical reports have suggested that posterior capsule changes in the lens were more prominent in microwave workers than in controls [6]. Also, a small number of epidemiological studies of cataracts in humans have appeared in the literature. A case-control study of World War II and Korean War veterans in the US, based on military service and hospital admission records, found that the frequencies of cataract formation were similar for radar and non-radar personnel [7]. A statistically significant difference in lenticular changes between the microwave-exposed and the control group was observed by

James C. Lin is with the University of Illinois at Chicago
851 South Morgan Street (M/C 154)
Chicago, Illinois 60607-7053 USA
Tel: +1 (312) 413-1052 (direct);
+1 (312) 996-3423 (main office)
Fax: +1 (312) 996-6465;
E-mail: lin@uic.edu

[Editor's note: Portions of this column also appeared in J. C. Lin, "Cataracts and Cell-Phone Radiation," *IEEE Antennas and Propagation Magazine*, **45**, 1, February 2003, pp. 171-174.]]

the same authors in a later study [8]. Moreover, an apparent, age-related increase in lens change made the authors postulate that military-type occupational exposure to microwave radiation may be implicated as a stress that increases the rate of lens aging. In the two related studies by Appleton et al. [9, 10], selected military personnel were subjected to ophthalmological examinations, and compared to other military personnel whose history of microwave exposure was deemed unlikely. They concluded that there was no association between military microwave operation and cataract or lens opacification. It is interesting to note that older age groups showed a trend toward lens opacities among exposed personnel. However, since the numbers in some age groups were small, a credible inference could not be made. Moreover, a fair conclusion from the above studies is that they all suffered from a lack of quantitative measures of microwave exposure.

Investigations on the effect of microwave radiation on the ocular system in laboratory animals were initiated soon after the introduction of radar in World War II. These studies have established a time and power threshold for cataractogenesis: induction of cataracts in animals exposed to near-field microwave radiation [11-14].

One of the most intensively investigated frequencies is 2450 MHz, which is in the same frequency band (2400-2500 MHz) used for some wireless local-area networks (WLANs), and for the proposed Bluetooth applications of wireless technology. Specifically, for rabbits exposed to near-field, 2450 MHz, continuous-wave (CW) microwaves, it has been shown that the minimum cataractogenic power density is 150 mW/cm2 for 100 min, which produces a maximum SAR of 138 W/kg in the vitreous body [13, 14]. A retrolental temperature (behind the lens) above 41°C was necessary for production of posterior lens opacities in these rabbits within a few days following exposure. The appearance of maximum temperature near the posterior capsule of the lens agreed with the observation that the peak SAR in the eye was also just behind the lens for the exposure conditions investigated. The maximum temperature in the eye for various ambient, orbital, and microwave exposure conditions has been simulated by using finite-element computer modeling [15]. It is interesting to note that when the retrolental temperature was kept from exceeding 41°C by means of whole-body hypothermia, a single, potentially cataractogenic microwave exposure did not produce any opacity in the lenses of exposed rabbits [13]. These findings support the notion of a thermal mechanism for microwave cataractogenesis.

There is, however, noticeable argument pertaining to whether a temperature rise, or heat, is the only factor, and whether chronic exposure to pulse-modulated radiation of low average power is significant in the production of lens opacity. Some reports allude to delayed biochemical changes that occur in the irradiated lens, i.e., a late decrease in the ascorbic acid and glutathione content of the lens [11]. Others report such ultra-structural changes as alteration of the equatorial and subcapsular cortical fibers in the absence of slit-lamp-detectable changes in lenses exposed repeatedly to near-threshold power densities [16]. Moreover, studies using isolated rat lenses have found that irradiation in vitro with high-power 918 MHz pulses of 10 microsecond width, delivered at various repetition rates, produced histopathological damages at the lens equator [17-19]. Although the threshold at which damage was observed in the lens differed depending on the type of damage, the lowest SAR at which holes within the fiber cells in the equatorial region were observed occurred at 231 W/kg after 6 min of exposure. The damage was about 4.7 times as great as for CW radiation. The ratio of damage decreased when the peak power was decreased. However, the significance of the ultra-structural or histopathological changes cannot be evaluated, since it is not known whether lenses with similar changes will ultimately sustain damage such as a cataract. In addition, extrapolation from in vitro to intact lenses in the whole animal is speculative. Nevertheless, these results suggest that repeated and/or high-power pulsed microwave radiation is capable of causing lenticular damage that is not related to average temperature elevation.

On the other hand, when rhesus monkeys were exposed to 200 mW/cm2 at 2450 MHz for 60 min, no cataract was observed [20]. Using a similar exposure system, a peak temperature of 39°C, which is below the threshold for rabbits, was measured near the posterior pole of the monkey lens. This result suggests an anatomic or species-dependent microwave cataractogenic threshold. Alternatively, and more likely, it may simply be a function of the difference in SAR distribution induced in the two species of animals by the exposure system. The absence of cataracts in the monkeys stems from the fact that the temperature in the lens was below the 41°C threshold, consistent with the thermal mechanism of induction.

An interesting aspect of the results from the recent publication is the expected increase in eye lens temperature of about 0.035°C for an incident power density of 1 mW/cm2 at 900 MHz to 2500 MHz under the most favorable transmission conditions of incidence angles [1]. A linear extrapolation leads to 115 mW/cm2 for the human eye to reach the 41°C cataractogenic threshold, which is slightly lower than the 150 mW/cm2 threshold incident power density for rabbits. The most favorable condition is defined as the most effective angles of incidence with the presence of both vertical and horizontal polarizations.

In addition to the 2.45 GHz frequency band for WLAN and Bluetooth applications, frequencies around 5.8 GHz also are used in WLAN to facilitate mobility of connected devices and appliances. In the case of an indoor WLAN system, the user of the mobile terminal may be in close proximity to the radiating antenna. Computer simulations have been reported for the frequency range between 6 GHz and 30 GHz, where the incident radiation can be approximated by a plane wave. It was shown that the computed SAR distribution in a human eye could give rise

to temperature elevations of the order of 0.04°C in the eye lens, with a normally incident power density of 1 mW/cm^2 at 6 GHz [21]. Accordingly, it would take a linearly extrapolated incident power density of 100 mW/cm^2 at this frequency to raise the temperature in the lens from 37°C to 41°C, compared to the situation at 900 MHz to 2500 MHz.

It is interesting to note that the frequency of 6 GHz has been implicated as the most effective frequency (also the highest frequency investigated in the paper) for inducing a maximum temperature elevation in the human eye. Specifically, the expected maximum temperature increase in the eye was about 0.06°C at an incident power density of 1 mW/cm^2 under the most favorable conditions [1]. However, it is not clear from the published results whether the location of the expected maximum-temperature rise coincides with the lens. In fact, an appraisal of the patterns of temperature distribution induced in the eye from their earlier publication would suggest a SAR distribution trending toward a maximum near the frontal surface of the eye as frequency increases, which is consistent with a diminished field-penetration depth at higher frequencies. Likewise, SAR maxima, or "hot spots," inside the eyeball tend to appear at lower frequencies [22], although it may not necessarily be in or near the lens. Clearly, both the SAR and temperature distributions vary with the frequency and angle of incidence of microwave radiation. Thus, a similar average value for the SAR and temperature of the entire eyeball would not necessarily augur the same for the amplitude or position of maximum SAR and temperature in the lens or the eye.

Taking the results of the recent paper [1] at their face value, the 0.06°C would imply a linearly extrapolated 4°C rise in lens temperature by 67 mW/cm2 of incident 6 GHz microwave radiation. This power density differs significantly from that of the Bernardi et al. study [21]. There are several plausible explanations. For example, the discrepancy could stem from the difference in incidence angles. However, the SARs are essentially maximum at normal incidence. While both studies employed the Finite-Difference Time-Domain (FDTD) numerical technique to compute the SAR values, and used the bio-heat equation to calculate the temperature distribution, there could have been subtle differences in their numerical implementation and parameter selection for their respective models. Although we will not address this issue for the time being, it would be beneficial to briefly compare the computed results on microwave-induced lenticular opacity or cataracts in humans and in animal models to the current safe exposure guidelines.

For example, guidelines promulgated for limiting general-population exposures to microwave radiation range from 1.0 to 10 mW/cm2 (10 to 100 W/m2) for frequencies between 800 MHz and 6000 MHz [23-26]. The linearly extrapolated temperature increases at 10 mW/cm2 are about 0.35°C at 900 MHz to 2500 MHz, and 0.6°C at 6 GHz. The temperature increases are a small fraction of the 4°C reported for cataractogenesis in rabbits. The exact conditions under which these changes may occur in human beings are disputable. However, linear extrapolations of computed results indicate that the incident density required for the human eye to reach the cataractogenic threshold may be only slightly lower than that needed for rabbits. Thus, any concern for microwave radiation, within the exposure guidelines, inducing cataracts in humans may be exaggerated.

References

1. A. Hirata, H. Watanabe, T. Shiozawa, "SAR and Temperature Increase in the Human Eye Induced by Obliquely Incident Plane Waves," *IEEE Transactions on Electromagnetic Compatibility*, **44**, 4, 2002, pp. 592-594.

2. A. Ishimaru, *Electromagnetic Wave Propagation, Radiation and Scattering*, Englewood Cliffs, NJ, Prentice-Hall, 1996.

3. J. C. Lin and O. P. Gandhi, "Computer Methods for Predicting Field Intensity," in C. Polk and E. Postow, (eds.), *Handbook of Biological Effects of Electromagnetic Fields*, *Second Edition*, Boca Raton, FL, CRC Press, 1996, pp. 337-402.

4. J. C. Lin, "Microwave Propagation in Biological Dielectrics with Application to Cardiopulmonary Interrogation," in L. E. Larsen and J. H. Jacobi (ed.), *Medical Applications of Microwave Imaging*, New York IEEE Press, 1986, pp. 47-58.

5. F. G. Hirsch and J. T. Parker, "Bilateral Lenticular Opacities Occurring in a Technician Operating a Microwave Generator," *Arch. Indust. Hyg.*, **6**, 1952, p. 512.

6. M. M. Zaret, "Selected Cases of Microwave Cataracts in Man Associated with Concomitant Annotated Pathologies," in P. Czerski, K. Ostrowski, M. L. Shore, C. Silverman, M. J. Suess, and B. Waldeskog (eds.), *Biologic Effects and Health Hazards of Microwave Radiation*, Warsaw, Poland, Polish Medical Publishers, 1974, pp. 294-301.

7. S. F. Cleary, S. B. Pasternack, and G. W. Beebe, "Cataract Incidence in Radar Workers," *Arch. Environ. Health*, **11**, 1965, pp. 179-182.

8. S. F. Cleary and S. B. Pasternack, "Lenticular Change in Microwave Workers: A Statistical Study," *Arch. Environ. Health*, **12**, 1966, pp. 23-29.

9. B. Appleton and G. C. McCrossen, "Microwave Lens Effects in Humans," *Arch. Ophthalmology*, **88**, 1972, pp. 259-262.

10. B. Appleton, S. Hirsh, R. O. Kinion, M. Soles, G. C. McCrossen, and R. M. Neidlinger, "Microwave Lens Effects in Humans," *Arch. Ophthalmol.*, **93**, 1975, pp. 257-258.

11. R. L. Carpenter and C. A. van Ummersen, "The Action of Microwave Radiation on the Eye," *J. Microwave Power*, **3**, 1968, pp. 3-19.

12. R. L. Carpenter, "Ocular Effects of Microwave Radiation," *Bull. New York Acad. Medicine*, **55**, 1979, pp. 1048-1057.

13. P. O. Kramar, A. F. Emery, A. W. Guy, and J. C. Lin, "The Ocular Effects of Microwaves on Hypothermic Rabbits: A Study of Microwave Cataractogenic Mechanisms," *Annals of New York Academy of Sciences*, **247**, 1975, pp. 155-156.

14.A. W. Guy, J. C. Lin, P. O. Kramar, and A. F. Emery, "Effect of 2450 MHz on the Rabbit Eye," *IEEE Trans. on Microwave Theory & Techniques*, **23**, 1975, pp. 492-498.

15.A. F. Emery, P. Kramar, A. W. Guy and J. C. Lin, "Microwave Induced Temperature Rises in Rabbit Eyes in Cataract Research," *J. of Heat Transfer*, **97**, 1975, pp. 123-128.

16.R. J. Williams, A. McKee, and E. D. Finch, "Ultrastructural Changes in the Rabbit Lens Induced by Microwave Radiation," *Annals NY Acad. Sci.*, **247**, 1975, pp. 166-174.

17.. J. Stewart-DeHaan, M. O. Creighton, L. E. Larsen, J. H. Jacobi, W. M. Ross, M. Sanwal, T. C. Guo, W. W. Guo, and J. R. Trivithick, "In Vitro Studies of Microwave-Induced Cataract. Separation of Field and Heating Effects," *Exp. Eye Research*, **36**, 1983, pp. 75-90.

18.P. J. Stewart-DeHaan, M. O. Creighton, L. E. Larsen, J. H. Jacobi, W. M. Ross, M. Sanwal, J. C. Baskerville, and J. R. Trivithick, "In Vitro Studies of Microwave-Induced Cataract. Reciprocity Between Exposure Duration and Dose Rate for Pulsed Microwaves," *Exp. Eye Research*, **40**, 1985, pp. 1-13.

19.M. O. Creighton, L. E. Larsen, P. J. Stewart-DeHaan, J. H. Jacobi, M. Sanwal, J. C. Baskerville, H. E. Bassen, D. O. Brown, and J. R. Trivithick, "In Vitro Studies of Microwave Induced Cataract. II Comparison of Damage Observed for CW and Pulsed Microwaves," *Exp. Eye Research*, **45**, 1987, pp. 357-373.

20.P. O. Kramar, C. Harris, A. F. Emery, and A. W. Guy, "Acute Microwave Irradiation and Cataract Formation in Rabbits and Monkeys," *J. Microwave Power*, **11**, 1978, pp. 135-136.

21.P. Bernardi, M. Cavagnaro, S. Pisa, and E. Piuzzi, "SAR Distribution and Temperature Increase in an Anatomical Model of the Human Eye Exposed to the Field Radiated by the User Antenna in a Wireless LAN," *IEEE Transactions on Microwave Theory & Techniques*, **MTT-46**, 1998, pp. 2074-2082.

22.. Hirata, S. Matsuyama, and T. Shiozawa, "Temperature Rises in the Human Eye Exposed to EM Waves in the Frequency Range 0.6-6 GHz," *IEEE Transactions on Electromagnetic Compatibility*, **EMC-42**, 4, 2000, pp. 386-393.

23.FCC, "Guidelines for Evaluating the Environmental Effects of Radiofrequency Radiation," FCC 96-326, Washington, DC, 1996.

24.NCRP, "Biological Effects and Exposure Criteria for Radiofrequency Electromagnetic Fields," NCRP Report No. 86, National Council on Radiation Protection and Measurement, Bethesda, MD,1986.

25.ICNIRP, "Guidelines for Limiting Exposure to Time-varying Electric, Magnetic, and Electromagnetic Fields (Up to 300 GHz)," *Health Physics*, **74**, 4, 1998, pp. 494-522

26.IEEE/ANSI, "Standard for Safety Levels with Respect to Human Exposure to Radio Frequency Electromagnetic Fields, 3 kHz to 300 GHz," IEEE Std. C95.1, Institute of Electrical and Electronics Engineers, Inc., New York, 1999.

Conferences

CONFERENCE REPORTS

EMC ZURICH '03

Zurich, Switzerland, 18 - 20 February 2003

The 15th International Zurich Symposium and Technical Exhibition on Electromagnetic Compatibility (EMC Zurich '03) was held from February 18 through 20, 2003 at the Swiss Federal Institute of Technology in Zurich (ETH Zurich), Switzerland. The meeting was attended by 475 participants from 41 countries and has included 31 exhibitor booths.

As in the preceding years, the Symposium was sponsored by the SEV Association for Electrical Engineering, Power and Information Technologies and has been jointly organized by the Communication Technology Laboratory and the Laboratory for Electromagnetic Fields and Microwave Electronics of the ETH Zurich. Prof. Dr. R. Vahldieck and Dr. G. Meyer acted as symposium president and symposium chairman, respectively. The technical program committee was chaired by Prof. Dr. F. Tesche (Clemson, USA).

A number of international and national professional organizations were cooperating, e.g. IEEE, ITU and URSI. As in the past URSI Commissions E has sponsored the participation of young scientists.

A total of 131 carefully selected technical papers were presented in 19 sessions devoted to: Signal integrity and CAD modeling, radio noise, EM field sensors, wired networks, intentional EMI, base stations and non-ionizing radiation, transmission lines and cables, test chambers, EMC modeling, EMC innovation, emission and immunity testing, power and rail system and components, large chip and package EMC modeling, automotive EMC, system EMC, lightning and its effects, analysis of electrically large systems, shielding and instrumentation and measurement. The sessions covered virtually all EMC "hot" topics and reviewed the current status as well as future trends of EMC technology. The full text of the presentations has been made available in the symposium proceedings and on a CD-ROM.

As in previous symposia the program did not exclusively address experts. An introduction to EMC technology for newcomers was offered by four tutorial lectures and four workshops. The Industrial Forum took place on Thursday and was intended to give the EMC industry a platform to present not so scientific and more practical issues with a total of seven contributions.

For the student paper competition, a total of 14 papers have been submitted. Of those the TPC has pre-selected the three best. A final presentation during the conference in front of a jury decided about final ranking.

Once again, a number of national and international organizations used the opportunity of the symposium to held open and closed meetings in coordination with EMC Zurich. An insight into the work of URSI Commission E was offered by an open meeting dealing with the progress in the different working groups and identifying outstanding topics and new lines of future research. The research cooperation on Sustainable Mobile Communication organized a meeting on "Exposure to GSM radiation". Their mission is to support innovative research on EMF risks attributed to cellular phone technology. A further open meeting was organized by the IARU (International Amateur Radio Union) on EMC problems experienced and caused by radio amateurs. The contributions of these joint events have been made available in a supplement to the symposium proceedings.

Centres of gravity of this symposium have been the field of EMC analysis and prediction with five sessions and two tutorials devoted to this area. These sessions focused on the continuous developments of numerical methods for modelling, analysis, prediction and mitigation of EMC effects. The basic strategies rely on a step-by-step treatment of well-structured EMC scenarios at different topological levels. Better defined and simpler test methods, with reduced measurement uncertainty, could significantly reduce the cost of design and testing of the final product. Four sessions and three workshops have dealt with this area. Testing gives the final answer to EMC, and sophisticated sensors and probes are prerequisites for efficient testing. Automotive EMC was also a main topic of this symposium.

It is difficult to point out general trends in the field of EMC but with the growing interest in theoretical models and numerical methods, the role of computers is becoming more and more important. Also with the trends to higher integration and to nanotechnology, EMC models and tools for MMCs, microsensors and nanomachines are gaining attention and new effects will have to be taken into account.

As usual, the Technical Exhibition has significantly contributed to the success of EMC Zurich'01 by demonstrating the fast conversion of theoretical knowledge into state-of-the-art hard- and software.

The traditional inquiry returned some very interesting suggestions for the next EMC Zurich Symposium which is planned for February 16 through 20, 2005. The call for papers of the 16th International Zurich Symposium and Technical Exhibition on EMC is scheduled for November 2003. This symposium will take place during the year in which the Swiss Federal Institute of Technology celebrates its 150th anniversary. EMC Zurich '05 will be one of the first events under the umbrella of this anniversary.

Dr. G. Meyer, Chairman
gmeyer@nari.ee.ethz.ch

Spatio-Temporal Analysis of Multipoint Measurements in Space (STAMMS)

Cluster input to Critical Issues in Magnetospheric Physics

Orléans, France, 12 - 16 May 2003

The Cluster mission, with its four identical spacecraft, has so far been one of the most successful missions of the European Space Agency, delivering data with unprecedented resolution and providing a wealth of novel information about the Earth's environment (magnetosphere and solar wind). Three years after its launch, it seemed appropriate to evaluate the contribution of Cluster to some of the key problems in magnetospheric and solar-terrestrial science.

More than 100 scientists from the space plasma physics community gathered during four days in Orléans for this STAMMS conference, which was organised in five topical sessions :

1) Remote sensing with Cluster: what new insight does Cluster provide into the localization of remote sources ?
2) Local plasma characterization with Cluster : how does the spatial resolution of Cluster contribute to our understanding of local plasma properties, such as turbulence ?
3) Thick layers : what is the contribution of Cluster to the understanding of discontinuities and boundaries in geospace ?
4) Boundary dynamics and transfers : our view of the Earth's bow shock and the magnetotail before and after Cluster.
5) Summary and perspectives : what are the strategies for future multipoint missions ?

Each session covered various aspects such as wave measurements, particle measurements, simulations and coordinated ground-space measurements.

Cluster represents a turning point, as it is the first mission in geospace to provide 3D spatial resolution. It has been and will remain a challenge to properly exploit this unique capacity. Even though a small fraction only of Cluster data has been studied so far, everyone agreed upon that this mission represents a breakthrough in our understanding of magnetospheric physics. And the best is probably still to come. The mission is planned to continue until the end of year 2005, and the scientific exploitation is expected to be pursued for many years after that. The session summaries of the conference are available on the website (http://web.cnrs-orleans.fr/~weblpce/stamms).

Our thanks are directed to the session conveners for helping set up the programme, and to the many sponsors (among which URSI commission H) who made it possible to organise this successful event in a pleasant environment.

Thierry Dudok de Wit
ddwit@cnrs-orleans.fr

Tenth International Workshop on Technical and Scientific Aspects of MST Radar - MST10

Universidad de Piura, Northern Peru, 13 - 20 May 2003

Tenth International Workshop on Technical and Scientific Aspects of MST Radar - MST10 - was held 13-20 May 2003 at the campus of the Universidad de Piura in northern Peru. These international workshops are held every 2-3 years and comprise major events gathering together experts from all over the world, engaged in research and development of radar techniques to study the mesosphere, stratosphere and troposphere (MST). It includes also ionospheric coherent scatter radars and planetary boundary layer radars. It offers excellent opportunities to young scientists, research students and also new entrants to the field for close interactions with the well-known experts on all technical and scientific aspects of MST radar methods.

As a new approach, the workshop consisted of two major parts: (Section I) standard workshop papers presented orally or as posters, and (Section II) a brain-storming session with the aim to highlight open questions and potential solutions, to produce proposals for innovative approaches, define new programs and prepare recommendations and resolutions.

The Universidad de Piura (UDEP) is known in radar circles due to its operation of ST and boundary layer radars, which are part of the activities of the Instituto Geofisico del Peru (IGP), operating the Jicamarca Radio Observatory (JRO), in collaboration with institutions like the University of Colorado (via CIRES) and NOAA (via the Aeronomy Laboratory).

Sponsors of MST10 were the Scientific Committee on Solar Terrestrial Physics (SCOSTEP), the International Union of Radio Science (URSI), the National Science Foundation (NSF) of USA, Consejo National de Ciencia y Technologia (CONCYTEC) of Peru and various research and development companies.

The International Steering Committee of MST10 consisted of J. Röttger (Chair, Germany), J. Chau (Peru), S. Fukao (Japan), E. Kudeki (USA), and R. Woodman (Peru). Adherent to the International Steering Committee were the Chairpersons of the MST Radar Permanent Working Groups P. Chilson (USA), D. Holdsworth (Australia), G. Nastrom (USA), P.B. Rao (India), and M. Yamamoto (Japan). Honorary Members of the Steering Committee were M.F. Larsen (USA), C.H. Liu (Taiwan), A.P. Mitra (India). The National Organizing Committee of MST10 consisted of: R. Woodman (Chair, IGP), J. Chau (JRO-IGP), Antonio Mabres (UDEP) and M. Sarango (Ciencia Internacional). The Local Organizing Committee consisted of Rodolfo Rodriguez (Chair), William Ipanaque, and Sergio Balarezo. Session conveners and session chair persons were drawn from the international scientific community.

The workshop was opened on Tuesday morning, 13 May 2003, in the presence of the President of the Piura region, Dr. César Trelles, the President of UDEP, Dr. Antonio Abruña, the Dean of the Faculty of Engineering of

Figure 1: Group Picture

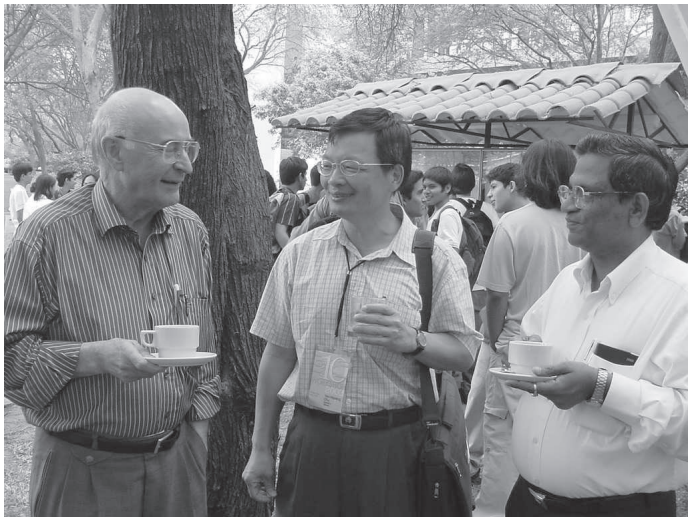

Figure 2: Informal discussions during a coffee break (Dr. Roettger from Germany, Dr. D.N. Rao from India, and Dr. Y.H. Chu from Taiwan)

UDEP, Dr. Sergio Balarezo, the President of the Instituto Geofisico del Perú, Dr. R.F. Woodman and the Chairman of the German Embassy and the Consulate in Piura were represented by R. Niemann and J. M. Irazola.

Participants were from 17 countries from all continents. A total of 175 abstracts had been submitted, and 109 oral papers (24 thereof invited) and 66 poster papers were presented. A tour of the university institutes and facilities as well as the radar systems took place on Thursday afternoon, which was followed by an outing to a nearby horse farm.

During the get-together on Monday evening and the workshop dinner on Thursday evening the workshop participants enjoyed north Peruvian-style folklore, and an extended tour took place on Sunday to visit the famous historical site of Sipan in the northern Peru region.

Public lectures at the university were given by R.F. Woodman on "Space exploration from the ground: Peruvian contributions to human knowledge", and by B.B. Balsley on "A half century of cooperation with my Peruvian colleagues". During the workshop dinner D.T. Farley spoke about his long-lasting experience with Jicamarca and corresponding episodes and adventures.

The hotel facilities were excellent, in short-walking distance to the university campus, and the local organizing committee, supported by Jicamarca personnel and university students, kept track of the very pleasant and highly functional workshop performance.

Session I.1 was on radar scattering processes in the neutral atmosphere (convened by H. Luce and A. Muschinski). This session dealt with observational and theoretical investigations (1) on how to separate the effects of different scattering mechanisms in the same data set, and on (2) radar echo characteristics in different radar configurations and their interpretations are presented. Emphasis of the papers was placed on contributions that discuss new observations (e.g., multi-beam, multi-frequency, multi-receiver, and/or multi-regime radar observations, also inter-comparisons with in situ measurements) on the basis of innovative, first-principle theoretical analysis. Invited talks were given by D. Fritts on direct numerical simulations of turbulence and radar backscatter, and by F. Dalaudier on combined radar and balloon observations. B. Balsley's kite observations, which show very thin structures in the lower troposphere point into the direction of understanding the highly specular radar returns as well.

Session I.2 was on D-, E-, and F-region coherent scattering (convened by D. Hysell and R.D. Palmer). It was devoted to the theory and observation of coherent scatter from ionospheric irregularities at all latitudes. Papers were presented. pertaining to such mature fields of study as the auroral and equatorial electrojets, PMSE, sporadic E-layers, and equatorial spread-F. Recent and planned campaigns like SEEK II, C/NOFS, and CIELO attest to the fact that numerous problems remain unsolved in these areas. In addition, papers on emerging areas of research were given, including long-lived meteor trails, 150 km echoes, daytime spread-F, and mid-latitude spread-F. Novel experimental techniques such as passive radar, networked radar, radar imaging, and coherent scatter Faraday rotation may promote rapid progress in the areas outlined above. Reports describing new experimental radar techniques were given also in section II. Invited papers were given by E. Kudeki on 150-km echoes, J. Chau on E region studies at low-latitudes,

W. Singer et al. on PMSE, F. Lind on E region irregularities at high latitudes, and S. Fukao on the SEEK-2 campaign. Due to short-notice travel cancellation P. Chilson could not give his invited talk on PMSE.

Session I.3 on winds, waves and turbulence in the lower and middle atmosphere and the lower thermosphere

was convened by W.K. Hocking and M.F. Larsen. This session examined recent developments of studies and observations of dynamics in the middle atmosphere and lower thermosphere. Topics of particular interest included wave-wave interaction, wave sources and generation mechanisms, wave deposition processes, non-linear interactions, wave propagation studies, turbulence anisotropy and turbulent transport processes. Correlations of wave events as a function of height, and multi-instrument studies were presented, and inter-comparisons of different techniques were considered to be important. One area of special interest was studies of wave velocity amplitudes and variability in the region above 90 km altitude, with particular interest in determining the frequency of occurrence of large amplitude events and large wind velocities (up to 100 m/s and higher) in this region. D. Fritts gave the invited presentation of P. Franke, who could not attend. This talk expanded the direct numerical simulation of turbulent structures. Investigations on gravity wave break down and the different kind of instabilities done by G. Klaassen were presented by W. Hocking. The invited review on turbulent diffusivity was presented by R. Wilson, and N. Gavrilov gave an invited talk on gravity wave and turbulence studies and drew attention on the possible relation of middle atmosphere gravity wave activity to El Nino.

K. Gage and D. Riggin convened **Session I.4** on meteorological phenomena and applications. It was concerned with recent developments in Doppler radar profiling in the lower neutral atmosphere, especially studies of lower atmospheric phenomena made with profilers in combination with other instruments during field campaigns. Topics of interest included the assimilation of profiler data in meteorological models, quality control of profiler data, operational networks of profilers and the impact of profiler data on forecasting. Of special interest were studies that demonstrate the utility of profiling for quantifying the vertical structure of turbulence, humidity, cloud and precipitation fields including drop size distributions and their variability. The invited talks were given by K. Gage (on behalf of S. Koch) on mesoscale analysis and prediction using wind profiler data and by C. Williams and K. Gage on rain drop size distributions deduced from profiler observations.

The operational aspects and recent system developments were handled in **Session I.5**, which was convened by I. Reid and D. Thorsen. The focus was on aspects related to the technical performance of radar systems and multi-instrument measurements. Papers pertaining to all aspects of technical performance of current and/or proposed facilities, including the unique problems associated with operation of remote stations were included. These aspects related as well to pros and cons of system configurations and measurement methods. It was addressed how multi-instruments can be used together to augment scientific research as well as how measurements from diverse instruments (including models) may be appropriately compared.

Short reports and summary presentations on the **Permanent Working Groups (PWGs)** activities were presented at the beginning of the second workshop week. These PWGs deal with (1) system calibration and definitions, (2) data analysis, validation, and parameter reduction methods, (3) accuracies and requirements for meteorological applications, and (4) international collaborations and education.

This was followed by **Section II on "Novel perspectives and unsolved issues".** To stimulate brain storming in this section, several invited talks were presented. T. Sato and K. Kamino introduced an adaptive clutter rejection scheme for MST radars, W. Hocking evaluated diagnostic capabilities of measurements of backscatter anisotropy, H. Luce reviewed the future of the multi-frequency techniques, J. Röttger asked what is turbulence seen by VHF radars, W. Hocking et al. reported about potential applications of a world-wide network of mesospheric radars with special emphasis on the Columbia space shuttle disaster, A. and E. Praskovsky presented a structure-function-based approach to data analysis for spaced antenna radars, and J. Sahr proposed VHF parasitic radar interferometry for MST zenith sounding. These presentations lead to distinct lively discussions. These were summarized in the final plenary session together with reports on the oral poster sessions prepared by the chairpersons.

The **Plenary and Closing Session** was held on Tuesday afternoon and chaired by J. Röttger. It included discussions of the highlights presented in the oral and poster workshop papers of Section I and in particular important issues and questions raised in the presentations of Section II.

The written reports of the session conveners and chairpersons formed a suitable input for the final discussions, which concentrated on topics such as (to mention just a few): Identification of backscattering mechanism by statistical analysis and the Direct Numerical Simulation. Here the questions were how DNS can model turbulence decay and how one can expand the modeling for multiple gravity waves and their breaking. The question on the realistic meaning of the effective diffusivity and turbulence energy dissipation rate remains to be studied. A dominant item seems to be the contributions of ST radars for the studies of stratosphere-troposphere exchange. Interesting and not yet solved topics are the scattering mechanism of polar mesosphere summer echoes, their structure and inter-hemispheric difference. The creation and propagation of gravity waves from low altitudes to higher altitudes in the mesosphere and lower thermosphere, and their momentum and energy dissipation. Also the E- and F-region

Other participants at lunch: D. Hysell (US), E. Kudeki (Turkey), J. Roettger (Germany), G. Lehmacher (Germany), H. Bahcivan (Turkey), J. Chau (Peru), C. Haldoupis (Greece), G. Hussey (Canada), G. Hassenpflug (South Africa)

irregularities, leading to coherent scatter, are still a relevant item and open questions were summarized, such as their generation mechanisms and their relation to coupling with above (electric fields) and below (gravity waves and tides).

Several approaches are in use to analyze and interpret spaced antenna and interferometer observations and the pros and cons are disputed. Imaging techniques are highlights of the recent developments to understand the structure and dynamics of the atmosphere. A promising idea is to apply the parasitic radar method for lower atmosphere studies. Combination with other techniques, such as the application aspects of the wind profilers, providing data for improving forecasting and modeling, are a most recognized spin-off of the MST radar technique.

The activities of the Permanent Working Groups were evaluated and it was resolved that these groups, which are mostly dormant between workshops, should become part of a discussion group on topical issues, which should be introduced and handled via the internet. The present workshop homepage http://jro.igp.gob.pe/mst10 forms a suitable forum for this purpose.

The normal abstracts of all papers were published by the local organizers in the abstract proceedings. Extended abstracts will be published on CD-ROM and as hardcopy, as usual, in the final workshop proceedings. An editorial team at the Jicamarca Radar Observatory takes care of this duty, supported by the steering committee. Full manuscripts can be submitted for potential publication in a special MST radar issue of the journal Annales Geophysicae. These manuscripts undergo the standard refereeing procedure, where the guest editors are D. Hooper and D.N. Rao. A call for papers has been distributed to all, who had submitted abstracts for MST10.

Several proposals for resolutions were discussed. The one on educational issues aims towards continuing and expanding the international radar schools, such as ISAR, but also supporting the tendencies for establishing regular schools on national levels as well as forming permanent departments on atmospheric radar at universities and other institutions. Concentrated efforts should be undertaken, supported by a resolution, to understand the hemispheric difference and frequency dependence of PMSE using calibrated radar systems. To improve the understanding of dynamical processes in low latitudes, special campaigns and in particular a tropical network of radars on a global scale was proposed and is laid down in a resolution. In general it was felt that the MST radar technique, although basically mature, still expects further and deeper understanding of the atmosphere by introducing new techniques, establishing new observation sites and upgrading existing facilities. Another resolution covers research requirements to understand mid-latitude E-region irregularities. These resolutions will be published in the final proceedings and submitted to the sponsoring organizations as well as other governing agencies.

The character of the workshop was discussed and it was felt that the addition of a brain storming section to foster new directions has raised the quality of the MST radar workshop. It was decided to continue with these workshops, and also keep the time frame of 8 days, not starting on Monday and including one weekend. Invitations to hold the next workshop - MST11 - were received from Australia, Germany and India. It was noted that Australia had twice been candidate before, but the final decision was postponed to allow more information of the community about the possible venue.

The workshop was closed on Tuesday afternoon leaving in the minds of the participants proper updates on scientific research and technical developments, potential approaches of open questions, views into a promising future and most delightful impressions on the University of Piura and the appreciation of the whole-hearted contributions by the members of the local organizing committee.

Those, who were still present after the workshop had the chance to see the tropical sunset at the nearby ocean front of Colan, - an ultimate finale of a successful workshop on atmospheric research. Our sincere particular thanks for the most efficient performance of MST10 are directed to the sponsors, the University of Piura and the staff of the local organizing committee.

Jürgen Röttger and Jorge Chau
roettger@linmpi.mpg.de
chau@jro.igp.gob.pe

CONFERENCE ANNOUNCEMENT

2004 URSI International Symposium on Electromagnetic Theory

Pisa, Italy, 23 - 27 May 2004

General Information

In a long tradition, Commission B, "Fields and Waves", of the International Union of Radio Science (URSI) organizes a triennial series of International Symposia on Electromagnetic Theory. The next symposium in this series is the 2004 International Symposium on Electromagnetic Theory, which will be held in Pisa, Italy, May 23-27, 2004. It is hosted by the Italian Member Committee of URSI and is organized by a Local Organizing Committee at the University of Pisa, in collaboration with the Italian Electromagnetic Society (SIEm). The scope of the Symposium covers all areas of electromagnetic theory and its applications. The working language of the Symposium is English. There will be a limited number of Young Scientist Awards (YSA) available for application.

Paper Submission

Authors addressing advancement and describing innovation in all areas of electromagnetic theory and its applications and other topics of interest to URSI are invited to submit contribution for review and eventual presentation in the symposium. Suggested topics and general information are listed in the next page. All submission must be electronic. Note: Two-times submission (Abstract and then final paper) is changed to one-time submission (Paper in 3-pages camera-ready format).

Contributions concerning all aspects of electromagnetic theory and its applications are welcome. Other organized sessions are also indicated on electronic paper submission page of the Web. Novel and innovative contributions are particularly appreciated.

Conference Website

The complete instructions for the electronic paper submission, the manuscript preparation, YSA application, registration and the updated information on the Symposium are available on the conference Web site: **www.ing.unipi.it/URSI-B2004.** Important and original papers will be selected and reviewed by the editorial board for inclusion in Radio Science. Details will be announced on the conference Web site.

Regular Topics

Basic Electromagnetic Theory
- R1 Electromagnetic theory
- R2 Mathematical modelling of EM problems
- R3 Solutions to canonical problems
- R4 Non-linear phenomena

Scattering and Diffraction
- R5 Scattering and diffraction
- R6 High-frequency methods
- R7 Inverse scattering and imaging

Random, Inhomogeneous, Nonlinear and Complex Media
- R8 Propagation and scattering in layered structures
- R9 Random media and rough surfaces
- R10 Complex media
- R11 Beam and pulse propagation and scattering in lossy and/or dispersive media

Computational Techniques
- R12 Numerical methods: general aspects
- R13 Numerical methods for integral and differential equations
- R14 Hybrid methods

Transient Fields
- R15 Time domain methods
- R16 Radiation, scattering and reception of transient fields and/or wide band signals

Guided Waves
- R17 Guided waves

EMC/EMI
- R18 Interaction of EM waves with biological tissues
- R19 Modelling Techniques for EMC/EMI

Antennas
- R20 Antennas: general aspects
- R21 Antenna arrays, planar and conformal
- R22 Smart antennas
- R23 UWB antennas

Systems
- R24 EM theory and applications for radio systems
- R25 Antennas and propagation for communication systems: Mobile, LAN etc.

Others
- R26 Others *(please indicate your specific field)*

Special Topics

- S1 Antennas, switches and circuits using RF MEMS
- S2 Artificial Magnetic, Soft and Hard Surfaces and other Complex Surfaces
- S3 Ground penetrating radars: EM modeling, antennas, imaging and inversion
- S4 Homogenization of electromagnetic material parameters
- S5 Hybrid techniques for large problems
- S6 Metamaterials
- S7 Radiation and Leakage effects in open planar structures
- S8 RF aspects of MIMO antenna systems
- S9 Space Solar Power Systems (Inter Commission WG in URSI)
- S10 The role of electromagnetism in micro- and nano-technologies
- S11 Time-reversal methods
- S12 UWB radio systems

Conference Contacts

Technical Program
Prof. **Makoto ANDO**, Chair,
Commission B of URSI
Department of Electrical and Electronic Engineering
Tokyo Institute of Technology
2-12-1, Oookayama, Meguro
Tokyo 152-8552, Japan
E-mail: mando@antenna.ee.titech.ac.jp
Phone: +81-3-57342563
Fax: +81-3-57342901

Local Arrangements
Prof. **Giuliano MANARA**, Chair
Local Organizing Committee
Department of Information Engineering,
University of Pisa, Via Diotisalvi 2
I-56126 Pisa, Italy
E-mail: g.manara@iet.unipi.it
Phone: +39 050 2217552
Fax: +39 050 2217522

Conference Secretariat

INCOR**,** D.G.M.P. srl
VIA G. Carducci, 62/E
I-56010 – Ghezzano, Pisa, Italy
E-mail: incor@sirius.pisa.it
Phone: +39 050 879740
Fax: +39 050 879812

Deadlines

1 November 2003: Deadline for receipt of YSA papers and YSA applications
15 November 2003: Deadline for receipt of papers
15 January 2004: Acceptance of papers
15 March 2004: Deadline for pre-registration

MSMW '04

Kharkov, Ukraine, 21 - 26 June 2004

The 5th International Kharkov Symposium on Physics and Engineering of Microwaves, Millimeter and Sub-Millimeter Waves (MSMW'04) will be organized in Kharkov, Ukraine on June 21-26, 2004. MSMW symposia were held several times in Kharkov since 1978 as a regular Soviet Union meeting on millimeter (mm) and submm waves and applications. It was owing to the fact that Usikov Institute of Radiophysics and Electronics of the National Academy of Sciences of Ukraine (IRE NASU) has always been one of the major research organizations in this field. It was established in 1955 with the main task of developing mm and submm wave systems for radars, communications, hot-plasma diagnostics in *Tokamak* controlled fusion machines. Institute of Radio Astronomy of the National Academy of Sciences of Ukraine (IRA NASU), which branched off IRE in 1985, performs research in mm-wave radio astronomy. Since 1998, MSMW symposia have English as single working language to facilitate closer interaction between the Western and Former Soviet Union (FSU) scientists and engineers.

Organizers

The National Academy of Sciences of Ukraine Scientific Council on the problem "Radio Physics and Microwave Electronics" in cooperation with IRE NASU, IRA NASU, KNU, IEEE Joint Chapters of Ukraine, and Ukrainian URSI Committee. Co-sponsorship of EuMA, URSI, IEEE ED and MTT Societies, and other international institutions is sought and expected.

Chairman: Prof. Vladimir M. Yakovenko (IRE NASU)
Co-Chairmen: Prof. Leonid M. Lytvynenko (IRA NASU) and Prof. Ilya I. Zalubovsky (KNU)
Co-Organizers: Dr. Alexei A. Kostenko and Prof. Alexander I. Nosich (IRE NASU)Prof. Vladimir M. Yakovenko (IRE NASU)

Suggested Topics

A. Electromagnetic theory and numerical simulation
B. Waves in semiconductors and complex media

C. Microwave superconductivity
D. Wave propagation, radar, remote sensing
E. Signal processing
F. Vacuum sources and amplifiers
G. Quasioptical techniques
H. Antennas
I. Waveguide and integrated circuits
J. Radio astronomy
K. Solid state devices
L. Nanoelectronics
M. Terahertz technology
N. Spectroscopy
O. Complex media and new materials
P. Scientific and industrial applications
Q. Electromagnetic metrology
R. Biomedical applications

Contact

MSMW'2004
IRE NASU, 12
Ac. Proskura St, Kharkov
61085, Ukraine
Phone/Fax: +380 (572) 441105
E-mail:msmw04@ire.kharkov.ua,
Internet: http://www.ire.kharkov.ua/MSMW04/msmw.htm

Deadlines

1-page abstracts by November 1, 2003, 3-page camera-ready papers by February 1, 2004. Instructions will be placed at the MSMW'04 Website.

35TH COSPAR SCIENTIFIC ASSEMBLY AND ASSOCIATED EVENTS

Paris, France, 18 - 25 July 2004

Topics

Approximately 90 meetings covering the fields of COSPAR Scientific Commissions (SC) and Panels.

Scientific Commissions

SC A: The Earth's Surface, Meteorology and Climate
SC B: The Earth-Moon System, Planets, and Small Bodies of the Solar System
SC C: The Upper Atmospheres of the Earth and Planets Including Reference Atmospheres
C0.1: Standards in Space Environments for ISO
C0.2: Advances in Remote Sensing of the Middle and Upper Atmosphere and Ionosphere from Ground and from Space
C1.1: Mesosphere, Thermosphere and Ionosphere Research: Coordinated Ground and Space Observations
C1.2: Thermospheric-Ionospheric Geospheric (TIGER) Symposium
C2.1: Coupling Processes in the MLT Region
C2.3: Long-term Changes of Greenhouse Gases and Ozone & their Influence on the Middle Atmosphere and Lower Thermosphere
C2.4: Atmospheric Electrodynamics and Climate Change
C2.5: Structure and Dynamics of the Arctic and Antarctic Middle Atmosphere
C3.1/B0.7/D3.3:Planetary Upper Atmospheres, Ionospheres and Magnetospheres
C3.2/B0.8: Planetary Atmospheres
C4.1: CIRA: The Development of a New Generation of COSPAR International Reference Atmospheres
C4.2: Advances in Specifying Plasma Temperatures and Ion Composition in the Ionosphere
C4.3/B0.9: Progress in the Development of Mars International Reference Atmosphere (MIRA)
C5.1/D4.1:Applications of Active Experiments for Space and Dusty Plasmas
C5.2/D4.2: Artificial Aurora: Predictions, Observations and Interpretation
SCD: Space Plasmas in the Solar System, Including Planetary Magnetospheres
SC E: Research in Astrophysics from Space
SC F: Life Sciences as Related to Space
SC G: Materials Sciences in Space
SC H: Fundamental Physics in Space

Panels

- Panel on Satellite Dynamics (PSD)
- Panel on Scientific Ballooning (PSB)
- Panel on Potentially Environmentally Detrimental Activities in Space (PEDAS)
- Panel on Standard Radiation Belts (PSRB)
- Panel on Space Weather (PSW)
- Panel on Planetary Protection (PPP)
- Panel on Space Research in Developing Countries (PSRDC)
- Panel on Capacity Building (PCB)
- The Public Understanding of Space Science
- Space Science Education and Outreach

Contact

Secretariat

COSPAR Secretariat
51 bd de Montmorency
75016 Paris, France
Tel: +33 1 45 25 06 79, Fax: +33 1 40 50 98 27
E-mail: cospar@cosparhq.org /
http://www.copernicus.org/COSPAR/COSPAR.html

Scientific Program Chair

Dr. M.L. Chanin
CNRS
Service d'Aeronomie
Verrrieres-le-Buisson, France

The **Abstract deadline** is 15 February 2004. The papers will be published in 'Advances in Space Research'.

URSI CONFERENCE CALENDAR

An up-to-date version of this Conference Calendar, with links to the various conference web sites can be found at http://www.ursi.org/Calendar.html

September 2003

11th Microcoll
Budapest, Hungary, 10-11 September 2003
Contact : Diamond Congress Ltd. – Microcoll, H-1027 Budapest, Fõ u. 68., Hungary, Phone: +36 1 2147701 Fax: +36 1 2012680, E-mail: diamond@diamond-congress.hu, http://www.diamond-congress.hu

CAOL 2003 - International Conference on Advanced Optoelectronics and Lasers
Alushta, Crimea, Ukraine, 16-20 September 2003
Contact : Igor A. Sukhoivanov, Organizing Committee Co-Chair, National University of Radioelectronics, KNURE, Lenin av, 14, 61166 Kharkov, Ukraine, Fax: (+380 572) 409107, Phone: (+380 572) 409484, E-mail: LFNM@kture.kharkov.ua , http://www.kture.kharkov.ua/caol/

October 2003

IRI Workshop
Grahamstown, South Africa, 6–10 October 2003
Contact : Dr. L McKinnell, Hermann Ohlthaver Institute for Aeronomy, Department of Physics and Electronics, Rhodes University, P O Box 94, Grahamstown, 6140, South Africa, Fax: +27 46 622 5049, L.McKinnell@ru.ac.za, (the preferred method of communication is e-mail), http://phlinux.ru.ac.za/hoia/IRI2003

Atmospheric Remote Sensing using Satellite Navigation Systems (Special Symposium of the URSI Joint Working Group FG)
Matera, Italy, 13-15 October 2003
Contact : ESTEC Conference Bureau, Attn. Ms Gonnie Elfering, P.O. Box 299 , NL-2200 AG Noordwijk , The Netherlands , Tel: +31-71-565-5005 , Fax: +31-71-565-5658 , e-mail: confburo@esa.int , http://www.congrex.nl/03c41

Telecom 2003 & JFMMA
Marrakech, Morocco, 15-17 October 2003
Contact : Prof. Ahmed Mamouni, IEMN, Cité Scientifique, Av. Poincaré, B.P. 69, F-59652 Villeneuve d'Ascq, France, Fax +33 3201 97 880, E-mail : ahmed.mamouni@iemn.univ-lille1.fr, http://www.fstg-marrakech.ac.ma/telecom2003.html

November 2003

APMC 2003
Seoul, Korea, 4-7 November 2003
Contact : Prof. Hyo Joon Eom, Dept. of Electrical Engineering, Korea Advanced Institute of Science and Technology, 373-1, Kusong-dong, Yusong-gu, Taejon, Korea, Fax : +82 42-869 8036, hjeom@ee.kaist.ac.kr , http://www.apmc2003.org

ClimDiff'03
Fortaleza, Brazil, 17-19 November 2003
Contact : Dr. Emanoel Costa, CETUC-PUC/Rio, Rua Marques de São Vicente 225, 22453-900 Rio de Janeiro RJ, Brazil, E-mail: "Emanoel Costa" epoc@cetuc.puc-rio.br , http://www.climdiff.com

May 2004

EMTS'04 - 2004 International Symposium on Electromagnetic Theory
Pisa, Italy, 23-27 May 2004
Contact persons : Prof. Makoto Ando, Commission B Chair, Dept. of Electrical and Electronic Engineering, Tokyo Institute of Technology, J2-12-1, Oookayama, Meguro, Tokyo152-8552, Japan, E-mail: mando@antenna.ee.titech.ac.jp and Prof. Lotfollah Shafai, Commission B Vice-Chair, Dept. of Electrical & Computer Eng., University of Manitoba, 15 Gillson Street, Winnipeg, MB R3T 5V6, Canada, E-mail: shafai@ee.umanitoba.ca

June 2004

EMC'04 Sendai - 2004 International Symposium on Electromagnetic Compatibilty/Sendai
Sendai, Japan, 1-4 June 2004
Contact : Prof. R. Koga, Dept. of Communications Network Engineering, Okayama University, Japan, koga@cne.okayama-u.ac.jp , www.dev.cne.okayama-u.ac.jp

August 2004

ISAP'04 - 2004 Int. Symp. on Antennas and Propagation
Sendai, Japan, 17-21 August 2004
Contact : ISAP'04, Attn. Dr. Tokio Taga, NTT DoCoMo, Inc., 3-5, Hikarino-oka, Yokosuka, 239-8536 Japan, E-mail : isap-2004@mail.ieice.org , http://www.ieice.org/cs/isap/2004

AP-RASC 2004 - 2nd Asia-Pacific Radio Science Conference
Beijing, China, 20-23 August 2004
Contact : Prof. Zong Sha, China Research Institute of Radio Propagation, P.O. Box 134-70, 100040 Beijing, China (CIE), Phone : +86 10-6821-2267, Fax : +86 10-6821-6857, E-mail : z.sha@ieee.org, or Mr. Liu Dayong, cient@public3.bta.net.cn, http://www.cie-china.org:ap-rasc/

September 2004

Bianisotropics '04
Ghent, Belgium, 22-24 September 2004
Contact: Isabelle Van Der Elstraeten, INTEC, Sint-Pietersnieuwstraat 41, B-9000 Gent, Belgium, Tel: +32 (0) 92643321, Fax: +32 (0) 92643593, E-mail : isabelle.vanderelstraeten@intec.ugent.be, http://www.intec.ugent.be/bian04

November 2004

JINA 2004 - International symposium on Antennas
Nice, France, 8-10 November 2004
Contact : Secretariat JINA, France Telecom R&D, Fort de La Tête de Chien, F-06320 La Turbie, France, Fax : +33 4 92 10 65 19, E-mail : jina.2004@wanadoo.fr, Web site : http://www.jina2004.com

An up-to-date version of this Conference Calendar, with links to the various conference web sites can be found at http://www.ursi.org/Calendar.html
Do you wish to announce your meeting in this Calendar? More information about URSI-sponsored meetings can be found on our Homepage at : http://www.ursi.org/Rules.html
URSI cannot be held responsible for any errors contained in this list of meetings

UTC Time Step

On n'introduira pas de seconde intercalaire à la fin de décembre 2003.
La différence entre UTI et le Temps Atomique International TAI est :
du 1er janvier 1999, 0h UTC, jusqu'à nouvel avis : UTC - TAI = -32 s
Des secondes intercalaires peuvent être introduites à la fin des mois de décembre ou de juin, selon l'évolution de UT1-TAI. Le Bulletin C est diffusé deux fois par an, soit pour annoncer un saut de seconde, soit pour confirmer qu'il n'y aura pas de saut de seconde à la prochaine date possible.

No positive leap second will be introduced at the end of December 2003.
The difference between UTC and the International Atomic Time TAI is :
from 1999 January 1, 0 h UTC, until further notice : UTC - TAI = -32 s
Leap seconds can be introduced in UTC at the end of the months of December and June, depending on the evolution of UT1-TAI. Bulletin C is mailed every six months, either to announce a time step in UTC, or to confirm that there is no time step at the next possible date.

Daniel GAMBIS
Director, Earth Orientation Center of IERS
Fax: +33 1-40 512291
E-mail: iers@obspm.fr

URSI Publications

Modern Radio Science 1999

Editor: Maria Stuchly
ISBN 0-7803-6002-8
List Price : USD 49.95 Member Price : USD 45.00
IEEE Product No. PC5837

Published by Oxford University Press
in cooperation with URSI and IEEE Press
Order 24 hours a day, 7 days a week :
1-732-981 0060 (Worldwide)
1-800-678 4333 (USA & Canada)
Fax 1-732 981 9667
E-mail : customer-service@ieee.org

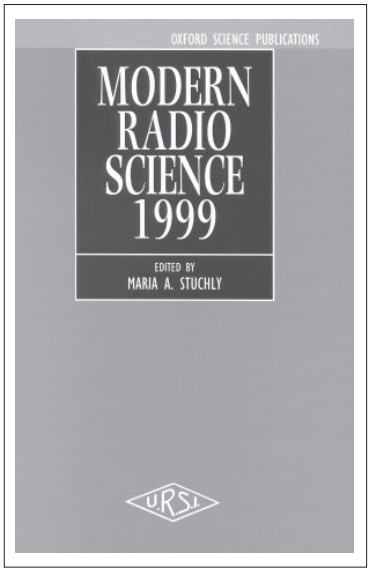

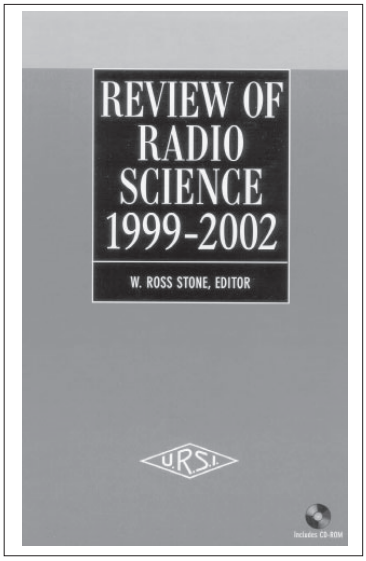

Review of Radio Science 1999-2002

Editor: W. Ross Stone
July 2002/Hardcover/977 pp
ISBN 0-471-26866-6
List Price : USD 125.00 Member Price : USD 106.25
IEEE Product No. #18493

Published by Wiley-Interscience
in cooperation with URSI and IEEE Press
Order can be sent to John Wiley & Sons, Inc.
from 8.30 a.m. to 5.30 p.m. :
1-732-469-4400 (Worldwide)
1-800-225-5945 (USA & Canada)
Fax 1-732 302-2370
E-mail : customer@wiley.com

Handbook on Radiopropagation Related to Satellite Communications in Tropical and Subtropical Countries

Editor: G.O. Ajayi
with the collaboration of :
S. Feng, S.M. Radicella, B.M. Reddy

Available from the URSI Secretariat
c/o Ghent University (INTEC)
Sint-Pietersnieuwstraat 41
B-9000 Gent, Belgium
tel. +32 9-264-33-20
fax +32 9-264-42-88
e-mail : ursi@intec.rug.ac.be

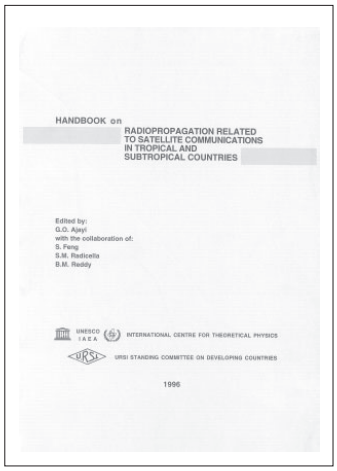

RADIO SCIENCE *Bimonthly!*

Radio Science contains original articles on all aspects of electromagnetic phenomena related to physical problems. Covers the propagation through and interaction of electromagnetic waves with geophysical media, biological media, plasmas, and man-made structures. Also included, but not limited to, are papers on the application of electromagnetic techniques to remote sensing of the Earth and its environment, telecommunications, signals and systems, the ionosphere, and radio astronomy.
ISSN 0048-6604.

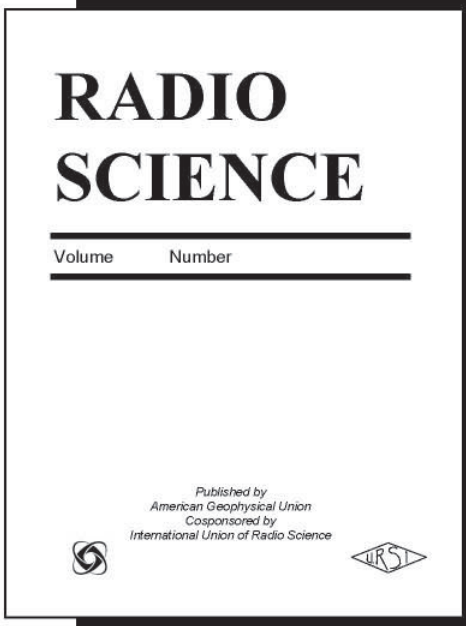

See a recent Table of Contents on the web!
www.agu.org/ pubs/inpress.html

2003 Subscription Rates: On-line / Print / On-line+Print

AGU Members & U.R.S.I. correspondents:	**$33 / $55 / $65**
Student AGU Members:	**$17 / $35 / $35**

Postal surcharges outside of North America: surface postage $22, air freight $51, air mail $84.

Subscribe Today!

	European Office	U.S. Office
Online:	www.agu.org	www.agu.org
E-Mail:	agu@copernicus.org	orders@.agu.org
Voice:	+49-5556-1440	+1-202-462-6900
Fax:	+49-5556-4709	+1-202-328-0566
Mail:	AGU - Orders Max-Planck Str. 13 37191 Katlenburg-Lindau GERMANY	AGU - Orders 2000 Florida Ave., NW Washington, DC 20009 USA

Submit to *Radio Science*!

Submissions to *Radio Science* are now done through the new **GEMS** electronic submissions system at **http://radioscience-submit.agu.org/**

For details on style, contact an editor's assistant listed below or consult the last pages of a recent issue of *Radio Science*.

Tarek M. Habashy, Editor
Schlumberger Doll Research
Electromagnetic Department
Old Quarry Road
RC, CT 06877
Ph: 203-431-5563
Fax: 203-438-3819
email: thabashy@ridgefield.oilfield.slb.com

Cosponsored by U.R.S.I. International and published bimonthly by AGU.

Members of the Network of U.R.S.I. Correspondents may subscribe at the AGU member rate!

AGU

Code: URSI03

Wireless Networks

The journal of mobile communication, computation and information

Editor-in-Chief:
Imrich Chlamtac
Distinguished Chair in Telecommunications
Professor of Electrical Engineering
The University of Texas at Dallas
P.O. Box 830688, MS EC33
Richardson, TX 75083-0688
email: chlamtac@acm.org

Aims & Scope:
The wireless communication revolution is bringing fundamental changes to data networking, telecommunication, and is making integrated networks a reality. By freeing the user from the cord, personal communications networks, wireless LAN's, mobile radio networks and cellular systems, harbor the promise of fully distributed mobile computing and communications, any time, anywhere. Numerous wireless services are also maturing and are poised to change the way and scope of communication. WINET focuses on the networking and user aspects of this field. It provides a single common and global forum for archival value contributions documenting these fast growing areas of interest. The journal publishes refereed articles dealing with research, experience and management issues of wireless networks. Its aim is to allow the reader to benefit from experience, problems and solutions described. Regularly addressed issues include: Network architectures for Personal Communications Systems, wireless LAN's, radio , tactical and other wireless networks, design and analysis of protocols, network management and network performance, network services and service integration, nomadic computing, internetworking with cable and other wireless networks, standardization and regulatory issues, specific system descriptions, applications and user interface, and enabling technologies for wireless networks.

Wireless Networks is a joint publication of the ACM and Baltzer Science Publishers. Officially sponsored by URSI

For a complete overview on what has been and will be published in Telecommunication Systems please consult our homepage:

BALTZER SCIENCE PUBLISHERSHOMEPAGE
http://www.baltzer.nl/winet

Special Discount for URSI Radioscientists

Euro 62 / US$ 65
(including mailing and handling)

Wireless Networks ISSN 1022-0038
Contact: Mrs. Inge Heleu
Fax +32 9 264 42 88 E-mail ursi@intec.rug.ac.be
Non members/Institutions: contact Baltzer Science Publishers

BALTZER SCIENCE PUBLISHERS
P.O.Box 221, 1400 AE Bussum, The Netherlands
Tel: +31 35 6954250 Fax: +31 35 6954 258 E-mail: publish@baltzer.nl

The Journal of Atmospheric and Solar-Terrestrial Physics

SPECIAL OFFER TO URSI CORRESPONDENTS

AIMS AND SCOPE

The *Journal of Atmospheric and Terrestrial Physics* (JASTP) first appeared in print in 1951, at the very start of what is termed the "Space Age". The first papers grappled with such novel subjects as the Earth's ionosphere and photographic studies of the aurora. Since that early, seminal work, the Journal has continuously evolved and expanded its scope in concert with - and in support of - the exciting evolution of a dynamic, rapidly growing field of scientific endeavour: the Earth and Space Sciences. At its Golden Anniversary, the now re-named *Journal of Atmospheric and Solar-Terrestrial Physics* (JASTP) continues its development as the premier international journal dedicated to the physics of the Earth's atmospheric and space environment, especially the highly varied and highly variable physical phenomena that occur in this natural laboratory and the processes that couple them. The *Journal of Atmospheric and Solar-Terrestrial Physics* is an international journal concerned with the inter-disciplinary science of the Sun-Earth connection, defined very broadly. The journal referees and publishes original research papers, using rigorous standards of review, and focusing on the following: The results of experiments and their interpretations, and results of theoretical or modelling studies; Papers dealing with remote sensing carried out from the ground or space and with in situ studies made from rockets or from satellites orbiting the Earth; and, Plans for future research, often carried out within programs of international scope. The Journal also encourages papers involving: large scale collaborations, especially those with an international perspective; rapid communications; papers dealing with novel techniques or methodologies; commissioned review papers on topical subjects; and, special issues arising from chosen scientific symposia or workshops. The journal covers the physical processes operating in the troposphere, stratosphere, mesosphere, thermosphere, ionosphere, magnetosphere, the Sun, interplanetary medium, and heliosphere. Phenomena occurring in other "spheres", solar influences on climate, and supporting laboratory measurements are also considered. The journal deals especially with the coupling between the different regions. Solar flares, coronal mass ejections, and other energetic events on the Sun create interesting and important perturbations in the near-Earth space environment. The physics of this subject, now termed "space weather", is central to the Journal of Atmospheric and Solar-Terrestrial Physics and the journal welcomes papers that lead in the direction of a predictive understanding of the coupled system. Regarding the upper atmosphere, the subjects of aeronomy, geomagnetism and geoelectricity, auroral phenomena, radio wave propagation, and plasma instabilities, are examples within the broad field of solar-terrestrial physics which emphasise the energy exchange between the solar wind, the magnetospheric and ionospheric plasmas, and the neutral gas. In the lower atmosphere, topics covered range from mesoscale to global scale dynamics, to atmospheric electricity, lightning and its effects, and to anthropogenic changes. Helpful, novel schematic diagrams are encouraged. Short animations and ancillary data sets can also be accommodated. Prospective authors should review the *Instructions to Authors* at the back of each issue.

Complimentary Information about this journal: http://www.elsevier.com/locate/JASTP? http://earth.elsevier.com/geophysics

Audience:
Atmospheric physicists, geophysicists and astrophysicists.

Abstracted/indexed in:
CAM SCI Abstr
Curr Cont SCISEARCH Data
Curr Cont Sci Cit Ind
Curr Cont/Phys Chem & Sci
INSPEC Data
Meteoro & Geoastrophys Abstr
Res Alert

Editor-in-Chief:
T.L. Killeen, National Centre for Atmospheric Research, Boulder, Colorado, 80307 USA

Editorial Office:
P.O. Box 1930, 1000 BX Amsterdam, The Netherlands

Special Rate for URSI Radioscientists 2003:
Euro 149.00 (US$ 149.00)
Subscription Information
2002: Volume 65 (18 issues)
Subscription price: Euro 2659 (US$ 2975)
ISSN: 1364-6826

CONTENTS DIRECT:
The table of contents for this journal is now available pre-publication, via e-mail, as part of the free ContentsDirect service from Elsevier Science. Please send an e-mail message to cdhelp@elsevier.co.uk for further information about this service.

For ordering information please contact Elsevier Regional Sales Offices:

Asia & Australasia/ e-mail: asiainfo@elsevier.com
Europe, Middle East & Africa: e-mail: nlinfo-f@elsevier.com
Japan: Email: info@elsevier.co.jp
Latin America : e-mail: rsola.info@elsevier.com.br
United States & Canada : e-mail: usinfo-f@elsevier.com

APPLICATION FOR AN URSI CORRESPONDENT

I have not attended the last URSI General Assembly, and I wish to remain/become an URSI Radioscientist in the 2003-2005 triennium. Subscription to *The Radio Science Bulletin* is included in the fee.
(please type or print in BLOCK LETTERS)

Name: Prof./Dr./Mr./Mrs./Ms. _____
Family Name *First Name* *Middle Initials*

Present job title: _____

Years of professional experience: _____

Professional affiliation: _____

I request that all information, including the bulletin, be sent to my ☐ home ☐ business address, i.e.:

Company name: _____

Department: _____

Street address: _____

City and postal / zip code: _____

Province / State: _____ Country: _____

Phone: _____ ext: _____ Fax: _____

E-mail: _____

Areas of interest (please tick)

☐ A Electromagnetic Metrology
☐ B Fields and Waves
☐ C Signals and Systems
☐ D Electronics and Photonics
☐ E Electromagnetic Noise & Interference
☐ F Wave Propagation & Remote Sensing
☐ G Ionospheric Radio and Propagation
☐ H Waves in Plasmas
☐ J Radio Astronomy
☐ K Electromagnetics in Biology & Medicine

The fee is 40 Euro.
(The URSI Board of Officers will consider waiving of the fee if the case is made to them in writing)

Method of payment: VISA / MASTERCARD (we do not accept cheques)

Credit Card No ☐☐☐☐ ☐☐☐☐ ☐☐☐☐ ☐☐☐☐ Exp. date: _____

Date: _____ Signed _____

Please return this signed form to:

The URSI Secretariat
c /o Ghent University / INTEC
Sint-Pietersnieuwstraat 41
B-9000 GENT, BELGIUM
fax (32) 9-264.42.88